INVESTIGATIONS INTO NANO-FORMULATIONS FOR ORAL DELIVERY OF DEFEROXAMINE IN THE TREATMENT OF HEMOCHROMATOSIS

by

ELIZABETH OLADOYIN AGBOLUAJE

(Under the Direction of May P. Xiong)

ABSTRACT

Hemochromatosis can be described as a medical condition with excessive iron accumulation in the body. There are two types of hemochromatosis, which include hereditary and acquired. Acquired hemochromatosis, as seen in patients with β-thalassemia and sickle cell disease, is due to transfusion-induced during the management of anaemia. When there is iron ++overload in the body, this can lead to the generation of reactive oxygen species, which can affect the heart, brain, liver, pancreas, joints, etc. One of the most established treatment strategies for hemochromatosis is iron chelation therapy, with deferoxamine being described clinically as the most successful in removing excess iron from the body. Deferoxamine is a clinically approved iron chelator and is a standard treatment in the management of hemochromatosis, but suffers from poor oral bioavailability, clinical toxicity, poor patient adherence, and suboptimal pharmacokinetics, necessitating prolonged intravenous infusion regimens. To address these issues, we developed two distinct: oral delivery strategies and which include:(1) self-assembled polymeric nanoparticles based on hyaluronic acid (HA, MW 15 kDa) conjugated with bile acids—deoxycholic acid (DOCA) or taurocholic acid (TCA)—and DFO, and (2) deferoxamine-loaded

nanostructured lipid carriers (DFO-NLCs) engineered using glyceryl monooleate and oleic acid, with poloxamer 188 as surfactant and a chitosan-alginate coating to enhance stability in gastric environments and gastrointestinal permeation.

In this dissertation, HA-BA-DFO conjugates were synthesized and formulated into self-assembled nanoparticles. The structural integrity was investigated with NMR, FTIR, and UV-Vis spectroscopy. It was observed that TCA9-HA-DFO displayed superior in vitro permeability and lower cytotoxicity compared to free DFO, while maintaining effective iron-chelating activity. For the second strategy, a Quality by Design (QbD) framework with Design of Experiments (DOE) was applied to optimize DFO-NLC formulations. Physicochemical characterization showed that formulations (F2, F3, and F5) demonstrated desirable particle size, encapsulation efficiency, DFO loading, and controlled release profiles, with F2 exhibiting the most sustained DFO release. With these two approaches, it was observed that both highlighted promising strategies that can be exploited to overcome the limitations of current DFO therapy. This offers huge potential for the development of safe, effective, and patient-friendly oral formulations that enhance therapeutic outcomes in iron-overload disorders.

INDEX WORDS: Deferoxamine, Iron overload, Oral, Polymeric nanoparticles, Hyaluronic acid, Bile acid, Nanostructured Lipid Carriers, Chitosan, Alginate

INVESTIGATIONS INTO NANO-FORMULATIONS FOR ORAL DELIVERY OF DEFEROXAMINE IN THE TREATMENT OF HEMOCHROMATOSIS

by

ELIZABETH OLADOYIN AGBOLUAJE

Bachelor of Pharmacy, Obafemi Awolowo University, Nigeria, 2016

MS, University of Toledo, US, 2021

A Dissertation Submitted to the Graduate Faculty of The University of Georgia in Partial

Fulfillment of the Requirements for the Degree

DOCTOR OF PHILOSOPHY

ATHENS, GEORGIA

2025

© 2025

Elizabeth Oladoyin Agboluaje

All Rights Reserved

INVESTIGATIONS INTO NANO-FORMULATIONS FOR ORAL DELIVERY OF DEFEROXAMINE IN THE TREATMENT OF HEMOCHROMATOSIS

by

ELIZABETH OLADOYIN AGBOLUAJE

Major Professor: Committee:

May P. Xiong Tamas Nagy Eugene Douglass Gurvinder Singh Rekhi

Electronic Version Approved:

Ron Walcott Vice Provost for Graduate Education and Dean of the Graduate School The University of Georgia August 2025

ACKNOWLEDGEMENTS

My eternal gratitude to God, the anchor of my soul, who made this day possible. All glory and adoration belong to the Father of lights, in whom there is no variableness or shadow of turning. Thank you, Lord, for all you have done for me. I extend my heartfelt appreciation to my advisor, Dr. May P. Xiong, for your unwavering support, counsel, and mentorship during my PhD program, which has shaped me into the scientist I am today. I would also like to thank my committee members, Dr. Tamas Nagy, Dr. Eugene Douglass, and Dr. Gurvinder Singh Rekhi, for their valuable suggestions and mentorship throughout my doctoral journey. Your expertise and support have been indispensable in my academic growth. My sincere thanks go to colleagues in the lab: Shuolin Cui, Joseph Manu, Cai Hong Li, and Sneha Ghosh for their great support, especially during my challenging life moments. To my wonderful parents, His Royal High Majesty, Oba Omisade Cornileus Agboluaje, and Her Royal High Majesty Olori Roseline Omolara Agboluaje, words can never be enough to tell you how much you mean to me. I thank you for your intentionality in giving me the best education possible. To my siblings: Agboluaje Abimisinuola, Agboluaje Miracle, and Agboluaje Hope, I could not have had a better set of sisters. To my husband, thank you so much for the strength you offered on days when my faith wavered; you are highly treasured.

Table of Contents

ACKNO	WLEDGEMENTSiv
LIST OF	TABLESvii
LIST OF	FIGURESviii
CHAPTI	ER
1. INTRO	ODUCTION1
1.1	Hemochromatosis
1.2	Current Management Approaches and Limitations
1.3	Oral Drug Delivery
1.4	Polymeric Nanoparticles 6
1.5	Nanostructured Lipid Carriers
1.6	Proposed Strategies8
2	BILE ACID-TARGETED HYALURONIC ACID FOR ENHANCED ORAL
ABSO	PRPTION OF DEFEROXAMINE
2.1	Abstract
2.2	Introduction
2.3	Experimental
2.4	Results23
2.5.	Discussion
2.6	Supplementary Information39

3. DEVELOPMENT AND OPTIMIZATION OF NANOSTRUCTUR	ED LIPID CARRIERS
FOR ENHANCED ORAL ABSORPTION OF DEFEROXAMINE	48
3.1 Abstract	49
3.2. Introduction	50
3.3 Experimental	54
3.4 Results	61
3.5 Discussion	74
3.6 Supplementary Information	78
4 CONCLUSIONS	85
4.1 Bile Acid-Targeted Hyaluronic Acid Nanoparticles for Enhan	nced Oral Absorption of
Deferoxamine	85
4.2 Development and Optimization of Nanostructured Lipid Carrie	ers for Enhanced Oral
Absorption of Deferoxamine	86
REFERENCES	88

LIST OF TABLES

Page
Table 3.1: Mixture variables output based on the experiment's constant inputs that can be
formulated and the corresponding response values for particle size, drug loading, and
encapsulation
efficiency64
Table S3.1. The experiment constants for the design of experiment included a drug: lipid ratio
(1:3-1:7), organic: aqueous phase (1:5- 1:15), and a surfactant concentration (0.5-
1.5%)
Table S3.2. Fusion pro predicted DFO-F2 as the overall best formulation with a drug: lipid ratio
(1:7), organic: aqueous phase (1:15), and a surfactant concentration
(1.5%)80
Table 4.1: Comparison of the bile acid–targeted hyaluronic acid nanoparticles for enhanced oral
absorption of deferoxamine efficiency and development and optimization of nanostructured lipid
carriers for enhanced oral absorption of deferoxamine
project86

LIST OF FIGURES

Page
Figure 2.1: Graphical abstract illustrating the proposed research strategy
Figure 2.2: Synthesis of TCA-HA-DFO polymeric conjugates26
Figure 2.3: Chemical structures were confirmed using 1H NMR in D2O and CD3OD (1:1 v/v).
Figure 2.4: TEM and DLS particle size of a DOCA9-HA-DFO, b TCA9-HA-DFO, and c HA-DFO. d Successful conjugation of DFO to the various polymer conjugates30
Figure 2.5: Cytotoxicity of free DFO (blue line), HA-DFO (red line), DOCA9-HA-DFO (green line), and TCA9-HA-DFO (purple line) after 24 h incubation
Figure 2.6: Ferritin reduction assay to monitor iron chelation efficacy of DFO, HA-DFO, DOCA9 HA-DFO, and TCA9-HA-DFO on a J774A.1 macrophage and b HepG2 iron-overloaded cells
Figure 2.7: Confocal imaging revealing cellular uptake of the polymeric conjugates34
Figure 2.8: In Vitro Permeation Studies
Figure S2.1: Synthesis of DOCA-HA-DFO polymeric conjugates
Figure S2.2: 1H NMR spectra of TCA, TCA-NPC, and TCA- NH2 showing the introduction of amino group on TCA backbone (B) 1H NMR spectra of DOCA, DOCA-NPC, and DOCA-NH2 showing the introduction of amino group on DOCA backbone42
Figure S2.3: (A). 1H NMR spectra of TCA, HA, TCA3-HA, TCA6-HA, TCA9-HA showing the successful conjugation of TCA-HA (B) 1H NMR spectra of DOCA, HA, DOCA3-HA, DOCA6 HA, DOCA9-HA showing the successful conjugation of DOCA-HA45
Figure S2.4: (A). FTIR spectra of OHA, TCA3-OHA, TCA6-OHA, and TCA9-OHA show the characteristic band for the creation of aldehyde groups at 1700 cm-1 following the oxidation reaction. (B). FTIR spectra of OHA, DOCA3-OHA, DOCA6-OHA, and DOCA9-OHA show the characteristic band for the creation of

Figure 3.1: Schematic illustration showing the design of deferoxamine-nanostructured lipid carriers coated with chitosan and alginate with improved oral bioavailability and iron-chelation efficacy
Figure 3.2: Schematic illustration showing the formulation of deferoxamine-nanostructured lipid carriers coated with chitosan and cross-linked with alginate
Figure 3.3: Three-dimensional (3D) response surface plots showing the effect of the variable on response at a surfactant concentration of 1.5%
Figure 3.4: Physicochemical characterization of F2 DFO-NLC showing particle size analysis for (a) DLS, (b) TEM and (c) successful loading of F2, F3 and F5 DFO to NLC67
Figure 3.5: FTIR spectra of DFO, chitosan, alginate, GMO, oleic acid, NLC, and F1-F10 DFO nanostructured lipid carriers showing characteristic peaks indicative of DFO loading and cross-linking between chitosan and alginate
Figure 3.6: Cumulative % drug release of DFO and F1, F2, F3, F5, F6, F7, and F10 DFO-NLCs (a) in simulated gastric fluid representative of pH 1.2, (b) in simulated fluid representative of pH 7.4
Figure 3.7: Cytotoxicity of free DFO (blue line), F2 DFO-NLC (green line), F3 DFO-NLC (purple line), and F5 DFO-NLC (red line) after 48 hrs. incubation on (a) J774A.1 cells, (b) HepG2 cells, and (C) Caco-2 cells
Figure 3.8: Ferritin reduction assay evaluating the iron chelation performance of DFO, F2 DFO NLC, F3 DFO-NLC, and F5 DFO-NLC in (a) J774A.1 macrophages, (b) HepG2 iron-overloaded cells
Figure 3.9. In Vitro Permeation Studies
Figure S3.1: Three-dimensional (3D) response surface plots showing the effect of the variable on response (A) the effect of organic/aqueous phase ratio on particle size at a surfactant concentration 76 of 0.5-1.%. (B) The effect of organic/aqueous phase ratio on % DL at a surfactant concentration of 0.5-1.%. (C) the effect of organic/aqueous phase ratio on % EE at a surfactant concentration of 0.5-1.%

CHAPTER 1

INTRODUCTION

Iron is a very important nutritional element for all forms of life and plays an important role in cell proliferation and differentiation, electron transport, cellular respiration, differentiation of hematopoietic cells, and gene expression regulation[1, 2]. While iron is very important, only 10 % of dietary intake gets absorbed into the bloodstream, with about 20mg of iron daily needed for hemoglobin synthesis, with about 18mg of the iron needed coming from aging red blood cells. The amount of iron can vary significantly from about 300mg in women that are not yet reached menopause to 1g in adult men. Iron homeostasis involves three main processes, which include absorption, storage, and export. Iron can be absorbed via binding to proteins such as transferrin, hemoglobin, or as free iron. Transferrin induces iron absorption by binding two Fe³⁺ ions, and this triggers interaction with transferrin receptor 1 (TfR1) on the cell surface, which causes endocytosis. When iron gets to the acidic environment of the endosome, there is a release of iron, reduction to Fe²⁺, and transportation by divalent metal transporter 1 (DMT1) into the cytoplasm. For hemoglobin, iron gets absorbed after it has been hemolyzed, with haptoglobin-bound hemoglobin entering macrophages via CD163.

There is a type of protein called ferritin, a protein which is the stored form of iron in hepatocytes and reticuloendothelial cells (macrophages and monocytes). When there is iron overload, there is more ferritin synthesis, and vice versa when there is iron deficiency. Iron gets exported by ferroportin, which can be found on the basolateral membrane of enterocytes and macrophages. There is more ferroportin expression when there is iron deficiency in the body, which will trigger

more iron release into the plasma. Ferroportin expression is regulated by hepcidin, a liver hormone that ultimately affects iron efflux. Hepcidin expression is controlled by various factors such as iron level, inflammation, and erythropoietic activity [3]. When there is iron overload in the body, the amount can reach up to 30 grams of iron in the body[4].

1.1. Hemochromatosis

Hemochromatosis is a common blood disorder that can be characterized by the gradual accumulation of iron in the body until it becomes very toxic to various organs in the body[5]. There are two types of hemochromatosis, and they include both acquired and hereditary hemochromatosis[6]. Hereditary hemochromatosis arises from genetic mutations that impact the regulation of iron absorption into the bloodstream. In 1996, Feder and his colleagues discovered the HFE gene as the main trigger for hereditary hemochromatosis[4]. Under hereditary hemochromatosis, there are different types based on genetic mutation. The first one is type 1 hereditary hemochromatosis or commonly called HFE-related hemochromatosis. The HFE gene is located on chromosome 6, where the C282Y mutation can occur. When this mutation is homozygous state, this leads to iron overload. About 10% of the Caucasian population has the mutation, and this makes it highly prevalent in them.

The second type of hereditary hemochromatosis is called juvenile hemochromatosis or type 2 hereditary hemochromatosis. It is a severe form of hemochromatosis that is not highly prevalent but affects mainly young adults above 30 years old. This type of hemochromatosis exhibits dominant cardiac and endocrine negative effects, and it exists either due to the hemojuvelin gene on chromosome 1 mutation or the hepcidin (HAMP) gene on chromosome 19 mutation.

Type 3 hereditary hemochromatosis is caused by transferrin receptor 2 gene on chromosome 7 mutation. Type 4 hemochromatosis is caused by the ferroportin (SLC40A1) gene located on chromosome 2 and can be divided into type A and type B. Type A has either normal or low plasma transferrin saturation and predominant macrophagic iron deposition, while type B can have increased plasma transferrin saturation and predominant parenchymal iron deposition. Other types of hereditary hemochromatosis include hereditary a(hypo)ceruloplasminemia, which is due to a ceruloplasmin gene mutation and an iron overload condition caused by a transferrin mutation[7]. For acquired hemochromatosis, iron overload can arise from medical intervention or based on lifestyle. For example, patients who have thalassemia or sickle cell diseases usually have an anemic condition and necessitate frequent blood transfusions, which can ultimately lead to iron overload in the body. Both hereditary and acquired hemochromatosis present similar symptoms clinically, such as diabetes, hepatomegaly, cardiomyopathy, splenomegaly, etc.

1.2. Current Management Approaches and Limitations

The diagnosis of hemochromatosis can combine several approaches, which include blood tests, imaging, and sometimes genetic analysis. The serum ferritin and transferrin levels are an indication of hemochromatosis in the blood. The imaging technique involves the use of magnetic resonance imaging (MRI), particularly R2 and T2* techniques, which allows non-invasive assessment of iron levels in organs like the liver and heart, offering an alternative to invasive procedures like liver biopsies. These imaging tools are especially useful in patients with thalassemia major who require frequent transfusions and are prone to iron accumulation. In the management of iron overload, the main goal is usually to reduce the iron level in order to prevent organ damage. Two major techniques have become the mainstay approaches in removing excess ions, and they include

phlebotomy and the use of iron chelation therapy. There are three types of iron chelators on the market, and they include deferoxamine, deferasirox, and deferiprone[7]. Deferoxamine (DFO), an iron-chelating drug that is clinically approved by the FDA, has been used for several years to treat the iron overload associated with constant blood transfusions.

DFO clinical use has been challenged by its poor pharmacokinetic properties in humans. Intensive infusion regimens, poor oral absorption, and nonspecific toxicity all contribute to poor patient compliance with DFO treatment[8]. Poor membrane permeability and low bioavailability of DFO have limited its use for oral drug delivery. An alternative to DFO, deferiprone was introduced clinically a few years ago for oral delivery, but its use has been plagued by limited chelation efficiency, and reports that some patients can develop a life-threatening reduction in their white blood cells while on deferiprone treatment, which has prevented its wider adoption [9]. There is still a great need for the development of a safe orally active iron chelator, according to the National Institute of Health and the National Heart, Lung, and Blood Institute[10].

1.4 Oral drug delivery

Oral drug delivery has become a mainstay approach of drug delivery over the years because of its desirable properties, which include patient compliance, non-invasiveness, and ease of drug administration [11, 12]. An oral drug delivery system includes several components from the mouth to the esophagus to the stomach to the small intestine and large intestine[13]. It is cheap, non-invasive, easy to manufacture, painless, and widely accepted by patients[14]. Also, the gastrointestinal tract (GIT) possesses a large surface area with a viscous mucosal lining for absorption, which is greater than 300m². The abundance of enterocytes, such as microfold cells, all over the intestines also makes the epithelium very absorptive. Absorption of drugs orally can

occur through four different main mechanisms, which include: paracellular, transcellular, carrier-mediated transcellular, and facilitated transport pathways[15]. The paracellular pathway involves drug diffusion via the small pores between the tight junctions of the mucosal enterocytes. The transcellular mechanism involves drug absorption through the phospholipid cell membrane of the intestinal enterocytes. In contrast, the carrier-mediated transport involves the interaction of mostly the protein carrier of the apical membrane of the enterocyte cell with the drug molecule, with the use of binding cassette transporters, adenosine triphosphate, superfamily, and solute carrier transporters, which can be found in the apical and basolateral membranes of the GI tract. Facilitated drug absorption also includes the interaction of the drug molecule with protein carriers, but without the use of energy[12].

Despite these desirable advantages, the gastrointestinal physiological barrier remains a great challenge in oral drug delivery. Gastrointestinal pH varies a lot from 1.2 in the fasting stomach to 5-7 in the small intestine and 6-7.5 in the colon[13, 16]. The use of nanocarriers with excellent gastrointestinal permeability has gained recent focus on improving the oral bioavailability of various drugs[17]. Nanocarriers can increase the residence time of drugs in the small intestine or prevent drug efflux transporters from pumping the drugs out[18]. Also, they can protect the medication from the acidic nature of the stomach while ensuring a controlled release of the medication into the target cells[19]. There are different types of nanocarriers, and they include micelles, nanoparticles, liposomes, dendrimers, carbon nanotubes, etc.[16]. Nanoparticles can range from polymeric nanoparticles to solid lipid nanoparticles to nanogels.

1.5 Polymeric Nanoparticles

Nanoparticles are colloidal, in which a drug can be entrapped, loaded, encapsulated, or conjugated to the nanoparticle matrix. Polymers are very desirable in making nanoparticles because of their impressive stability, controlled drug release kinetics, high drug loading, and safety[16]. Polymeric nanoparticles can range from a size of 10-1000nm[20]. The size of nanoparticles will determine the oral absorption and biodistribution of the drug loaded, which will then ultimately impact its therapeutic efficacy. A particle size of less than 600nm is desirable for an oral drug delivery system [21]. Biomaterials, in particular, make attractive drug polymeric nanoparticles due to their nontoxicity, biocompatibility, and biodegradability. For biodegradable polymers, examples include chitosan, alginate, hyaluronic acid, pectin, polylactic acid, etc. Some of the preparation methods for polymeric nanoparticles include some of the following: complex coacervation, ionic gelation, solvent evaporation, ionotropic gelation, polyelectrolyte complexation, polymerization of monomers, etc.[22].

Hyaluronic acid is a linear polysaccharide made up of repeating units of N-acetylglucosamine and d-glucuronic acid linked by β (1,4) and β (1,3) glycosidic bonds[23]. Hyaluronic acid's molecular weights can range from 1000 to 10,000,000 Da. Hyaluronic acid is found in the extracellular matrix and in the synovial fluid of human tissues[24]. It plays an important role in wound healing, tissue hydration, lubrication, etc.[25]. There has been an extensive investigation into the biomedical application of hyaluronic acid due to its desirable properties. Studies have reported that hyaluronic acid can adhere and penetrate the intestinal epithelial layer[26]. Hyaluronic acid has been shown in recent studies to enhance the oral absorption of poorly absorbable drugs [23]. It can improve drug absorption through the Caco-2 cell layer by endocytosis uptake[27]. There is also overexpression of hyaluronic acid in epithelial cells of the colon [28]. Various functional groups

on hyaluronic acid such as carboxyl, acetamido, and hydroxyl groups to further improve the desired polymeric nanoparticle being developed [29]

Chitosan is a linear polysaccharide that is generated by the partial deacetylation of chitin, with primary building blocks of *N*-acetyl-glucosamine and glucosamine. Some of the factors that can influence chitosan's properties include degree of acetylation, molecular weight, and the pH of the environment. Studies have reported that the positively charged group of chitosan can interact with the negatively charged group in mucin, which enables chitosan to be able to have mucoadhesive properties and prolonged residence time. Chitosan can also open tight junctions reversibly, thereby increasing paracellular pathway absorption of drug molecules[30-32].

Alginate, which is one of the most abundant materials in nature, is also a very desirable biomaterial due to its biocompatibility, biodegradability, and chemical versatility in biomedical applications[33]. It is an anionic polysaccharide made up of β -D-mannuronic acid (M) and α -L-guluronic acid (G) repeating units linked by a $1\rightarrow4$ linkage[34]. Alginate has been used extensively in the biomedical field for tissue engineering, wound dressing, drug delivery, etc.[35]. Alginate has been used in the delivery of medications such as doxorubicin, insulin, cisplatin, etc.[36]. Bile acids are amphiphilic biomaterials that are synthesized in the liver and stored in the gallbladder. They can bind to different target sites based on their hydrophilicity or hydrophobicity [37]. They have a short aliphatic side chain and a steroid nucleus that is very tough[38]. Bile acids (i.e., deoxycholic acid, taurocholic acid), which are also bioactive materials, have been recently proven to be oral absorption enhancers [24, 25].

1.5 Nanostructured Lipid Carriers

Studies have shown that lipid nanoparticles can be employed to improve the oral absorption of drugs. This is because lipids can boost the absorption of drugs in the GIT by enhancing mucosal adhesion and prolonging the residence time. Also, lipid nanoparticles have the potential to shield loaded drugs from chemical and enzymatic degradation. They exhibit a gradual release of drug molecules from the lipid matrix into the bloodstream, leading to enhanced therapeutic profiles compared to free drugs. Nanostructured lipid carriers (NLCs) have been described as an effective lipid system for oral delivery of various drugs[39]. NLCs contain a mixture of solid lipid and liquid lipid, which can enhance drug loading capacity while minimizing drug expulsion during storage.

1.6 Proposed Strategies

DFO clinical use has been limited to the parenteral route due to its low bioavailability of 2% when given orally. There is a great need to develop oral formulations of DFO that can improve the pharmacokinetic profile and reduce the toxic side effects of DFO[9]. Although other chelators have developed their oral formulations like deferiprone, their clinical use has shown a life-threatening reduction in white blood cell counts and has made the drug untenable as an alternative for many patients. Most studies have been focused on increasing the plasma half-life and decreasing the non-specific toxicity of deferoxamine by exploring various drug delivery routes apart from the oral drug delivery route. For example, Rassu and his team have developed solid microparticles with the use of chitosan chloride and methyl-β-cyclodextrin for the nasal drug delivery of DFO. Increased nose-to-brain permeation of DFO was observed with limited systemic exposure [40]. Although some studies have been developed for oral formulations of conjugating DFO by hyperbranched polyglycerol and hydroxyethyl starch to increase the plasma half-life, these approaches did not increase the permeability

of DFO across the intestinal membrane. The development of an oral delivery form of DFO with the use of intestinal permeable nanocarriers can be instrumental in addressing the challenges of DFO oral delivery. Therefore, two strategies were investigated in this report to address the low oral bioavailability of DFO.

The first study was focused on the development of an oral delivery form of deferoxamine using a polymeric nanocarrier that has been shown to increase intestinal drug permeation, and this will be the optimal way of addressing DFO delivery challenges[41, 42]. We hypothesize that selfassembled nanoparticle conjugates of deferoxamine using hyaluronic acid and sodium deoxycholate/ taurocholate as nano drug carriers and oral absorption enhancers will show improved intestinal permeation of deferoxamine. We also hypothesize that the nanoparticles formed from DFO polymeric conjugates will increase the ion chelating efficiency and reduce the non-specific toxicity of deferoxamine. It is anticipated that this study will be instrumental to translational studies for the clinical use of improved orally bioavailable deferoxamine. The development of an orally bioavailable form of DFO with the use of HA as a polymeric nanocarrier and two types of bile acids as oral absorption enhancers makes this proposed project innovative. Most reports in the literature have focused on developing other drug delivery routes such as intravenous, topical, nasal, etc., for DFO. Therefore, this innovative project is focused on developing an oral delivery form of deferoxamine with the use of a polymeric nanocarrier that is safe, biocompatible, and biodegradable.

The second study focused on developing and optimizing polymer-coated nanostructured lipid carriers for the oral delivery of deferoxamine. The experimental approach was focused on two aims.

Aim 1 involves the design, formulation, and characterization of DFO-NLCs. Five different DFO-NLC

formulations were designed and developed with the use of quality by design. Method preparation involves the solvent diffusion method for the primary emulsion development, followed by chitosan and alginate coating. Aim 2 involves an in vitro investigation into the oral absorption, cytocompatibility, and iron chelation efficiency of the DFO-NLCs. It is imperative to investigate the oral absorption of the developed DFO-NLCs. Oral absorption will be determined by trans transwell assay setup with the use of colon carcinoma cell line. Cytocompatibility will also be done with macrophages and a hepatic cell line for DFO-NLCs to determine whether the use of lipid nanoparticles reduces the toxicity of DFO. An iron chelation study will also be done to determine whether the formulation will impact the ion chelation efficiency of DFO.

The two strategies will then be quantitatively compared to selecting a better approach for future translational studies for oral delivery of DFO.

CHAPTER 2

BILE ACID-TARGETED HYALURONIC ACID FOR ENHANCED ORAL ABSORPTION $\label{eq:constraint} \text{OF DEFEROXAMINE}^1$

¹ Agboluaje, Elizabeth Oladoyin, et al. "Bile acid—targeted hyaluronic acid nanoparticles for enhanced oral absorption of deferoxamine." The AAPS Journal 26.3 (2024): 46. Reprinted here with permission of the publisher.

2.1 Abstract

Patients with β-thalassemia and sickle cell disease often rely on blood transfusions, which can lead to hemochromatosis and chronic oxidative stress in cells and tissues. Deferoxamine (DFO) is clinically approved to treat hemochromatosis but is suboptimal for patients due to its poor pharmacokinetics, which require long-term infusion regimens. Although the oral route is preferable, DFO has limited oral bioavailability. Studies have shown that hyaluronic acid (HA) and bile acid (BA) can enhance the oral absorption of poorly absorbed drugs. To improve upon the oral delivery of DFO, we report on the synthesis and characterization of HA (MW 15 kD) conjugated to two types of BA, deoxycholic acid (DOCA) and taurocholic acid (TCA), and DFO. The resulting seven polymeric conjugates all formed self-assembled nanoparticles. The degree of BA and DFO conjugation to the HA polymer was confirmed at each step through nuclear magnetic resonance, Fourier transform infrared spectroscopy, and UV-Vis spectroscopy. The best formulations for further in vitro testing were determined based on physicochemical characterizations and included HA-DFO, TCA₉-HA-DFO, and DOCA₉-HA-DFO. Results from in vitro assays revealed that TCA9-HA-DFO enhanced the permeation of DFO the most and was also less cytotoxic to cells compared to the free drug DFO. In addition, ferritin reduction studies indicated that the conjugation of DFO to TCA9-HA did not compromise its chelation efficiency at equivalent free DFO concentrations. This research provides supportive data for the idea that TCA conjugated to HA may enhance the oral absorption of DFO, improve its cytocompatibility, and maintain its iron chelation efficiency.

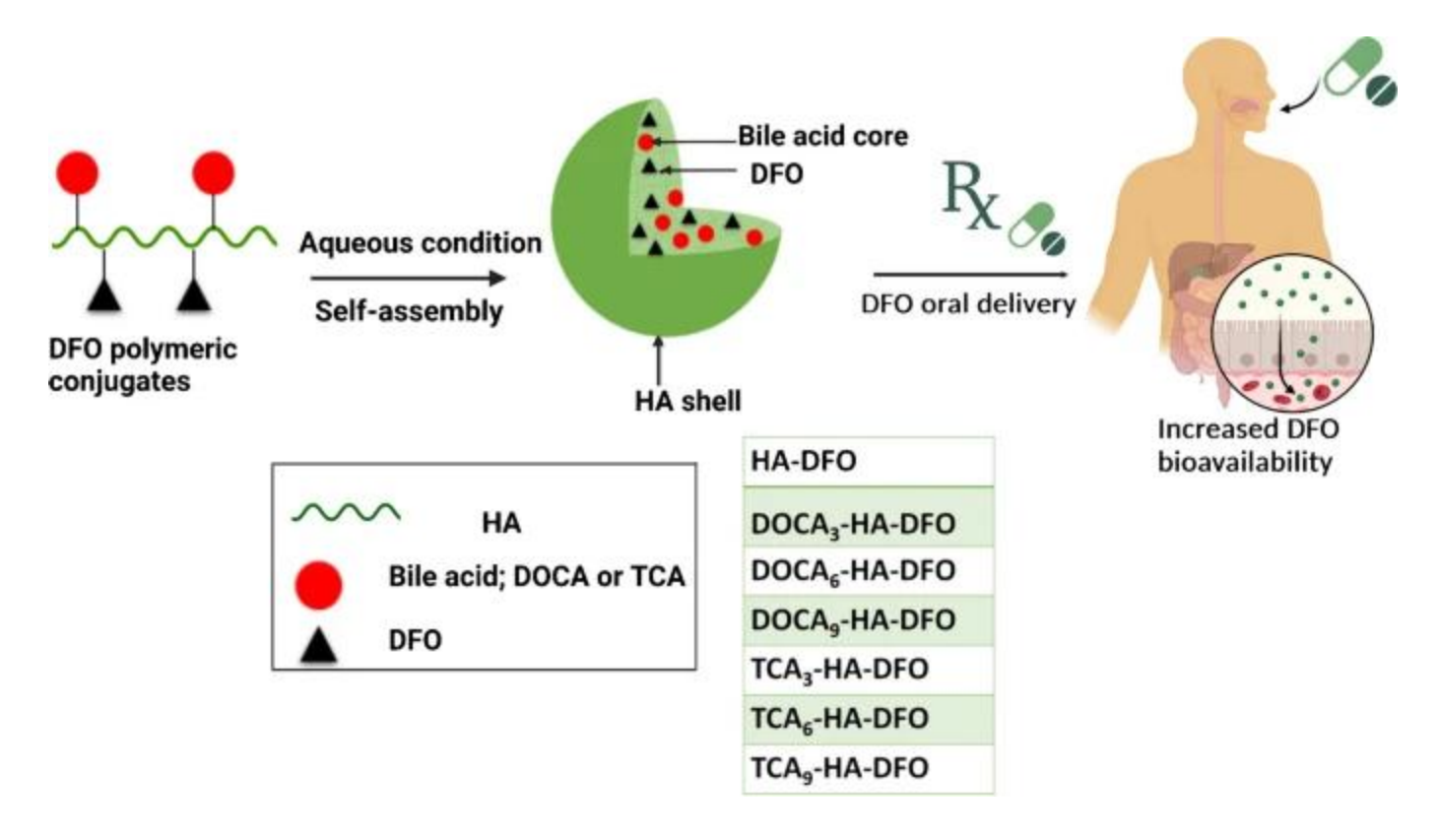


Figure 2.1. Graphical abstract illustrating the proposed research strategy

2.2 Introduction

Hematological disorders such as sickle cell and thalassemia are hereditary conditions caused by point mutations on the beta-globin gene and can lead to the production of defective hemoglobin, causing severe anemia and the need for lifetime blood transfusions to infuse healthy hemoglobin to alleviate the symptoms of anemia [43-46]. Although the first cure for sickle cell using the genediting tool CRISPR was recently approved by the FDA (Casgevy, December 2023), the cost of this therapy hovers around 2 million dollars per patient and makes it inaccessible to people in developing countries where the disease is more prevalent [47, 48]. In addition, there are still questions regarding possible off-target side effects of CRISPR as a curative tool for treating genetic disorders [48]. Under normal conditions, liver macrophages and hepatocytes store excess

iron as ferritin and hemosiderin. Transferrin transports iron to body tissues, while spleen macrophages recycle iron from old red blood cells for new cell production in the bone marrow [49]. Repeated transfusions cause iron overload, leading to the formation of reactive oxygen species (ROS) through the Fenton reaction, damaging vital organs [50]. The first FDA-approved chelation therapy was DFO which can be administered as an infusion or a subcutaneous injection. Intravenous DFO is clinically recognized as a highly effective iron chelator due to its hexadentate structure which allows it to bind at a 1:1 stoichiometric ratio to iron with a stability constant on the order of 10³⁰ [51], unlike oral chelators such as deferiprone and deferasirox which bind more weakly to iron at a 3:1 and 2:1 stoichiometric ratio, respectively [9, 40, 52]. Despite the long positive history of intravenous DFO, its oral use is still hampered in patients, mainly due to poor absorption (2% oral bioavailability) [9, 53]. Consequently, there remains a significant need to develop a safe and orally active DFO formulation [9, 10], mainly because oral drug delivery is preferable to patients due to its non-invasiveness [54]. Because the gastrointestinal physiological barrier remains a challenge for some drugs, the use of polymers with excellent gastrointestinal permeability has gained interest in improving their bioavailability [17].

Natural polymers such as HA in particular make attractive drug carriers for oral delivery and can enhance the oral absorption of poorly absorbable drugs such as paclitaxel, metformin, and insulin [23, 32, 42, 55]. HA is a natural linear polysaccharide that is nonimmunogenic, biocompatible, and biodegradable [41, 56, 57]. HA's molecular weights (MW) can range from 10³ to 10⁷ Da with alternating disaccharide units of D-glucuronic acid and N-acetyl-d-glucosamine, with a lower MW more preferred for oral drug delivery applications [24, 27, 58-60]. HA can enhance drug absorption by adhering to mucous membranes and binding to receptors for endocytosis on GI tract cells [61]. Another advantage of HA is the ability to functionalize this polymer as needed with small targeting

molecules of interest [62]. For example, the use of BA, such as natural DOCA and synthetic TCA was shown to increase the oral absorption of drugs [55, 63, 64]. In this paper, we investigated whether the absorption of HA-DFO polymer conjugates could be further enhanced through functionalization with BA.

DOCA and TCA are small amphiphilic BA with distinct partition coefficients of 3.50 for DOCA and 0.20 for TCA [65-67] and were assessed for their ability to further enhance the oral absorption of DFO polymeric conjugates [68]. We chose 15 kD HA for the study based on prior reports, suggesting its effectiveness in improving the oral delivery of other HA-drug conjugates [69]. The synthesis of HA-DFO, DOCA-HA-DFO, and TCA-HA-DFO involved investigations into various reaction conditions to covalently conjugate these molecules at different levels to the HA polymer backbone. The final 7 polymer conjugates synthesized were further analyzed *in vitro* to gain insight into their cytocompatibility, absorption, and iron chelation properties. Our results suggest that BA, such as DOCA and TCA, conjugated to HA can indeed enhance intestinal permeation of DFO compared to HA-DFO or DFO alone. Additionally, we also demonstrate that these polymer conjugates can still efficiently chelate iron in iron-overloaded cells, similar to free DFO, and that their use is also associated with a reduction in cytotoxicity (typically associated with free DFO) at equivalent concentrations.

2.3. Experimental

Detailed information about the materials used can be found in the Supplementary Information.

2.3.1 Synthesis of TCA-HA and DOCA-HA

Preparation of TCA-NH2 and DOCA-NH2

TCA-HA and DOCA-HA were synthesized by first functionalizing TCA and DOCA with primary amines before conjugation to HA (**Figs. 2.2A and S1A**). First, 1.86 mmol of TCA or 2.8 mmol DOCA in 6 ml of dimethylformamide (DMF) was reacted with 4-nitrophenyl chloroformate (NPC) (2.23 mmol for TCA and 3.36 mmol for DOCA) and triethylamine (3.72 mmol for TCA and 5.6 mmol for DOCA) at 0°C for 30 min and then 12 h at room temperature at a feed mole ratio of 1:1.2:2 of TCA to NPC to TEA and 1:1.2:2 of DOCA to NPC to TEA, respectively. At the end of the reaction time, the solvent was evaporated by rotary evaporation, followed by lyophilization to generate TCA-NPC and DOCA-NPC. Next, TCA-NPC (0.147 mmol) or DOCA-NPC (0.188 mmol) in 2 ml of DMF was reacted with 4-methyl morpholine (1.17 mmol for TCA and 1.128 mmol for DOCA) and ethylenediamine (14.7 mmol for TCA and 18.8 mmol for DOCA) for 24 h at room temperature. TCA-NH₂ and DOCA-NH₂ were recrystallized by the addition of cold acetonitrile four times, followed by centrifugation and lyophilization to obtain the dry TCA-NH₂ and DOCA-NH₂. The functionalized BAs were confirmed by ¹H NMR (Bruker Advance 400 MHz spectrometer).

Conjugation of TCA-NH2 and DOCA-NH2 to HA

The carboxyl groups of HA (15 kD) were conjugated to TCA-NH₂ and DOCA-NH₂, respectively, via EDC NHS coupling chemistry at various test ratios (**Figs. 2.2A and S2.1A**). HA (0.1 g) was dissolved in 5 ml of formamide with gentle magnetic stirring at room temperature. Various amounts of EDC and NHS (the feed ratio of EDC to NHS to HA was 10:10:1, 20:20:1, and 30:30:1, respectively) were added. Next, TCA-NH₂/DOCA-NH₂ (the feed ratio to HA was 10:1, 20:1, and 30:1, respectively) dissolved in DMF were added to the mixed solution of HA, EDC, and NHS under gentle stirring at 50°C. The whole mixture was allowed to cool to room temperature and

stirred under a nitrogen atmosphere for 24 h. The resulting solution was dialyzed serially against an excess amount of water/methanol (1:3 v/v then 1:1 v/v) for 1 day and DI water for 2 days, respectively. This was followed by lyophilization to generate the dried TCA-HA and DOCA-HA polymer conjugates. The degree of substitution (DS), defined as the number of TCA and DOCA conjugated per one HA molecule under the various conditions tested, was assessed by 1 H NMR in $D_{2}O/CD_{3}OD$ (1:1, v/v).

2.3.2. Synthesis of TCA-HA-DFO and DOCA-HA-DFO Conjugates

Oxidization of TCA-HA and DOCA-HA

Previous studies have reported using NaIO₄ to oxidize sugar ring hydroxyl groups in HA to form two aldehyde groups per monomeric unit [70, 71]. These aldehydes can then be employed to conjugate DFO's amino group to the HA backbone via Schiff base chemistry. To conjugate the TCA-HA and DOCA-HA polymeric conjugates to DFO, the HA backbone was oxidized through NaIO₄ (Figs. 2.2 B and S2.1B). In brief, each (1%w/v) of the various ratios of TCA-HA and the DOCA-HA polymeric conjugates was dissolved in DI water, and the equimolar ratio of NaIO₄ to HA (1:1) was added in dropwise amounts. The reaction was allowed to proceed in a dark room at room temperature for 8 h under gentle stirring. Next, 1 ml of ethylene glycol was then added to inactivate the unreacted NaIO₄. This was followed by dialysis of the resultant solution against an excess amount of DI water for 3 days and lyophilization to generate the dried oxidized "OHA, TCA₃-OHA, TCA₆-OHA, TCA₉-OHA, DOCA₃-OHA, DOCA₆-OHA, and DOCA₉-OHA" polymeric conjugates wherein the under script indicates the number of each respective BA that

was conjugated to the HA backbone. Confirmation of the oxidized conjugates was assessed by ATR-CRYSTAL FTIR (Fourier transform infrared spectroscopy) (Bruker).

Conjugation of DFO to TCA-OHA and DOCA-OHA

The coupling of DFO to varying degrees of BA_n-HA polymer conjugates (OHA, TCA₃-OHA, TCA₆-OHA, TCA₉-OHA, DOCA₃-OHA, DOCA₆-OHA, and DOCA₉-OHA) was done through a Schiff base reaction (Figs. 2.1b and S1B). In brief, various ratios of oxidized polymeric conjugates were dissolved with DFO at a molar ratio of 1:20 in DI water, and the reaction proceeded at room temperature for 24 h with gentle stirring. This was followed by purification with a dialysis bag (cutoff of 3500 MW) against an excess amount of DI water for 3 days to remove unconjugated DFO and subsequently lyophilized to generate the various DFO-HA-BA conjugates. The fluorescent Cy5.5-polymeric conjugates for cell studies were prepared through an amide coupling reaction similar to the one used for coupling the terminal amine of DFO, where 20 μl of Cy5.5-NH₂ (5 mg/ml) was added to 5 mg/ml to the oxidized polymeric conjugates (5 mg/ml) in DI H₂O in a 25-ml round flask covered with aluminum foil and stirred overnight. Unreacted Cy5.5 was removed through dialysis (10,000 MW) against DI H₂O for 24 h. Confirmation of successful synthesis and conjugation ratio was done by ¹H NMR, FTIR, and UV–Vis spectroscopy (SpectraMax® Plus 384 Microplate Reader (Molecular Devices)).

2.3.3. Preparation of DFO Self-Assembled Nanoparticles

All final polymeric conjugates synthesized were dissolved in DI water at a concentration of 1 mg/ml. The solution was then sonicated three times at 2 min each with the use of a probe-type sonicator (Fisher Scientific Sonic Dismembrator model 500) at 25 W.

2.3.4. Physicochemical Properties

The size and polydispersity of the self-assembled DFO nanoparticles formed were determined using Dynamic Light Scattering (DLS) (Zetasizer Nano ZS instrument; Malvern Instruments, UK), specifically, the z-average diameter (intensity) of the nanoparticles in PBS (2 mg/ml w/v) was measured at a scattering angle of 90°. Additionally, the surface properties and electrical mobility of the DFO nanoparticles were characterized by monitoring the zeta potential. To confirm the morphology and size of the DFO nanoparticles, Transmission Electron Microscopy (JEOL-JEM1011) was employed. The ability of the DFO nanoparticles to chelate ferric iron was investigated by monitoring UV–Vis absorption spectra in the range of 350–650 nm. Iron chelated to DFO at a 1:1 ratio exhibits a specific absorption peak at 430 nm, which can be used to determine the DFO conjugation level to the polymeric conjugates. One milligram per milliliter of DFO nanoparticles was reacted with saturated Fe(III) solution, and their absorbances at 430 nm were measured. The DFO conjugation ratio as %w/w was determined using Eq. 1:

%DFO (w/w) =
$$\frac{\text{weight of DFO}}{\text{weight of polymeric conjugate-DFO}} \times 100$$
-----Eq.1

2.3.5. Cytotoxicity Study in Mammalian Cells: Caco-2, J774A.1, and HEPG2

When properly cultivated over several weeks, Caco-2 cells can undergo spontaneous differentiation into a monolayer of polarized cells with features similar to those on small intestinal enterocytes, making these cells particularly attractive for in vitro modeling of drug absorption and permeability (41). Caco-2 cells were cultivated following a previously reported procedure [72].

The cells were seeded at passage 13 using 500 ml DMEM (without pyruvate) supplemented with 5 ml of PEST (penicillin 10,000 U/ml + streptomycin 10,000 μg/ml solution, 100 ×), 5 ml of 100 × nonessential amino acids, and 50 ml FBS as constituents of the culture media. They were seeded at a density of 2.5 × 105 cells /cm2 and cultured at 37°C, 5% CO2 in a humidified incubator for 21–29 days. During this period, Caco-2 cell differentiation into a monolayer was monitored by TEER (transepithelial electrical resistance) measurements. For the cytotoxicity assay, differentiated Caco-2 cells were passage into 96-well plates and incubated for 6 days before adding the polymer conjugates. It was also important to assess mammalian cell viability in model cells such as J774A.1 macrophage cells and liver HepG2 because oral absorption of the conjugates could lead to the conjugates getting into the systemic circulation and potentially localizing to the liver, where hepatocytes and Kupffer cells in humans store excess iron [49]. In the case of the J774A.1 cells and HepG2, they were cultivated following a previously reported procedure [49]. Briefly, cells were seeded in 96-well plates at a density of 10,000 cells/well and incubated at 37°C, 5% CO2 in a humidified atmosphere in DMEM complete medium. An MTT resazurin metabolism-based assay was performed with the following nanoparticles: free DFO, HA-DFO, TCA9-HA-DFO, and DOCA9-HA-DFO. More specifically, final concentrations tested in all 3 cell lines ranged from 1200 to 2.34 µM equivalent DFO. After 24 h incubation at 37°C, cells were washed with PBS, and 100 µl of resazurin (44 µM) was added to each well and incubated for 4 h. Fluorescence measurements were taken using a SpectraMax Gemini EM microplate reader (excitement at 560 nm, emission at 590 nm). Wells without cells served as the blank, and cells without treatment represented 100% cell viability. The viability of cells was determined based on fluorescence readings using Eq. 2:0

Caco-2 cell viability (% decrease) =
$$\frac{F(Sample) - F(Blank)}{F(Control) - F(Blank)} \times 100$$
-----Eq.2

2.3.6. In Vitro Iron Chelation Efficacy Studies

J774A.1 macrophage cells or liver HepG2 were plated in six-well plates at a density of 30,000 cells per well and incubated for 24 h at 37°C, 5% CO2 in a humidified incubator in DMEM complete medium. After the initial incubation, the cells were treated with 100 μM ferric ammonium citrate (FAC) solution in complete media for 24 h to induce iron overload in the cells. Subsequently, the cells were washed with PBS and exposed to DFO, HA-DFO, TCA9-HA-DFO, and DOCA9-HA-DFO nanoparticles at equivalent concentrations of 10 μM and 50 μM DFO for 48 h. Two control groups were included: group A cells were not iron-overloaded with FAC (normal cells), whereas group B cells were iron-overloaded with FAC but left untreated. After 48 h of incubation with nanoparticles, the cells were lysed using cell lysis buffer (150 mM NaCl, 10 mM Tris, 1% Triton X-100, and protease inhibitor cocktail, pH 7.4). Cellular ferritin concentration was measured using mouse and human ferritin ELISA kits, and the total protein concentration was measured using the BCA protein assay kit. The results were presented as the ratio of nanogram of ferritin per microgram of total protein concentration.

2.3.7. Cellular Uptake Studies in Caco-2 Cells

The cultivation of Caco-2 cells was carried out following the procedures outlined in the "Cytotoxicity Study in Mammalian Cells: Caco-2, J774A.1, and HEPG2" section. To assess the cellular uptake of the nanoparticles, a confocal laser scanning microscope (Zeiss LSM-800)

microscope, Jena, Germany) was utilized. Caco-2 cells were seeded in an 8-well chamber slide (Lab-Tek) and then incubated for 21 days at 37°C in a 5% CO₂ environment. After the incubation period, the cells were washed three times with DPBS (Dulbecco's Phosphate Buffered Saline) and then exposed to 200 μ g/ml of Cy5.5, and Cy5.5 labeled with HA, DOCA₉-HA, and TCA₉-HA in each 500 μ l well and incubated for 3 h. Subsequently, the solutions were removed, and the cells were washed again with DPBS. The cells were then fixed using a 4% formaldehyde solution and labeled with the cell membrane dye (FMTM 1–43 FX). Using the confocal laser scanning microscope and LD LCI PApo 40×1.2 ImmCorrDIC objective, a minimum of six regions of interest were collected from each condition while retaining identical pinhole settings, laser intensities, and thresholding within each repeat. Using a confocal image depth of 0.27 μ m, the relative fluorescence intensity for Cy5.5 was measured in each ROI using the Zen Blue 3.0 software. Values from three independent repeats were collected and compared to assess the cellular uptake of the experimental nanoparticles.

2.3.8. In Vitro Permeation Studies

To investigate whether cellular uptake correlates with improved drug permeability across Caco-2 cells, we measured DFO concentration differences in the apical vs. basolateral layers. To assess the absorption of DFO nanoparticles across Caco-2 cells as a model for intestinal epithelial cells, cell permeability studies were conducted. The cells were seeded at a density of 1×10^5 cells per well onto 12-well transmembrane plates with filters having a pore size of 400 μ m to create a dual-layer culture system with apical and basolateral compartments. Over 21 days, the medium in both the apical and basolateral layers was replaced every 2 days to allow the formation of cell monolayers. After the cell monolayers were established, the medium was removed, and the cells

were washed with HBSS. Subsequently, 500 μl of 400 μM DFO or DFO equivalent in HA-DFO, TCA₉-HA-DFO, and DOCA₉-HA-DFO nanoparticles in HBSS solution were added to the apical layer of the transmembrane plates. At various time points (0, 0.5, 1, 2, 4, 8, and 24 h), 50 μl samples were collected from the basolateral chamber and mixed with saturated Fe (III) solution. The mixed solution was then characterized by its absorbance at a wavelength of 430 nm. Also, the TEER values of the Caco-2 cell monolayers were measured using EVOM2 (WPI, 240 V 50 Hz with STX2 electrode). The samples were incubated with the Caco-2 cells in the transwell setup, and the TEER values were measured at time points (0, 0.5, 1, 2, and 4 h). After 4 h, the samples were discarded and the cells were incubated with DMEM without pyruvate followed by TEER values measurement (8, 12, and 24 h). The percentage change in the TEER value was calculated using Eq. 3.

TEER (% decrease) =
$$\frac{T (Final) - T (Blank)}{T (Initial) - T (Blank)} \times 100$$
-----Eq. 3

2.3.9. Statistical Analysis

Statistical analysis was performed with GraphPad Prism 5.0 software. Statistical significance between groups was assessed with one-way ANOVA; *p* less than 0.05 was considered statistically significant.

2.4. Results

2.4.1. Synthesis of TCA-HA-DFO and DOCA-HA-DFO Polymeric Conjugates

The study employed two BA (TCA and DOCA), which were linked to HA through EDC and NHS reactions. The conjugation of TCA and DOCA to HA involved linking the amino groups of TCA and DOCA to the carboxyl group of HA via carbodiimide-catalyzed amidation (Figures S2.2A and S2.2B). The configuration of TCA-HA and DOCA-HA polymeric compounds was analyzed using 1H NMR in D2O and CD3OD (1:1 v/v) (Figures S2.3A and S2.3B). The characteristic signals of HA were identifiable within the 2.0 ppm and 3.3-4.9 ppm range [73, 74], while the successful incorporation of TCA and DOCA was verified by distinct signals at 0.6–1.8 ppm [75, 76]. The amount of HA and TCA/DOCA was quantitatively characterized from the integration ratio between the characteristic peaks of the N-acetyl group in HA ($\delta = 2.01$ ppm [3H, -COCH3-]) and the methyl group in TCA/DOCA ($\delta = 0.6$ ppm [3H, -CH3]). To subsequently conjugate DFO to TCA-HA or DOCA-HA, there was a need to oxidize the HA backbone. Using NaIO4, aldehyde functional groups were introduced by cleaving the C2-C3 hydroxyl groups of vicinal diols. The presence of the dialdehyde groups was confirmed by the identification of new peaks at 1700 cm-1 and 1650 cm-1 for TCA and DOCA, respectively, corresponding to the strong C = O stretching vibration of the aldehyde group (Figure S4A and S4B) [77]. For the conjugation of DFO to the TCA-OHA and DOCA-OHA polymeric conjugates, the amino group of DFO was reacted with the dialdehyde group on HA by a Schiff base reaction. The chemical structure of TCA-HA-DFO and DOCA-HA-DFO polymeric conjugates was analyzed using 1H NMR in D2O and CD3OD (1:1 v/v). The characteristic signals of HA, TCA, and DOCA were identifiable while the successful conjugation of DFO to the polymeric conjugates was identified by the presence of DFO 1H NMR peaks: 2.90–3.07(m, -CH2-NHCO- of DFO), 2.39–2.81 (m, -CH2-CO- of DFO), and 1.18–1.79 (m, –CH2- of DFO) (**Fig. 2.3a, b**) [43].

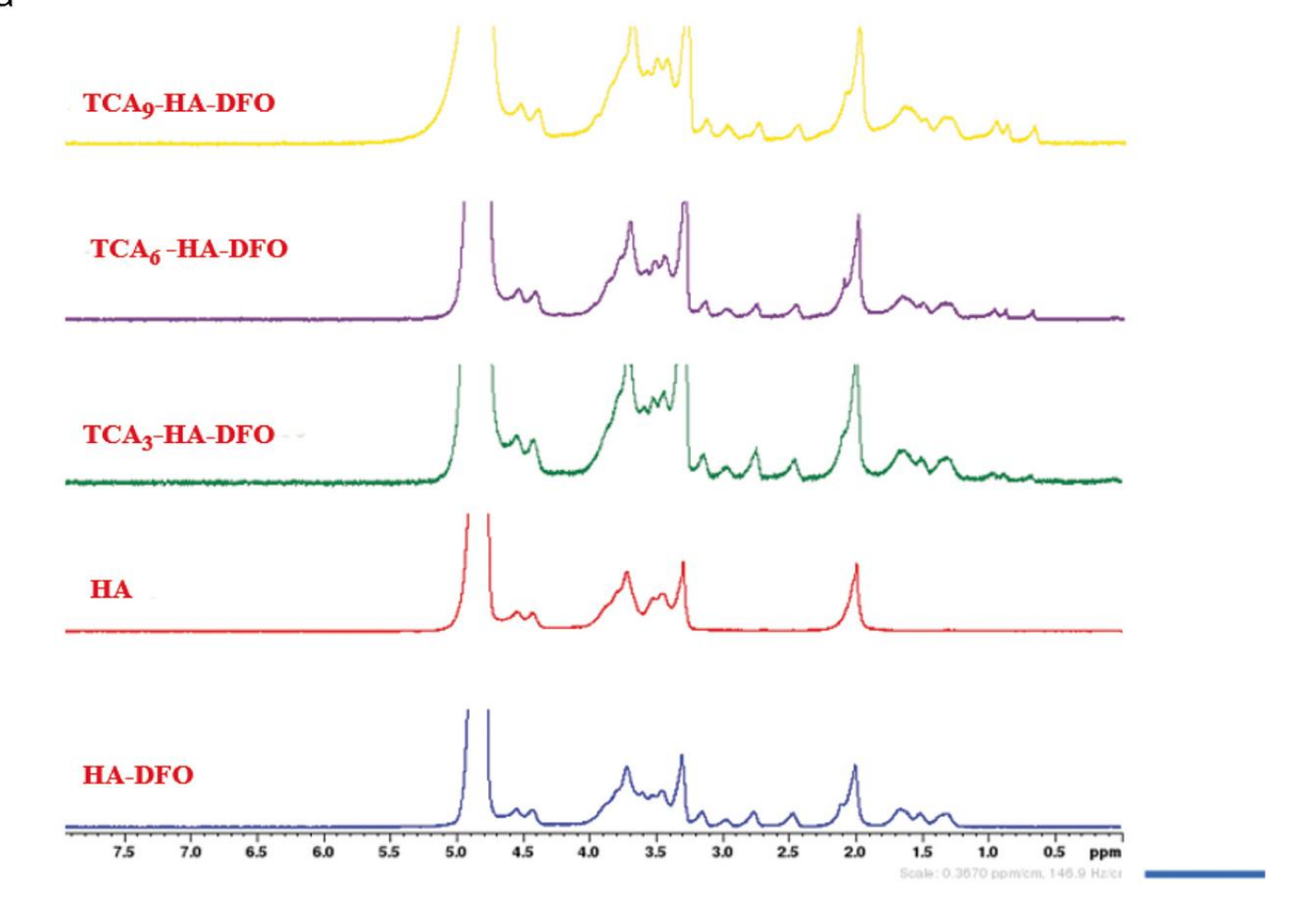
2.4.2. Physicochemical Characterizations

The seven DFO polymeric conjugates spontaneously formed nano-sized particles in DI water by probe-type sonication. The average sizes and polydispersity (PDI) of the DFO nanoparticles were in the range of 391.1–71.28 nm and 0.51–0.135, depending on the DS values. The TEM images showed spherical nanostructures for all the DFO conjugates. The physicochemical characterization data of all the DFO seven polymeric conjugates are summarized in Table 1. The DLS and TEM data of DOCA₉-HA-DFO, TCA₉-HA-DFO, and HA-DFO are shown in **Fig. 2 .4a–c**. Based on the physicochemical characterization of the seven polymeric conjugates, DOCA₉-HA-DFO, TCA₉-HA-DFO, and HA-DFO polymeric conjugates were chosen as the representative candidates for further studies because they had the highest DFO conjugation level and were able to form self-assembled nanoparticles with smaller particle sizes and PDI. Next, DFO conjugation to the polymeric conjugates was confirmed through UV–Vis by the addition of an excess concentration of Fe(III) solution to the DFO polymeric conjugates and noting the chelation peak at 430 nm (**Fig. 2 .4d**).

Fig 2.2. Synthesis of TCA-HA-DFO polymeric conjugates. **a** Functionalization at various ratios of TCA to HA. TCA-HA conjugation chemistry was accomplished by coupling the carboxyl group of HA with TCA-NH₂ in the presence of EDC and NHS. **b** Oxidization of TCA-HA with NaIO₄ to introduce aldehyde groups onto HA followed by conjugation of DFO to TCA-OHA via Schiff base reaction.

2.4.3. Cytotoxicity Study

The cell viability study done on Caco-2 cells showed no cytotoxicity based on mitochondrial metabolism when up to 500 μM free DFO or equivalent HA-DFO, DOCA₉-HA-DFO, and TCA₉-HA-DFO were added to the cells. However, for HepG2 and J774A.1 cells, free DFO significantly reduced cell viability but was significantly improved with polymeric conjugates consisting of HA and BA (TCA /DOCA) conjugated to DFO at equivalent free DFO concentrations. For example, IC₅₀ for DFO was ca. 19 μM but increased to ca. 80 μM for HA-DFO, ca. 233 μM for DOCA₉-HA-DFO, and ca. 522 μM for TCA₉-HA-DFO in J774A.1 cell. Also, IC₅₀ for free DFO was ca. 30 μM but increased to ca. 120 μM for HA-DFO, ca. 211 μM for DOCA₉-HA-DFO, and ca. 910 μM for TCA₉-HA-DFO in HEPG2 cells (**Fig. 2.5 a–c**).



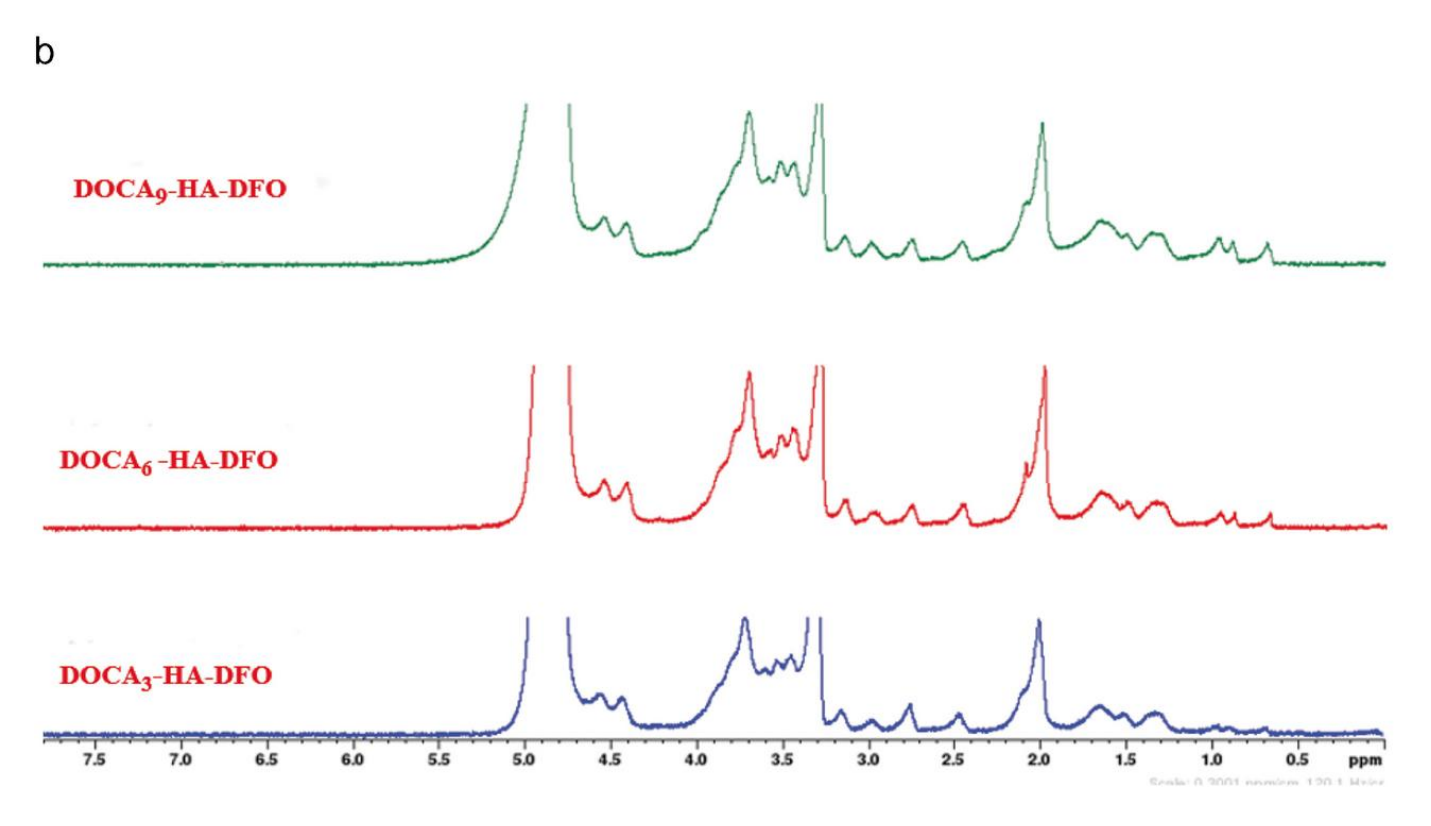
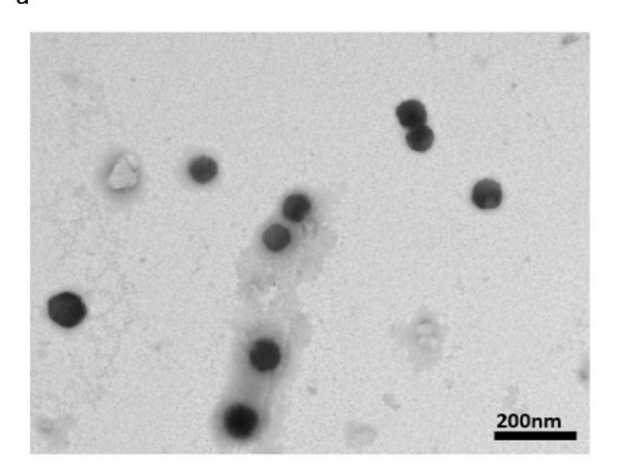
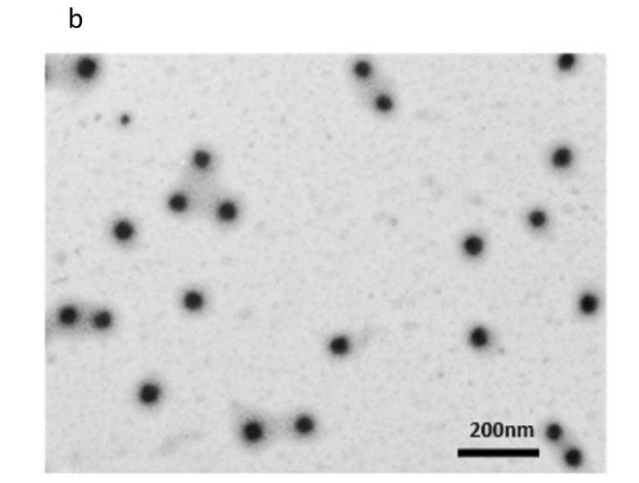


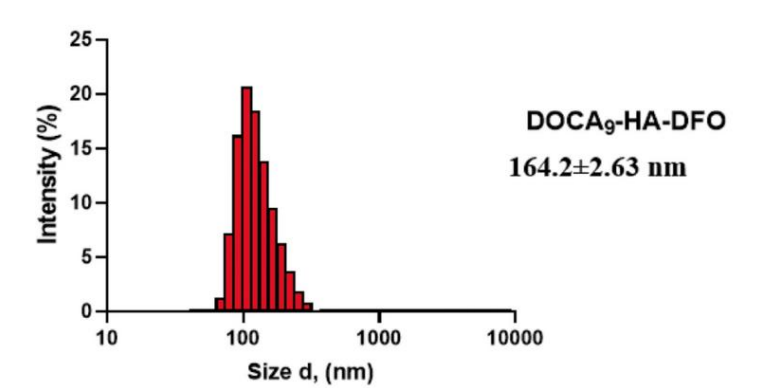
Fig 2.3. Chemical structures were confirmed using ¹H NMR in D₂O and CD₃OD (1:1 v/v). **a** TCA ¹H NMR peaks were between 0.6 and 1.8 ppm and **b** DOCA ¹H NMR peaks were between 0.6 and 1.8 ppm. For both TCA/DOCA, HA ¹H NMR peaks were at 2.0 ppm and 3.3–4.9 ppm. The amount of TCA/DOCA to HA was quantitatively characterized by the integration ratio between the characteristic peaks of the HA and TCA/DOCA

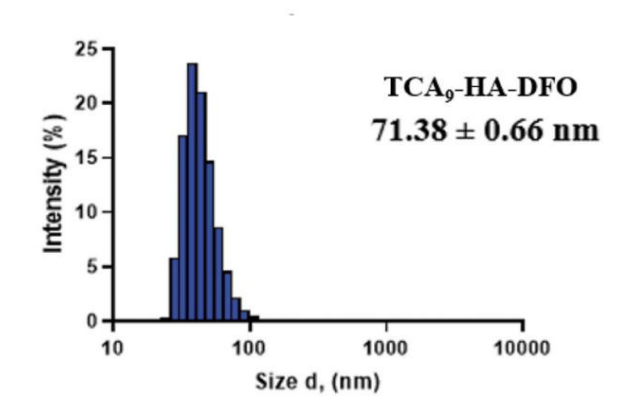
2.4.4. In Vitro Iron Chelation Efficacy Studies

As shown in Fig. 2.6a, 100 μM FAC treatment increased cellular ferritin from baseline levels of 6.44 ng/μg total protein (blue bar) to 10.29 ng/μg (red bar) in the J774A.1 macrophage cell. Free DFO (3.34 ng/μg total protein, green bar) and TCA₉-HA-DFO (2.67 ng/μg total protein, wine bar) showed comparable treatment effects based on similar declines in ferritin concentrations at 50 μM and 10 μM equivalent DFO concentrations whereas HA-DFO and DOCA₉-HA-DFO had a smaller decrease in ferritin concentration at equivalent DFO concentrations. Also, as shown in Fig. 2.6 b, 100 μM FAC treatment increased cellular ferritin from baseline levels of 3.96 ng/μg total protein (blue bar) to 12.31 ng/μg (red bar) in the HepG2 liver cells. Free DFO (4.01 ng/μg total protein, green bar), DOCA₉-HA-DFO (4.31 ng/μg total protein, brown bar), and TCA₉-HA-DFO (3.93 ng/μg total protein, wine bar) showed comparable treatment effects based on similar declines in ferritin concentrations at 50 μM and 10 μM equivalent DFO concentrations, whereas HA-DFO had a smaller decrease in ferritin concentration at equivalent DFO concentrations.

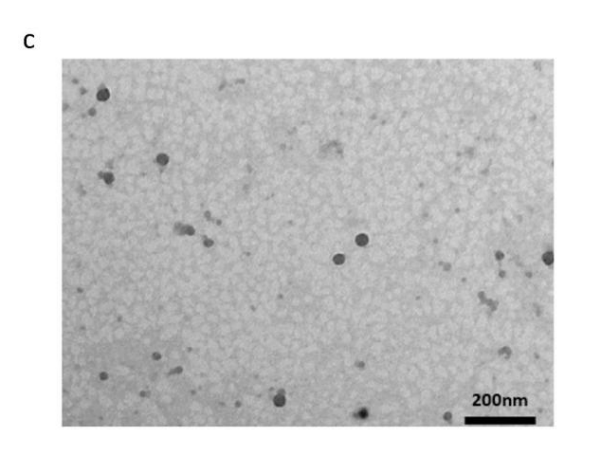


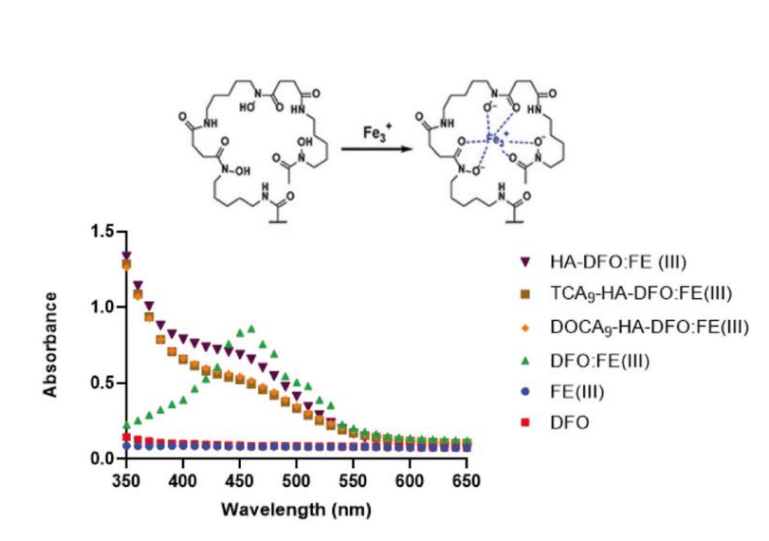






d





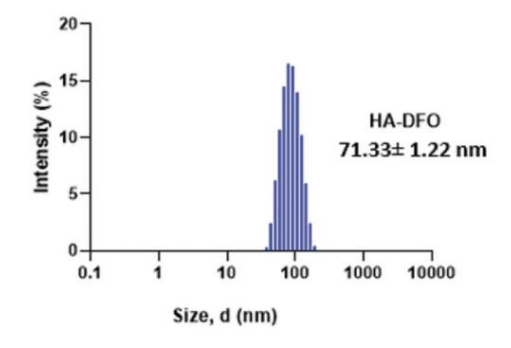


Fig 2.4. TEM and DLS particle size of a DOCA₉-HA-DFO, **b** TCA₉-HA-DFO, and **c** HA-DFO. **d** Successful conjugation of DFO to the various polymer conjugates was confirmed by UV-Vis in the presence of excess Fe(III) by the presence of a strong absorbance peak at 430 nm, which is characteristic of DFO:Fe(III) complexation

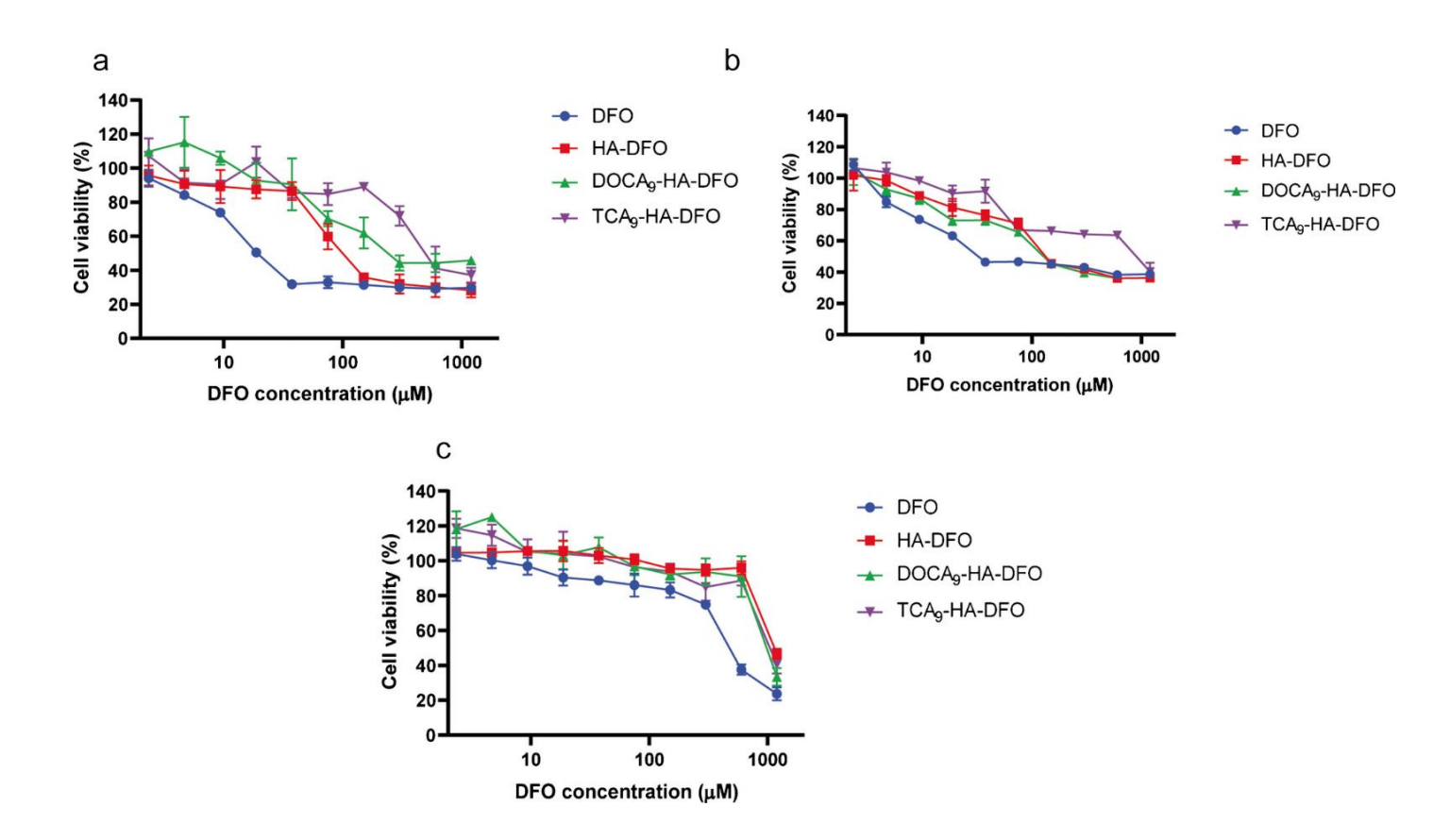


Fig 2.5. Cytotoxicity of free DFO (blue line), HA-DFO (red line), DOCA₉-HA-DFO (green line), and TCA₉-HA-DFO (purple line) after 24 h incubation on **a** J774A.1 cells, **b** HepG2 cells, and **C** Caco-2 cells, where each data point is presented as the mean \pm SD (n = 3)

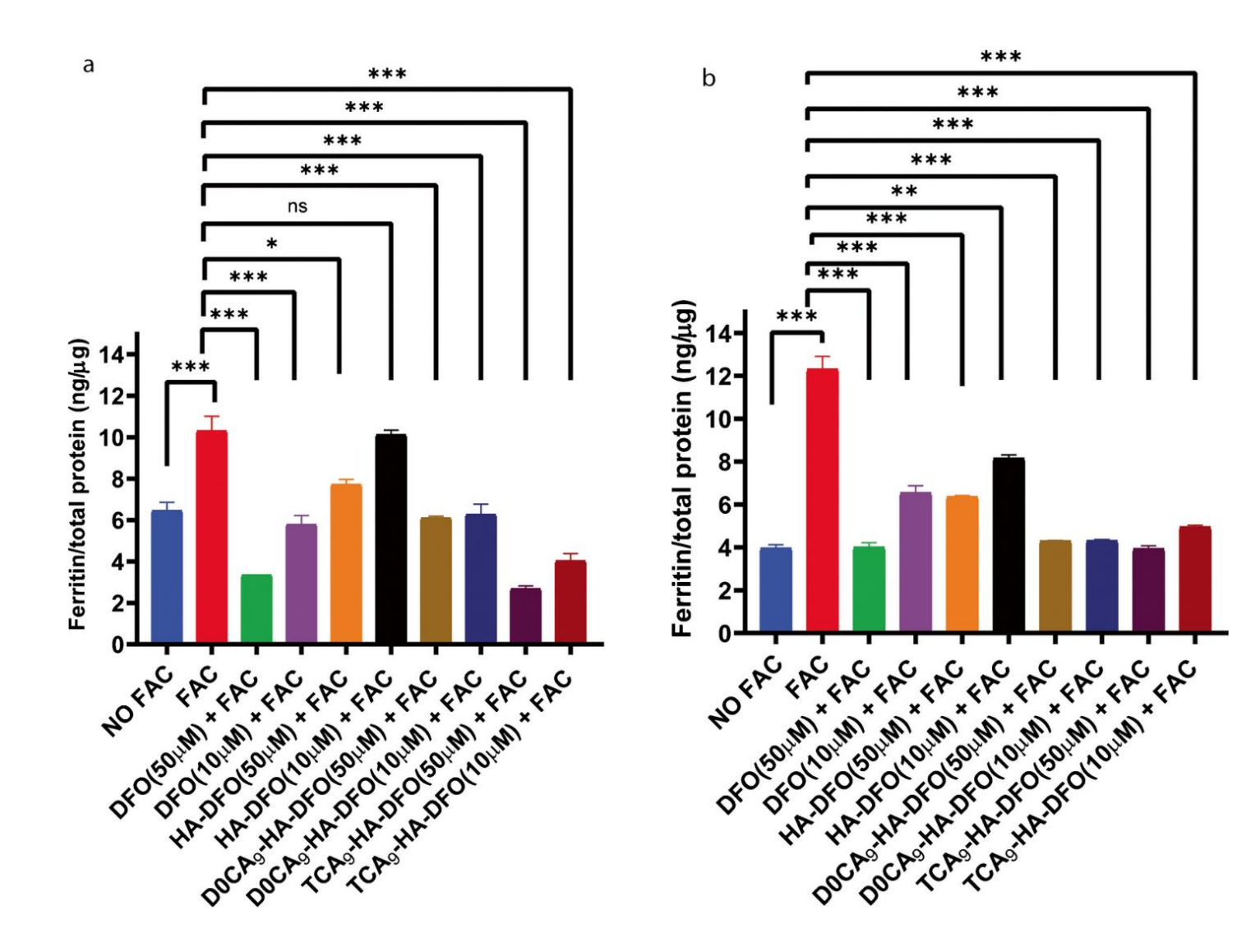


Fig 2.6 Ferritin reduction assay to monitor iron chelation efficacy of DFO, HA-DFO, DOCA₉-HA-DFO, and TCA₉-HA-DFO on **a** J774A.1 macrophage and **b** HepG2 iron-overloaded cells. The cells were treated with DFO or HA-DFO or DOCA₉-HA-DFO or TCA₉-HA-DFO at 10 μM or 50 μM for 48 h. The cellular ferritin level was measured by a mouse ferritin ELISA assay. Results

are normalized to total protein (ng/µg) and presented as mean \pm SD (n = 3). "ns" means the difference was not significant. *p < 0.05, **p < 0.01, and ***p < 0.001

2.4.5. Cellular Uptake Studies in Caco-2 Cells

The ability of the nanoparticles to permeate the *in vitro* Caco-2 cell monolayer through the transcellular route was investigated with confocal laser scanning microscopy (CLSM). The dye Cy5.5 was used as the control, while the test samples included Cy5.5 conjugated to the polymeric conjugates. It was key to understand if HA itself could be internalized into Caco-2 cells or whether either of the BA (DOCA/TCA) could play a role in enhancing the internalization process. Results showed that HA had an intracellular fluorescent intensity of 7.81×10^6 . It was also observed that DOCA and TCA improved the cellular uptake with fluorescent intensities of 1.87×10^7 for DOCA₉-HA-Cy5.5 and 2.18×10^7 for TCA₉-HA-Cy5.5, respectively (**Fig. 2.7a, b**).

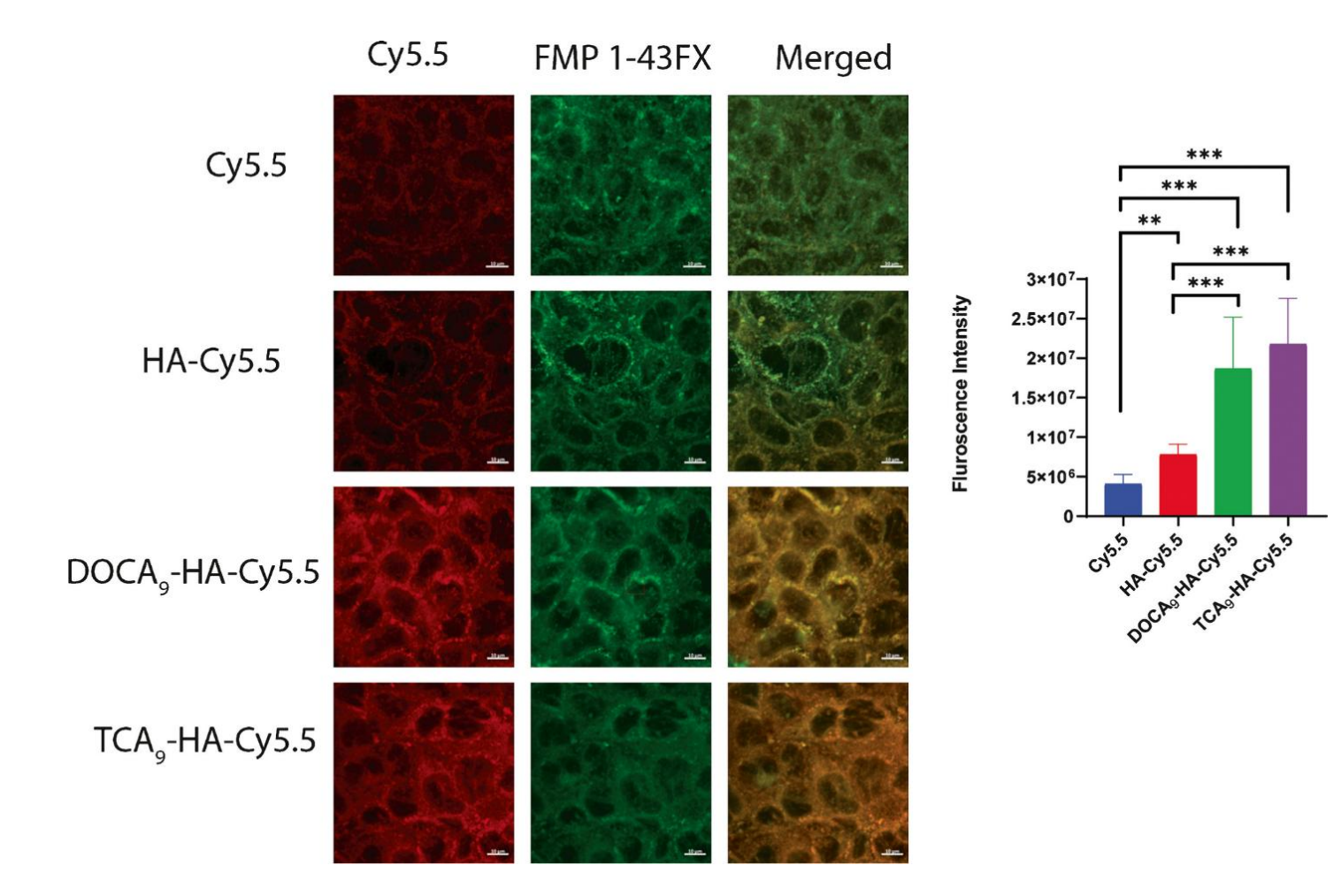


Fig 2.7. Confocal imaging revealing cellular uptake of the polymeric conjugates. a Cellular uptake study at 3 h performed in Caco-2 cells treated with polymeric conjugates (HA, DOCA₉-HA, and TCA₉-HA) labeled with Cy5.5. The control was free Cy5.5. b Quantitative cell polymeric conjugates localization by confocal fluorescence microscopy to show fluorescence intensity. Results are presented as mean \pm SD (n = 3). "ns" means the difference was not significant. *p < 0.05, **p < 0.01, and ***p < 0.001. All images were captured using CLSM (scale of 10 μM)

2.4.6. In Vitro Permeation Studies

To further quantify the permeability of the DFO nanoparticles across this Caco-2 model of the GI tract, we monitored the degree to which DFO successfully crossed the monolayer from the apical to basolateral chambers (Fig. 2.8a) [78]. The results obtained from the absorbance readings of the DFO to Fe(III) complex indicated that the DFO nanoparticles were able to permeate the Caco-2 monolayer increasingly over time, with TCA9-HA-DFO and DOCA9-HA-DFO having the highest significant DFO permeation when compared with the free drug at equivalent DFO concentrations (Fig. 2.8b). Also, beyond the drug permeation study, TEER values were measured to monitor the integrity of all the monolayers treated with free DFO or DFO nanoparticles (Fig. 2.8c). Per previous reports and using similar insert sizes, Caco-2 cells that have differentiated properly should have tight junctions with TEER values above 200 Ω cm² [25]. To assess the potential for TEER recovery, the monolayers underwent a rinsing process and were allowed to regenerate in fresh medium following a 4-h incubation period with the samples. During this phase, the cell monolayers exhibited a temporary and reversible rise in TEER. It was observed that nearly full restoration of these effects occurred within 24 h, suggesting that alterations in TEER did not result in permanent tight junction damage.

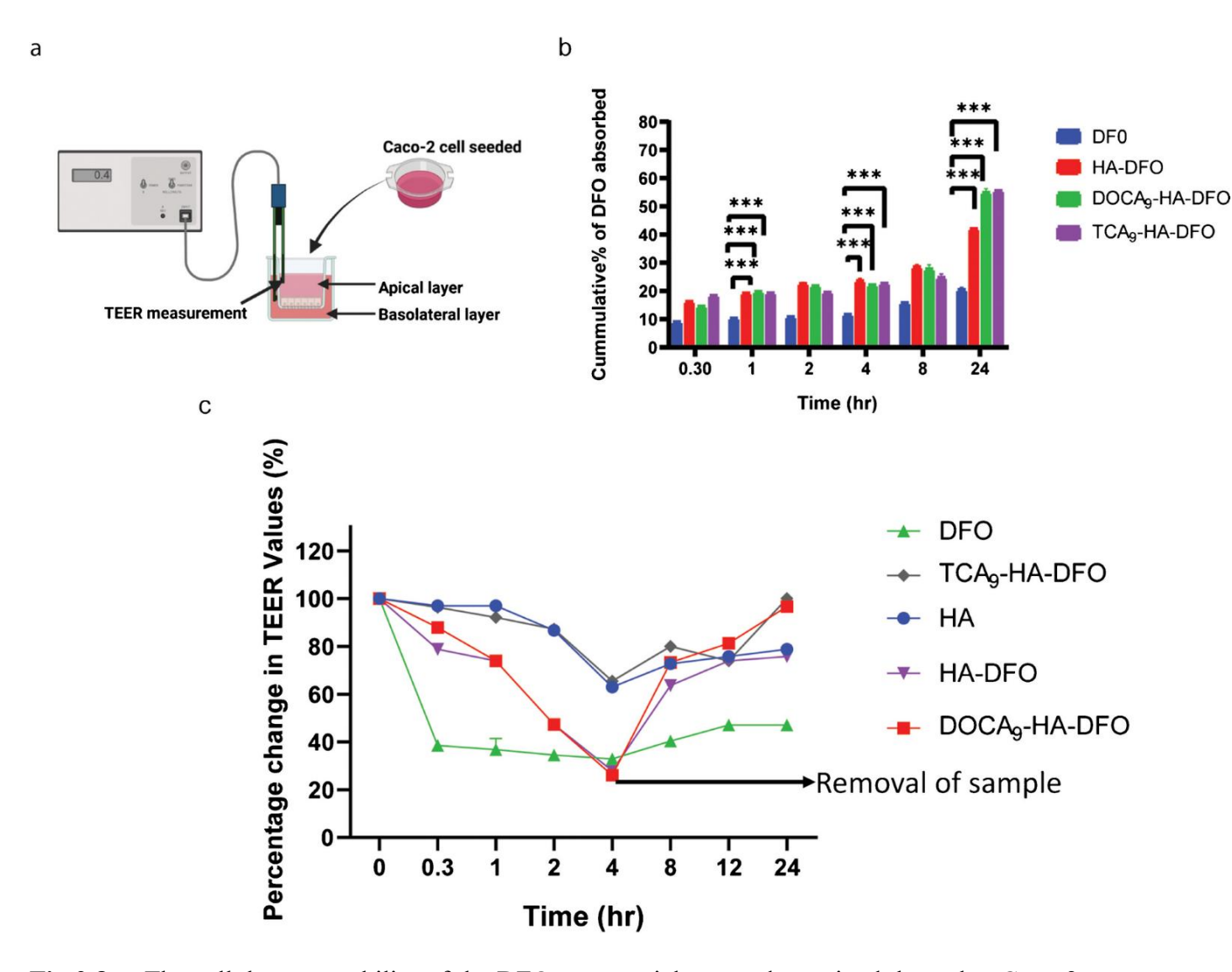


Fig 2.8. a The cellular permeability of the DFO nanoparticles was determined through a Caco-2 monolayer permeability assay. The transwell assay shows the various parts of the setup. b Caco-2 cells were treated with either 400 μM of equivalent DFO or HA-DFO or DOCA₉-HA or TCA₉-HA nanoparticles and incubated for 24 h. At each time point, 50 μl from the basolateral layers of each setup was added with Fe(III) and tested for absorbance at 430 nm. c TEER value measurements after incubation with DFO nanoparticles and removal of the DFO nanoparticles after 24 h.

2.5. Discussion

The HA backbone was successfully functionalized with two different types of BA (DOCA/TCA) as shown in the results (Figure 2.3 A and S2.3B). With an increasing feed molar ratio from 10:1 to 30:1, the DS of DOCA and TCA in HA progressively rose from 3 to 9. The HA backbone was oxidized before DFO conjugation, and it involved oxidation of the vicinal hydroxyl groups of the sugar ring with the use of NaIO₄ [79]. The various percentages of DFO (9.7 to 42%) were conjugated to the HA backbone (Table 1). The particle sizes and PDI decreased as the DS increased, which reflects the formation of nanoparticles with more compact hydrophobic inner cores. The body cells primarily store iron in the intracellular protein known as ferritin in storage cells, and ferritin concentration is therefore highly indicative of the indirect level of iron being stored in the body [49]. The ferritin ELISA assay was used to evaluate the ability of the DFO nanoparticles to reduce ferritin concentration. To model iron overloading of these cells, J774A.1 macrophage cells and HepG2 liver cells were pretreated with 100 µM FAC for 24 h and then treated with various iron chelation formulations. Data revealed that TCA₉-HA-DFO nanoparticles were the most effective at chelating excess iron stored in cells at levels similar to free DFO (Fig. 2 .6a, b) and that they had the advantage of being less cytotoxic to the cells at concentrations tested (Fig. 2.5a-c). This suggests that DFO's toxicity may be reduced best by conjugating the drug's reactive primary amino group to a polymer backbone as previously reported [44]. Free DFO and conjugates were less toxic to Caco-2 cells in comparison to J774A.1 mouse macrophage cells and HepG2 human liver cells with an IC₅₀ of 500 μM for free DFO and 1020 μM for TCA₉-HA-DFO, respectively, in Caco-2 cells in comparison to similar studies conducted in J774A.1 mouse

macrophage cells (IC₅₀ of 19 μM for free DFO) and HepG2 human liver cells (IC₅₀ of 30 μM for free DFO). Reducing the cytotoxicity of DFO by delivering it through polymeric conjugates is important since high doses of free DFO (> 2.5 g per infusion) have been reported to impair renal and liver function in elderly patients or patients with underlying renal or hepatic issues [53, 80, 81].

Previous research has documented that the incorporation of HA into a nano formulation can enhance its binding affinity to the GIT wall [23]. To evaluate whether the absorption could be further enhanced, we investigated whether the addition of BA, such as DOCA/TCA, onto HA could further enhance the uptake by Caco-2 cells. Since BA receptors such as apical sodiumdependent bile acid transporter (ASBT) are abundantly expressed on the surface of Caco-2 cells [82], this may explain the significant internalization of DOCA₉-HA-Cy5.5 and TCA₉-HA-Cy5.5 across the Caco-2 cell monolayer by a factor of 2-2.5 over HA alone (Fig. 2 .7a-c). It should be noted that the apical membrane of enterocytes in the ileum also naturally expresses the ASBT, which has garnered considerable attention as a focal point for drug absorption through the use of BA [83]. In our experiments, after the removal of the test samples, the TEER values returned to normal, which might indicate that the DFO nanoparticle absorption may be due to a transcellular mechanism involving binding of HA to the cell membrane and absorption by ASBT-mediated endocytosis through binding of the BA [84]. Although the focus of this study was not to investigate the mechanism of action of absorption, our studies are very encouraging and point to the possibility of enhancing DFO absorption through the use of HA and BA. One additional advantage of DFO nano formulations over free DFO administration is that they have consistently been reported to be much less cytotoxic to cells at equivalent concentrations [44, 49]. In our studies, we observed that DFO drug absorption was seen to increase as the number of BA molecules conjugated to HA increased, with TCA-HA-DFO performing better than DOCA-HA-DFO (**Fig. 2.8 a–c**) [85, 86]. This could be due to the more hydrophilic nature of TCA which may allow for this BA to more readily extend out towards the aqueous environment compared to the more lipophilic DOCA which may remain more shielded within the nanoparticle and thus less accessible for binding to BA receptors [87].

2.6. Supplementary Information: BILE ACID-TARGETED HYALURONIC ACID FOR ENHANCED ORAL ABSORPTION OF DEFEROXAMINE

S2.1. Materials and Instruments

Deferoxamine mesylate (DFO) was procured from Hospira, Inc. (Lake Forest, IL). Sodium HA (Mw = 15 KDa) was purchased from Life-core Biomedical LLC. (Chaska, MN). Deoxycholic acid (DOCA), Taurocholic acid (TCA), N-hydroxysuccinimide (NHS), 1 N-ethyl-N'-(3- dimethyl aminopropyl)-carbodiimide hydrochloride (EDC), sodium periodate (NaIO4), N, N-dimethylformamide (DMF), and were formamide were purchased from Sigma Aldrich (St. Louis, MO). Ferric ammonium citrate (FAC) and triethylamine (TEA) were purchased from VWR (Radnor, PA). Dulbecco's modified eagle medium (DMEM) without pyruvate, Dulbecco's modified eagle medium (DMEM), penicillin/streptomycin solution (100×), nonessential amino acids (100×), heat-inactivated fetal bovine serum (FBS), DMSO (99.5% purity), Cypate 5.5 (Cy5.5), N-(3-triethylammonium propyl)-4-(4-(dibutyl amino)styryl) pyridinium dibromide (FMTM 1-43 FX), Hank's Balanced Salt solution (HBSS), Dulbecco's Phosphate-Buffered Saline without CaCl₂ and MgCl₂, Resazurin, and Pierce BCA protein assay kit were purchased from

Thermo Fisher Scientific Inc. The human epithelial colorectal adenocarcinoma (Caco-2) cell line was purchased from the American Type Culture Collection (ATCC). Trypsin and Corning 12-well transwell plates were purchased from Fisher Scientific. The hepatoma cell line HepG2 mouse macrophage cell line J774A.1 were purchased from American Type Culture Collection (ATCC). The Human and Mouse ELISA kit was purchased from Immunology Consultants Laboratory, INC (Portland, OR). Ltd. The remaining reagents were procured from commercial sources and used without any additional purification.

Figure S2.1. A.

Figure S2.1. B.

Figure S2.1. Synthesis of DOCA-HA-DFO polymeric conjugates. (A) Functionalization of various ratios of DOCA with HA. DOCA-HA conjugate was synthesized by coupling the carboxyl group of HA with DOCA-NH₂ in the presence of EDC and NHS (B) Oxidization of the DOCA-

HA polymeric conjugates with sodium periodate (NaIO₄) to create aldehyde groups on HA and conjugation of DFO to DOCA-OHA by a Schiff base reaction.

Figure S2.2A

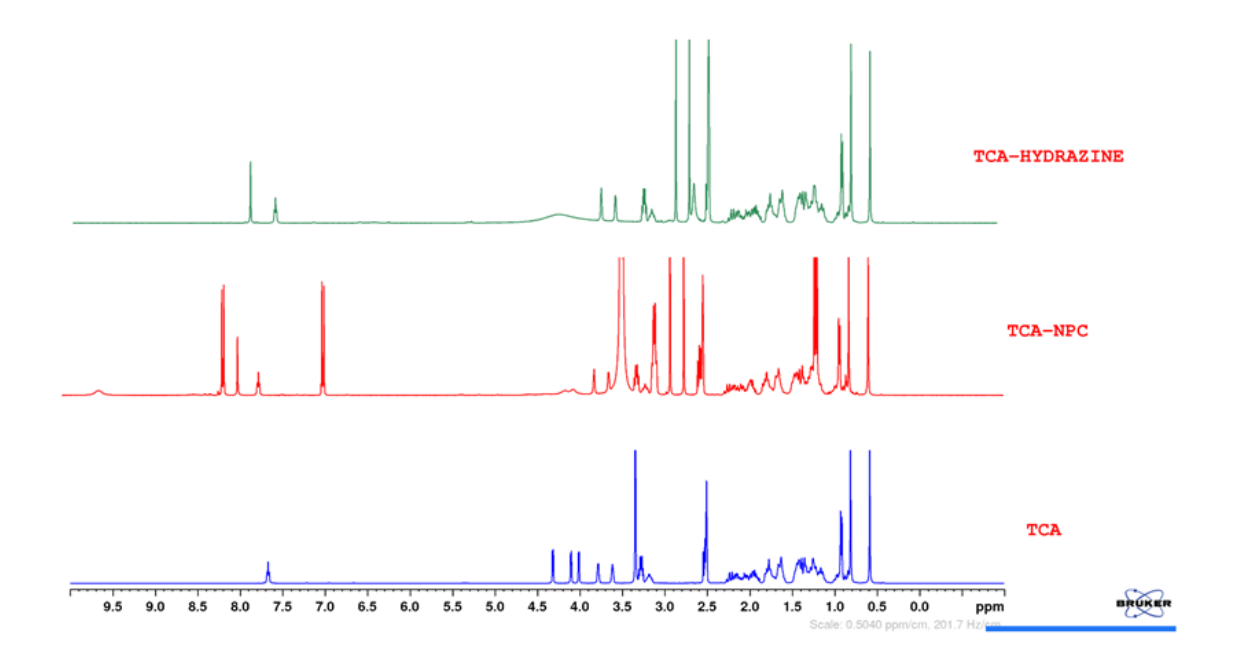


Figure S2.2. B

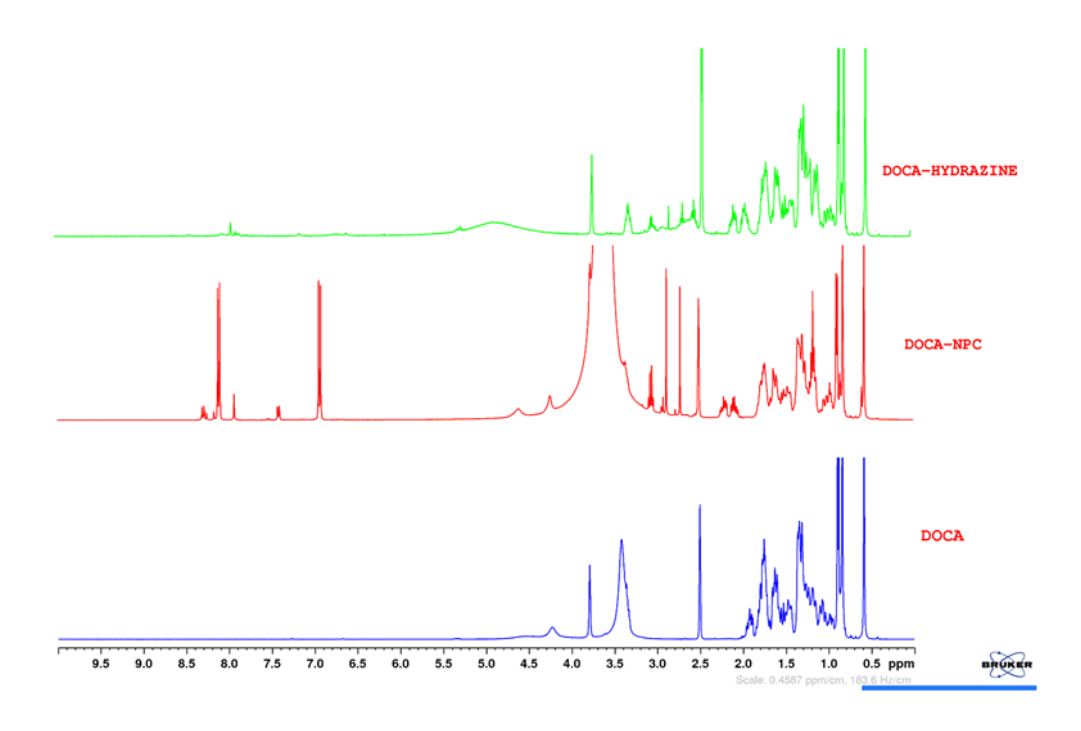


Figure S2.2 (A). ¹H NMR spectra of TCA, TCA-NPC, and TCA- NH₂ showing the introduction of amino group on TCA backbone (B) ¹H NMR spectra of DOCA, DOCA-NPC, and DOCA-NH₂ showing the introduction of amino group on DOCA backbone.

Figure S2.3A.

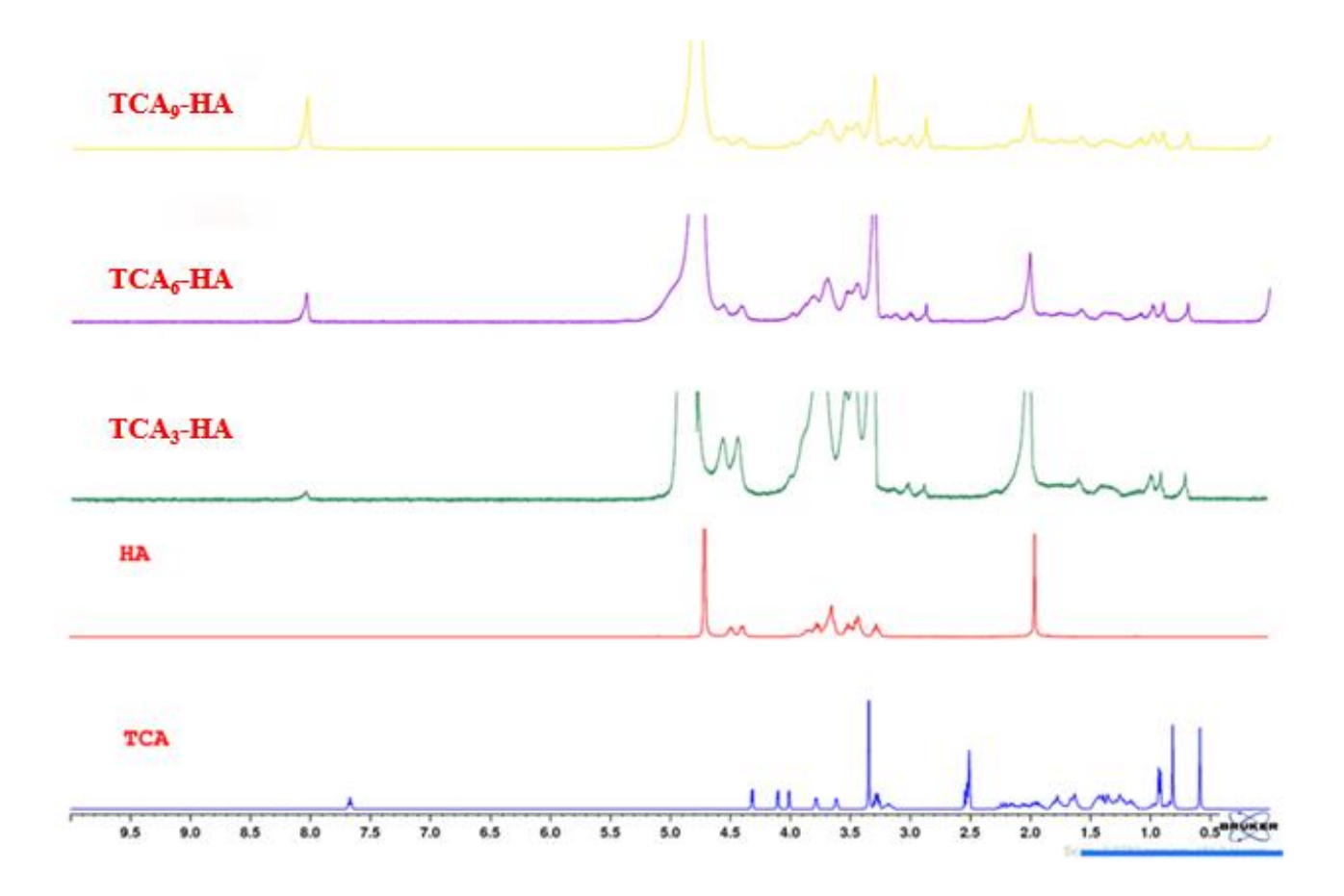


Figure S2.3B.

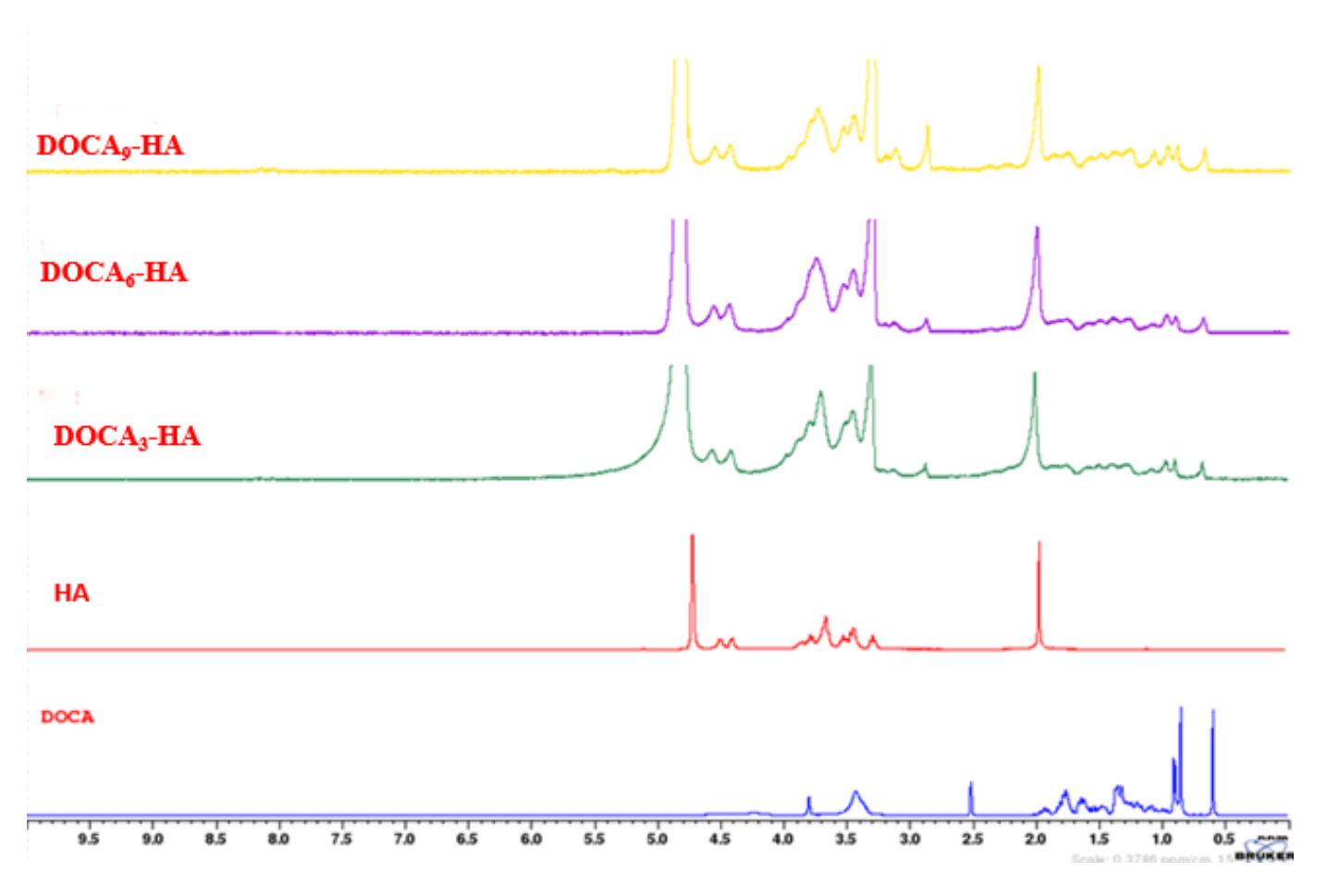


Figure S2.3 (A). ¹H NMR spectra of TCA, HA, TCA₃-HA, TCA₆-HA, TCA₉-HA showing the successful conjugation of TCA-HA (B) ¹H NMR spectra of DOCA, HA, DOCA₃-HA, DOCA₆-HA, DOCA₉-HA showing the successful conjugation of DOCA-HA.

Figure S2.4A.

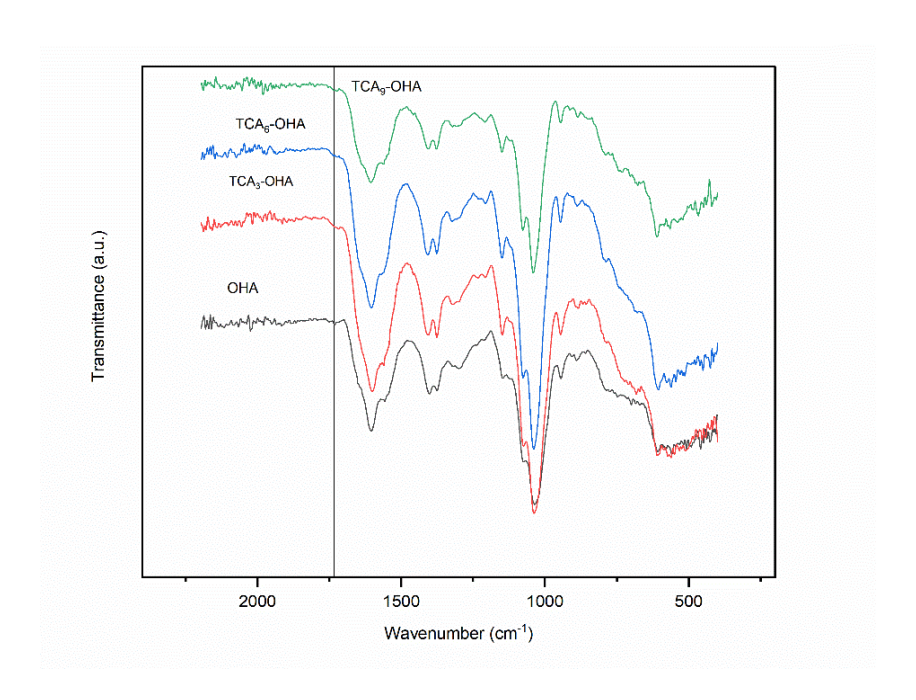


Figure S2.4B.

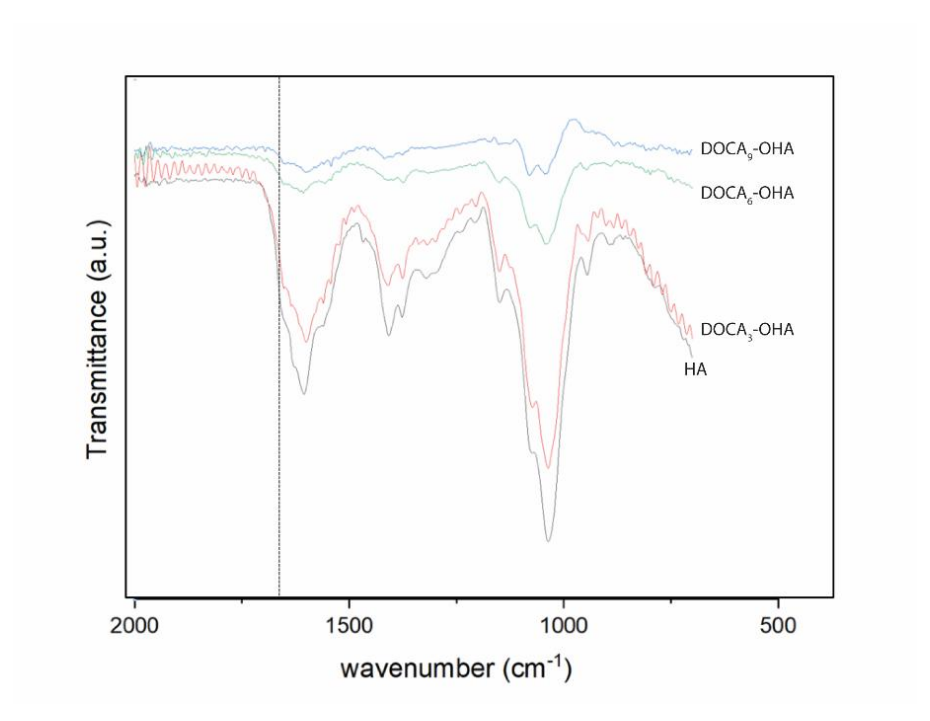


Figure S2.4 (A). FTIR spectra of OHA, TCA₃-OHA, TCA₆-OHA, and TCA₉-OHA show the characteristic band for the creation of aldehyde groups at 1700 cm⁻¹ following the oxidation

reaction. (B). FTIR spectra of OHA, DOCA₃-OHA, DOCA₆-OHA, and DOCA₉-OHA show the characteristic band for the creation of aldehyde groups at 1650 cm-1 following the oxidation reaction.

CHAPTER 3

DEVELOPMENT AND OPTIMIZATION OF NANOSTRUCTURED LIPID CARRIERS FOR ENHANCED ORAL ABSORPTION OF DEFEROXAMINE

²Agboluaje, Elizabeth Oladoyin, et al. "Development

And Optimization of Nanostructured Lipid Carriers for

Enhanced Oral Absorption of Deferoxamine."

To be submitted to a peer-reviewed journal.

3.1. Abstract

Hemochromatosis, which can either be genetic or acquired, is a medical condition characterized by excessive iron accumulation and can ultimately lead to chronic oxidative stress in various organs such as the heart, liver, brain, etc. Deferoxamine (DFO) is a clinically established iron chelator but is limited by its poor oral bioavailability, necessitating intravenous administration. To address the need for effective oral DFO therapy, this study focuses on the development and optimization of deferoxamine-loaded nanostructured lipid carriers (DFO-NLCs). Nanostructured lipid carriers, combining solid and liquid lipids, offer enhanced drug loading, stability, and controlled release compared to traditional solid lipid nanoparticles. Glyceryl monooleate and oleic acid were selected as lipid components, with poloxamer 188 as surfactant and chitosanalginate coating to protect the formulation in gastric environments. A Quality by Design (QbD) approach, utilizing Design of Experiments (DOE), was employed to systematically optimize the formulation parameters and achieve desirable physicochemical properties. The optimized DFO-NLCs were characterized for particle size, zeta potential, polydispersity index, drug loading, encapsulation efficiency, drug release behavior, cytotoxicity, iron chelation efficacy, and in-vitro oral absorption. The physicochemical analysis demonstrated that F2, F3, and F5 DFO-NLCs had the best properties, and in-vitro studies with F2 DFO-NLC exhibiting the most controlled release rate for DFO. This strategy offers a promising pathway for the development of a safe, patientpreferred with controlled-release for oral deferoxamine formulation with enhanced therapeutic potential.

Keywords: Iron overload, Deferoxamine, Oral, Nanostructured Lipid Carriers, Chitosan, Alginate

3.2. Introduction

Hemochromatosis commonly referred to iron overload (IO) is a medical condition marked by the excessive accumulation of iron and damage of vital organs such as the heart, liver, pancreas, joints and skin, etc.[44, 88]. Hemochromatosis is categorized into two types: primary and secondary. Primary hemochromatosis arises from genetic mutations, most commonly in the HFE gene[89]. In contrast, secondary hemochromatosis develops as a consequence of other medical conditions or treatments that result in excessive iron accumulation. These include chronic blood transfusions associated with disorders like thalassemia or sickle cell anemia, chronic liver diseases, or excessive dietary iron consumption [90]. With secondary hemochromatosis, which is usually acquired, the body loses its ability to regulate iron homeostasis, and this can lead to metal irons from storage proteins (i.e., ferritin, hemosiderin) being leaked into the bloodstream in the form of highly reactive non-transferrin-bound iron (NTBI)[8]. NTBI is known to increase cellular oxidative stress by improving the generation of reactive oxygen species (ROS) via the Haber-Weiss reaction The implications of excess metals extend beyond blood disorders, as accumulating evidence suggests that elevated levels of iron and other essential metals contribute to the progression of diseases such diabetes, cardiomyopathy, Alzheimer's, Parkinson's, liver cirrhosis, angiogenesis[49, 91].

Deferoxamine is the most established and widely used iron chelator for removing excess irons in the body[92]. DFO, which can be administered intravenously, can stoichiometrically bind to iron at a 1:1 ratio due to its hexadentate structure, while other oral chelators, deferasirox and deferiprone, stoichiometrically bind to iron at 2:1 and 3:1 ratios [90]. While intravenous DFO has

been clinically established, its oral use remains limited due to its poor absorption, with an oral bioavailability of 2%. Therefore, there is a pressing need to develop a safe and effective orally active deferoxamine (DFO) formulation, as oral drug delivery is highly preferred by patients due to its non-invasive nature. Also, oral delivery presents a promising alternative for enhancing the pharmacokinetics and reducing the toxicity profiles of deferoxamine (DFO)[93]. To address this issue, lipids and lipid nanoparticles can be employed to improve the oral absorption of hydrophilic drugs. This is because lipids can boost the absorption of drugs in the gastrointestinal tract (GIT), especially when formulated as lipid nanoparticles, due to the small particle size, by enhancing mucosal adhesion and prolonging the residence time. Also, lipid nanoparticles have the potential to shield loaded drugs from chemical and enzymatic degradation. They exhibit a gradual release of drug molecules from the lipid matrix into the bloodstream, leading to enhanced therapeutic profiles compared to free drugs. Also, lipid molecules have been reported to reduce the toxicity and adverse side effects of various drug delivery classes when compared with others of polymeric nature[39].

While the use of solid lipid nanoparticles (SLNs) has been demonstrated to have high entrapment efficiency and excellent sustained release for various drugs, their use is still limited because of particle enlargement, unpredictable gelation behavior, unforeseen polymorphic transformations, and low encapsulation efficiency due to the crystalline nature of the solid lipid[39, 94, 95]. Nanostructured lipid carriers (NLCs) are a class of lipid nanoparticles that address the challenges of SLNs with a matrix that consists of a mixture of liquid lipid and solid lipid, which enables an imperfect matrix that enhances drug loading, controlled drug release, and permeability of hydrophilic drugs across the biological membrane[96-100]. NLCs' properties include high drug loading capacity, limited drug expulsion from the matrix during storage, small particle size,

improved stability, etc. [101-103]. In selecting the materials for the formulation of deferoxaminenanostructured lipid carrier (DFO-NLCs), key factors were considered based on the hydrophilic nature of DFO.

Glyceryl monooleate was selected as the solid lipid because it can encapsulate large amounts of water in its liquid crystalline phases. Oleic acid was selected as the liquid lipid because prior studies have shown that DFO is highly soluble in oleic acid, and it can stabilize water in oil emulsions[39, 93]. Poloxamer 188 served as a surfactant, while sodium alginate was utilized as a crosslinking agent. To protect the DFO-NLCs in the highly acidic environment of the stomach, it was coated with low molecular-weight with 85 % degree of deacetylated chitosan cross-linked with sodium alginate [104, 105]. Studies have shown that chitosan with low molecular weight and a higher degree of deacetylation can ensure there is greater re-dispersibility of smaller particles in water [106]. While DFO is very soluble in water, chitosan-alginate polymeric coating for the NLCs will ensure a more efficient controlled drug release rate with high drug loading percentage. Regulatory authorities such as the Food and Drug Administration (FDA) and the European Medicines Agency (EMA) advocate for the implementation of the Quality by Design (QbD) approach as an ongoing process in pharmaceutical development to ensure the final product meets high standards of quality, safety, and efficacy[107]. An experiment of design (DOE) was applied to ensure quality by design (QbD) for the formulation optimization process. Several studies have reported on the efficiency of QbD to ensure safe and effective optimized formulations [100, 108]. DOE is a systematic approach that can be used to identify relationships between input variables (X) and output variables (Y) while enabling a deeper understanding of the process and its optimization[109, 110]. DOE can also be used to reduce the number of experiments to be done while ensuring that all possible attributes are considered with formulations that portray highquality properties[111-113]. The DOE was used to investigate how variations in the ratio of solid lipid, liquid lipid, and surfactant would influence the attributes of the DFO-NLCs. The responses analyzed included particle size, zeta potential, polydispersity index, drug loading, and encapsulation efficiency[114]. The optimized DFO-NLC formulations were then characterized by their drug release rates, cytotoxic profile, iron chelation efficiency, and oral absorption in vitro models (**Figure 3.1**).

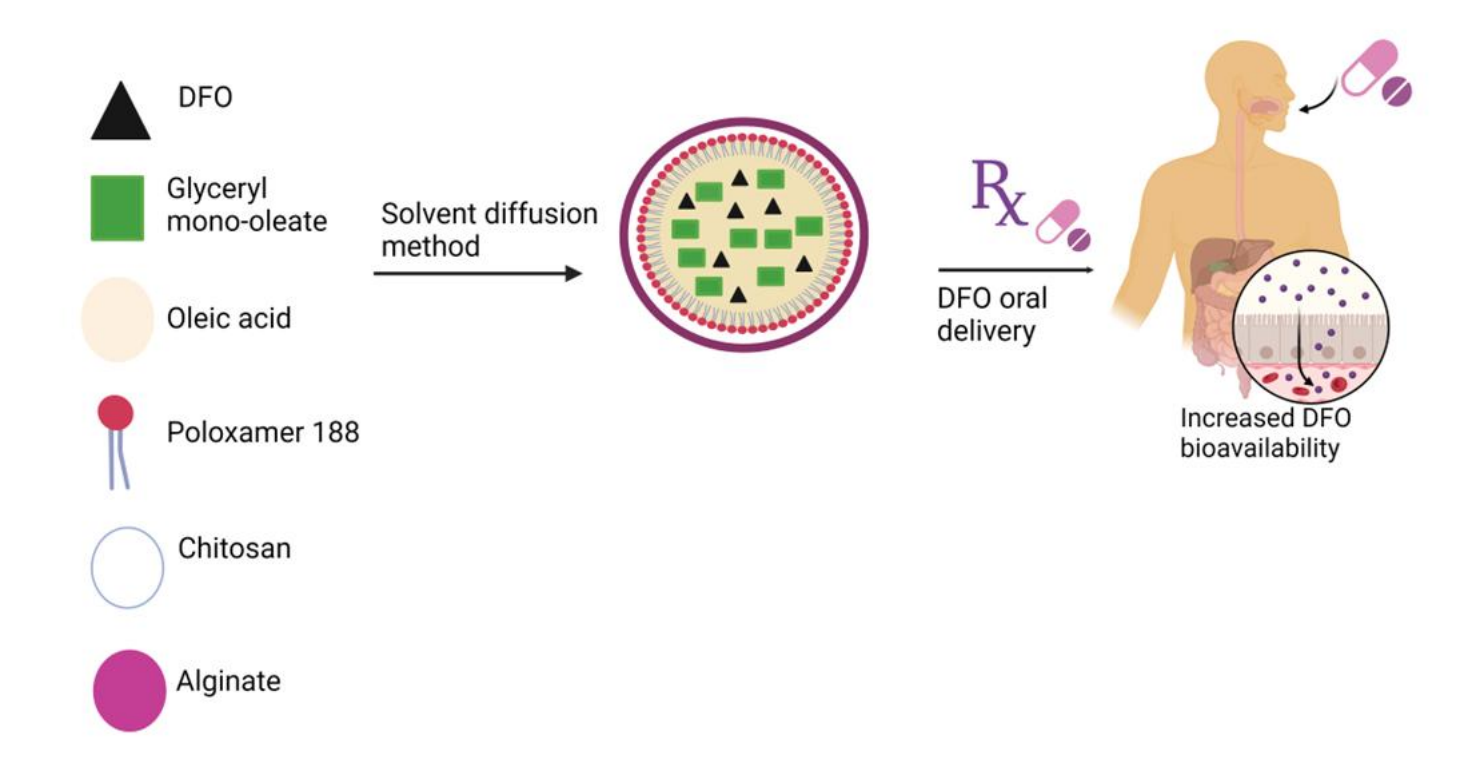


Figure 3.1. Schematic illustration showing the design of deferoxamine-nanostructured lipid carriers coated with chitosan and alginate with improved oral bioavailability and iron-chelation efficacy.

3.3. Experimental

3.3.1. Preparation of DFO-NLCs formulations

Different amounts of DFO, glyceryl mono-oleate, and oleic acid were dissolved in 5 mL of a solvent blend consisting of ethanol and acetone (1:1 v/v) using a water bath set at 35 °C. The organic mixture was then quickly added into 50 mL of an aqueous Poloxamer 188 solution (1% w/v) at 25 °C while sonicating for 2 minutes. This was followed by adding 6.25 mL of a 2% w/v chitosan solution (prepared by dissolving 2.4 g of chitosan in 100 mL of water containing 2% w/v acetic acid) into the emulsion and sonicating again for 2 minutes. Subsequently, 10 mL of a sodium alginate solution was added while continuously stirring magnetically for 30 minutes, leading to the formation of DFO-NLCs formulations. The formulations were dried in a vacuum desiccator at room temperature for 24 hours to remove any residual organic solvent, followed by storing the final products in a dry, cool environment for future use. A schematic overview of the DFO-NLCs formulation process is illustrated in **Figure 3.2.**

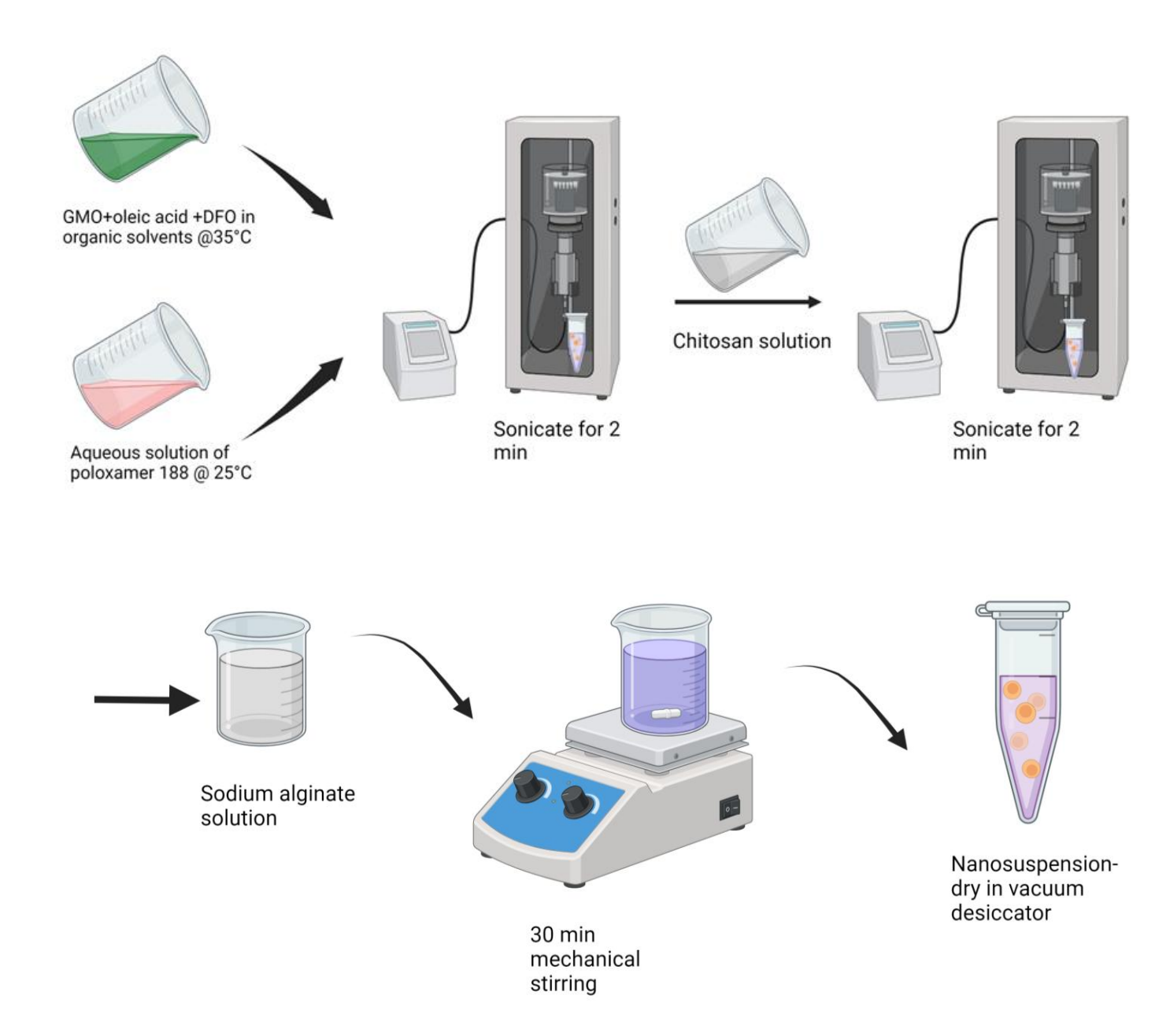


Figure 3.2. Schematic illustration showing the formulation of deferoxamine-nanostructured lipid carriers coated with chitosan and cross-linked with alginate.

3.3.2. Design of Experiment

The DOE is an instrumental experimental design that was used to accommodate all possible variables and statistically predict the best possible conclusion. Previous studies have reported that variables such as drug: lipid concentration, organic: aqueous phase volume, and surfactant concentration were the main factors that influence the properties such as particle size, zeta potential, polydispersity, drug loading, and entrapment efficiency of NLCs[114]. Thus, a software called Fusion Pro by S-Matrix (Fusion Pro Software Version 9.9.0 Build 690, S-Matrix Corporation (www.smatrix.com)) was used to investigate the impact of these variables on the properties of the prepared DFO-NLC formulations and to select the optimized DFO-NLC to investigate further. Different ranges of the key ingredients in the mixture variables that were considered include the following: drug: lipid ratio (1:3-1:7), lipid phase: aqueous ratio (1:5-1:15), and surfactant concentration (0.5 - 1.5%). Also, the percentage of chitosan and alginate used was kept constant across all formulations. Statistical analysis was also performed using Fusion Pro software. Although the software generated 17 possible formulations, only 15 formulations were prepared because runs 11 and 12 were duplicates of run 10. The details of the design and the different ratios predicted can be found in **Table S3.1**.

3.3.3. Physicochemical Characterization of DFO-NLCs

The mean particle size and polydispersity index of the DFO-NLCs formulations were determined with the use of Dynamic Light Scattering (DLS) (Zetasizer Nano ZS instrument; Malvern Instruments, UK) at a scattering angle of 90°. DFO-NLC formulations were diluted with distilled water at a concentration of 2 mg/ml w/v. Also, the zeta potential was used to investigate the surface properties and electrical mobility of the DFO-NLCs. Transmission Electron Microscopy (JEOL-

JEM1011) was employed to confirm the shape and size of the DFO-NLCs. The DFO-NLCs needed to retain their ability to chelate ion, which was done by monitoring the UV-Vis absorption spectra in the range of 350-650 nm with an absorbance peak indicative of the DFO-ferritin reaction (at a 1:1 ratio) assay at 430nm. Fourier transform infrared (FT-IR) spectroscopy was determined by ATR-CRYSTAL FTIR (Fourier transform infrared spectroscopy) (Bruker) to assess possible interactions between the excipients and the drug at a region of 4000- 500 cm⁻¹.

The drug loading and entrapment efficiency of DFO into the NLCs were determined by the centrifugation method. 0.5 mL of each prepared sample of DFO-NLC was filled into the Amicon ultracentrifugation tubes (10 kDa cut off, United States) and centrifuged at 14000 rpm for 20 mins at 4°C. The aqueous medium was collected and analyzed by the DFO-ferritin reaction assay by measuring the absorbance at 430nm due to iron chelating DFO at a 1:1 ratio, which can be used to confirm the amount of DFO loaded into NLCs. The standard calibration curves were generated by reacting serial dilutions of 1mg/ml of DFO with saturated Fe (III) solution for reference absorption curves at 430 nm. The collected ultracentrifuged medium was reacted with saturated Fe (III) solution, and their absorbances at 430 nm were measured to determine DFO concentrations. The percentage DFO loading and encapsulation efficiency ratio were determined using Eq. 1 and Eq. 2;

% DFO loading =
$$\left(\frac{\text{DFO total weight - DFO free weight}}{\text{Weight of the lipid}}\right) \times 100$$
-----Eq. 1

% DFO encapsulation efficiency =
$$(\frac{DFO\ total\ weight\ -DFO\ free\ weight}{DFO\ total\ weight}) \times 100$$
-----Eq 2

3.3.4. In Vitro DFO Release Study

The in vitro drug release of DFO-NLCs was investigated by the dialysis bag method[115]. Two different release media were used in the study, which included simulated gastric fluid (pH 1.2) for a 1-hr study and simulated intestinal fluid (pH 7.4) for 4 hrs. study. Briefly, the suspension containing DFO-NLCs formulations equivalent to 5mg of DFO in 5 mL of phosphate buffer saline (PBS) was filled into a dialysis bag (3.5 kDa MWCO) and suspended separately into 42 mL of release media while stirring at 80 rpm and 37°C for 24 hrs. At different time points between (0, 0.30,1, 2,4,6,8, and 24 hrs.), 2ml was collected and replaced with an equal volume of fresh medium. DFO in the collected samples was quantified by UV-Vis spectrophotometry at 430 nm and calculated against the calibration curve.

3.3.5. Cytotoxicity Study in Mammalian Cells: J774A.1, HEPG2 and Caco-2

It was important to test the DFO-NLC formulations in mammalian cell lines such as J774A.1 macrophages and HepG2 liver cells because orally absorbed NLCs can enter the systemic circulation and accumulate in the liver, where hepatocytes and Kupffer cells in humans store excess iron. Both J774A.1 and HepG2 cells were cultured using a previously described protocol [90]. J774A.1 and HepG2 cells were seeded in 96-well plates at a density of 10,000 cells per well and incubated for 24 hrs. at 37°C with 5% CO₂ in DMEM medium (with sodium pyruvate) supplemented with 1% of PEST (penicillin 10,000 U/ml + streptomycin 10,000 μg/ml, 100×), 1% of 100× nonessential amino acids, and 5% of fetal bovine serum (FBS). Prior studies have reported that Caco-2 cells can spontaneously differentiate into a polarized monolayer that closely mimics the characteristics of small intestinal enterocytes, and this has made them a widely used in vitro

model for studying drug absorption and permeability [116]. Caco-2 were also cultivated according to a previously established method [90] where cells at passage 4 were seeded at a density of 10,000 cells per well and incubated for 7 days at 37°C with 5% CO₂ in DMEM medium (without sodium pyruvate) supplemented with 1% of PEST (penicillin 10,000 U/ml + streptomycin 10,000 μg/ml, 100×), 1% of 100× nonessential amino acids, and 10 % of fetal bovine serum (FBS). A resazurin-based MTT metabolic assay was performed using free DFO, DFO-NLCs (F2, F3, and F5). In all three cell lines, final tested concentrations ranged from 1000 to 3.90 μM DFO equivalent. After 48 hrs. sample incubation with the cells, the cells were washed with PBS and incubated with 100 μl of 44μM of resazurin for 4 hours. Fluorescence intensity was measured using a Spectra-Max Gemini EM microplate reader (excitation at 560 nm, emission at 590 nm). Wells without cells served as blank, while untreated cells represented 100% viability. Cell viability was calculated from fluorescence values using Equation 3.

Cell viability (% decrease) =
$$\frac{F(sample) - F(Blank)}{F(control) - F(Blank)} \times 100$$
-----Eq. 3

3.3.6. In Vitro Iron Chelation Efficacy Studies

J774A.1 macrophage cells and HepG2 liver cells were seeded in six-well plates at a density of 30,000 cells per well and incubated for 24 hours at 37°C in a humidified atmosphere containing 5% CO₂, using DMEM supplemented with 10% FBS, 1% PEST and 1% essential amino acid (DMEM complete media). This was followed by cell treatment with 100 μM ferric ammonium citrate (FAC) in complete media for 24 hrs. to trigger intracellular iron overload. After the iron overload induction, the cells were rinsed with PBS and treated with various formulations, including free DFO, F2, F3, and F5 DFO-NLCs at equivalent concentrations of 10 μM and 50 μM for 48

hours. The study included two control groups; group A consisted of normal, untreated cells, and group B contained iron-loaded cells without any subsequent treatment. After treating the cells with the test samples for 48 hrs., cells were lysed with a buffer composed of 150 mM NaCl, 10 mM Tris, 1% Triton X-100, and a protease inhibitor cocktail at pH 7.4. The intracellular ferritin levels were determined using specific mouse and human ferritin ELISA kits, and total protein content was quantified via the BCA protein assay. Ferritin values were normalized to total protein and reported as nanograms of ferritin per microgram of total protein concentration.

3.3.7. *In Vitro* Permeation Studies

To explore whether the inclusion of NLCs coated with chitosan and alginate in the formulation of free DFO improved the permeability of DFO across Caco-2 cell monolayers, transport studies were carried out using a dual-chamber trans-well system. The dual-chamber trans-well system consists of 12-well trans-well plates with 400 μ m pore-size filters, creating distinct apical and basolateral compartments. Caco-2 cells were seeded at a density of 1×10^5 cells per well in the apical layer for 21 days, while the media in both apical and basolateral layers were replaced every 2 days to establish tight, polarized monolayers. Once the cells reached confluency and the monolayer integrity was confirmed, the complete media was removed from the cells, and they were washed with HBSS. After which, 500 μ l of 400 μ M free DFO or equivalent DFO doses in F2, F3, and F5 DFO-NLCs in HBSS were added to the apical side. At various time intervals (0, 0.5, 1, 2, 4, 8, and 24 hours), 100 μ l samples were withdrawn from the basolateral chamber and reacted with a saturated Fe (III) solution. The mixed solution was then evaluated by its absorbance measurements at 430 nm to quantify the amount of DFO transported from the apical layer to the basolateral layer. Additionally, the transepithelial electrical resistance (TEER) of the Caco-2 monolayers was

measured using an EVOM2 volt-ohm meter (WPI, 240 V, 50 Hz) and an STX2 electrode. TEER readings were taken at the various time intervals (0, 0.5, 1, 2, 4, 8, and 24 hours) during drug treatments, and then after 24 hrs., the samples were discarded, and TEER measurements were taken at 25, 26, 28, and 48 hrs. The percentage changes in TEER values were computed using Equation 4.

TEER (% decrease) =
$$\frac{T (Final) - T (Blank)}{T (Initial) - T (Blank)} \times 100$$
------ Eq. 4

Statistical Analysis

Data was analyzed using GraphPad Prism version 5.0. Comparisons between groups were performed using one-way analysis of variance (ANOVA). A p-value of less than 0.05 was considered statistically significant.

3.4.Results

3.4.1. Optimization of Formulations

The design of experiments with the use of Fusion Pro by S-Matrix was selected for the efficient optimization process because it accommodates the possibility of investigating all possible variables and statistically predicting the optimized formulation with the use of a selected number of experimental runs[117]. While the independent variables included the drug/lipid ratio, organic/aqueous phase ratio, and the surfactant concentration, the dependent variables included the entrapment efficiency (EE), drug loading (DL), particle size (PS), polydispersity index (PDI), and zeta potential (ZP). The measured values for EE, DL, and PS ranged from 49.41 ± 0.89 to

90.25 \pm 0.67% (w/w), 4.63 \pm 0.08 to 29.01 \pm 0.86% (w/w), and 108.5 \pm 4.06 to 616.4 \pm 42.23 nm, respectively, as reported in **Table 3.1**. Based on the response values for the 15 formulation runs, fusion pro software predicted that the best formulation to accommodate all desired properties would be F2 DFO-NLC with a drug: lipid ratio (1:5), organic: aqueous phase (1:15), and a surfactant concentration (1.5%), with a predicted particle size of 281.34 nm, DL of 28.08 % w/w and EE of 91.34 % w/w as shown in Table S3.2.. After F2 DFO-NLC formulation and optimization, the experimental values included a particle size of 215.90 \pm 22.8 nm, DL of 26.07 \pm 0.19 % w/w, and EE of 91.34 % w/w. While Fusion Pro predicted F2 DFO-NLC as the best, other formulations that had desirable response values were also considered for further studies before further streamlining. Also, the three-dimensional (3D) response surface plots for the effects of the investigated variables on the evaluated response values with a surfactant concentration of 1.5% are shown in **Figure 3.3**, while the evaluated response values with a surfactant concentration of 0.5% and 1.5% are shown in **Figure S3.1a - c**. The fusion pro predicted acceptable performance region can be found in **Figure S3.2**.

Run	Variables				Response values					
no	DFO	Lipid	Organic	Aqueous	Surfactant	Drug	Entrapment	Particle	Zeta	PDI
			phase	phase	(%)	loading	efficiency	size (nm)	potential	
						(%)	(%)		(mV)	
F1	1	5	1	15	1	21.50±0.17		237.80 ±	-32.53 ±	0.52
							83.38±0.67	19.7	0.05	±0.02

F2	1	7	1	15	1.5	26.07±0.19		215.90 ±	-34.9	±	0.37
							90.25±0.67	22.8	0.50		±
											0.03
F3	1	3	1	10	1	10.88±1.91		198.47 ±	-55.07	±	0.416
							63.68±1.54	1.08	1.32		±
											0.04
F4	1	3	1	15	1.5	4.63±0.08		602.01 ±	-19.4	±	0.588
							57.62±0.99	27.4	0.22		±
											0.01
F5	1	3	1	5	0.5	29.01±0.86		245.37 ±	-35.77	±	0.45
							69.63±2.07	18.9	0.45		±
											0.02
F6	1	7	1	5	1.5	12.97±0.16		108.5 ±	-		0.45
							75.75±0.95	4.06	41.4	±	±
									1.13		0.019
F7	1	5	1	5	1	19.39±0.14		145.23 ±	-		0.47
							73.55±0.54	8.73	33.20	±	±
									0.50		0.043
F8	1	5	1	10	1.5	5.16 ± 0.14		552.34 ±	-32.45	±	0.61
							51.49±1.44	31.41	0.42		±
											0.13
F9	1	5	1	10	1	6.81 ± 0.12		162.93 ±	-32.40	±	0.53
							49.41±0.89	5.45	0.37		±
											0.01

F10	1	7	1	5	0.5	12.47 ±		275.23 ±	-43.43 ±	0.51
						0.19	61.73±0.96	2.13	0.40	±
										0.00
F11	1	7	1	10	1	6.77 ± 0.72		616.4 ±	-41.13 ±	0.73
							50.0±5.36	42.23	0.21	±
										0.02
F12	1	7	1	15	0.5	7.31 ± 0.08		232.43 ±	-27.60 ±	0.53
							58.57±0.68	5.54	0.28	±
										0.08
F13	1	3	1	5	1.5	7.29 ± 0.10		218.34 ±	-38.67 ±	0.42
							60.38±0.90	19.57	0.33	±
										0.073
F14	1	3	1	15	0.5	9.38 ± 0.09		242.6 ±	-32.13 ±	0.60
							51.04±0.49	4.94	0.98	±
										0.05
F15	1	5	1	10	0.5	10.22 ±		178.7 ±	-45.17 ±	0.53
						0.244	49.67±1.18	5.03	1.13	±
										0.04

Table 3.1. The experiment constants for the design of experiment included a drug: lipid ratio (1:3-1:7), organic: aqueous phase (1:5-1:15), and a surfactant concentration (0.5-1.5%). Table 1 shows the mixture variables output based on the experiment's constants inputs that can be formulated and the corresponding response values for Particle size, drug loading and encapsulation efficiency.

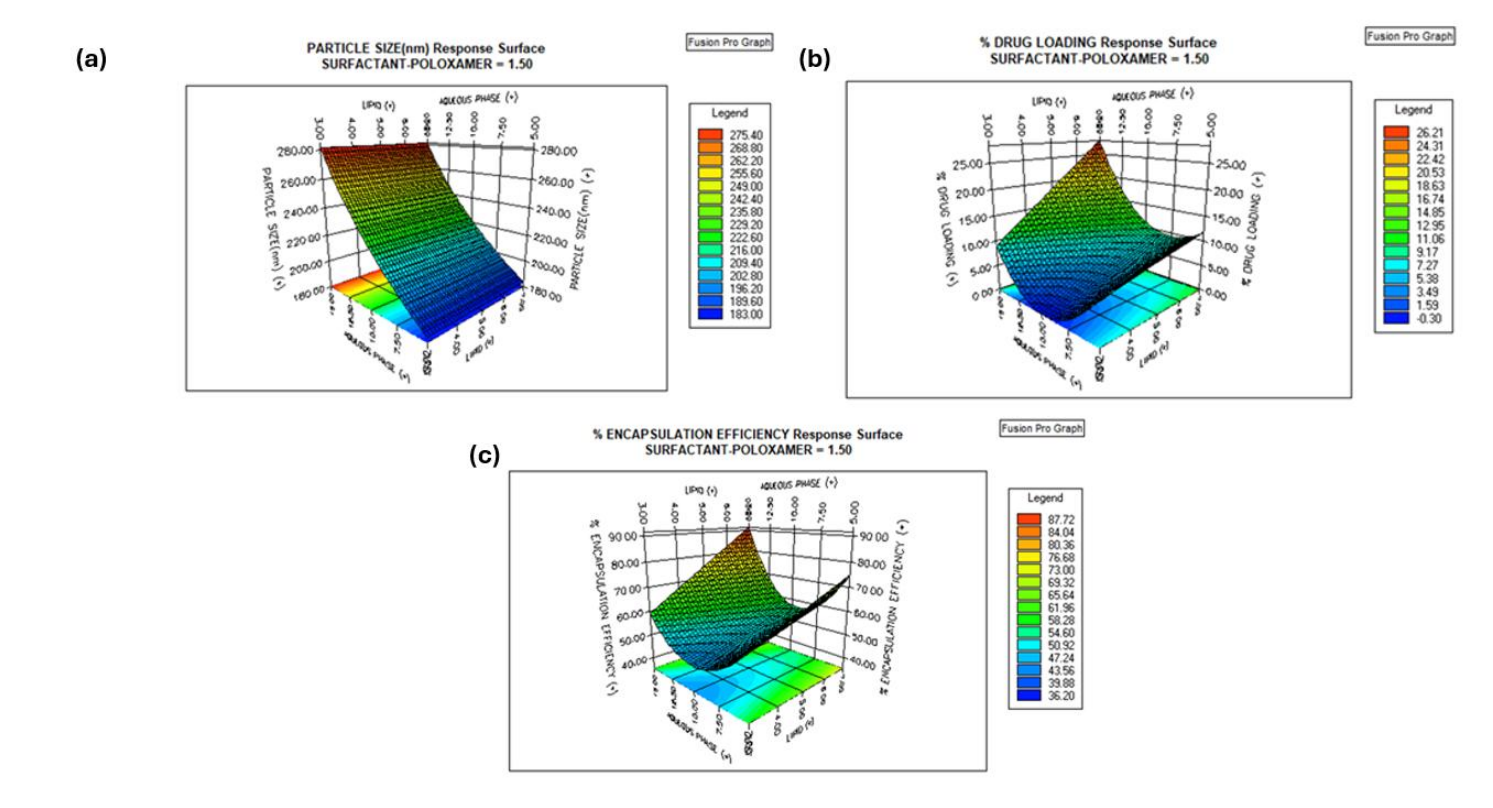


Figure 3.3. Three-dimensional (3D) response surface plots showing the effect of the variable on response at a surfactant concentration of 1.5%. (A) The effect of organic/aqueous phase ratio on particle size (B), The effect of organic/aqueous phase ratio on % drug loading, (C) The effect of organic/aqueous phase ratio on % EE.

3.4.2. Physicochemical Characterization of DFO-NLCs

The optimized formulation (F2-DFO NLC) had a particle size of 215.90 ± 22.8 nm, DL of 26.07 ± 0.19 % w/w, EE of 91.34 % w/w, Zeta potential of -32.53 ± 0.05 , and a PDI of 0.37 ± 0.03 . The TEM images for F2 DFO-NLC showed NLC with a spherical shape coated with chitosan and alginate. UV-vis was also used to confirm DFO loading into the NLCs by the reaction of Fe (III) solution with DFO and observing the absorbance at 430nm. The DLS, TEM, and UV-Vis of F2

DFO-NLC are shown in Figure 3.4a-c. In addition, F1, F3, F5, F6, F7, and F10 with reported values as seen in Table 3.2 were also characterized by FTIR and drug release studies prior in vitro studies. The FTIR spectra obtained in the attenuated total reflectance (ATR) mode for the alginate cross-linked loaded with DFO can be seen in Figure 3.5. The scanning range used was 4000-400 cm⁻¹ at a resolution of 8 cm⁻¹ and 16 scans per sample. For DFO, the bands at 2857–2932 cm⁻¹ and 3085 cm⁻¹ are due to the asymmetric and symmetric CH₂ and N-H stretching vibrations while the peaks at 1038, 1170, 1480, 1566 and 1621 cm⁻¹ are due to the stretching vibrations of (N-O of the hydroxamate groups and of C-C respectively), the bending vibration of (CH₂ and N-H (amine II) respectively), and stretching vibration of C=O (amine I)[118]. For alginate, the peaks at 3300 cm⁻¹, 2928 cm⁻¹, and 1624 cm⁻¹ are due to the stretching vibration of O-H, CH stretch, and C=O stretch, respectively. For chitosan, the peaks at 3300⁻¹, 1621 cm⁻¹, and 1560 cm⁻¹ are due to the NH₂ and O-H stretch, C=O stretch from amide I, and NH₂ bending vibrations, respectively[119, 120]. Oleic acid is a straight-chain carboxylic acid consisting of 18 carbons, while GMO is an ester of glycerol and oleic acid. For oleic acid, the peaks at 2924–2855 cm⁻¹, 1709 cm⁻¹, and 936 cm⁻¹ are due to C-H, C=O, and out-of-plane O-H stretching vibrations, respectively. For GMO, the peaks at 3459 cm⁻¹, 2926–2853 cm⁻¹, 1735 cm⁻¹, 1454 cm⁻¹, 1162 cm⁻¹ are due to O-H bending, C-H stretching, C=O stretching, CH3 bending and C=O bending vibrations respectively [121].

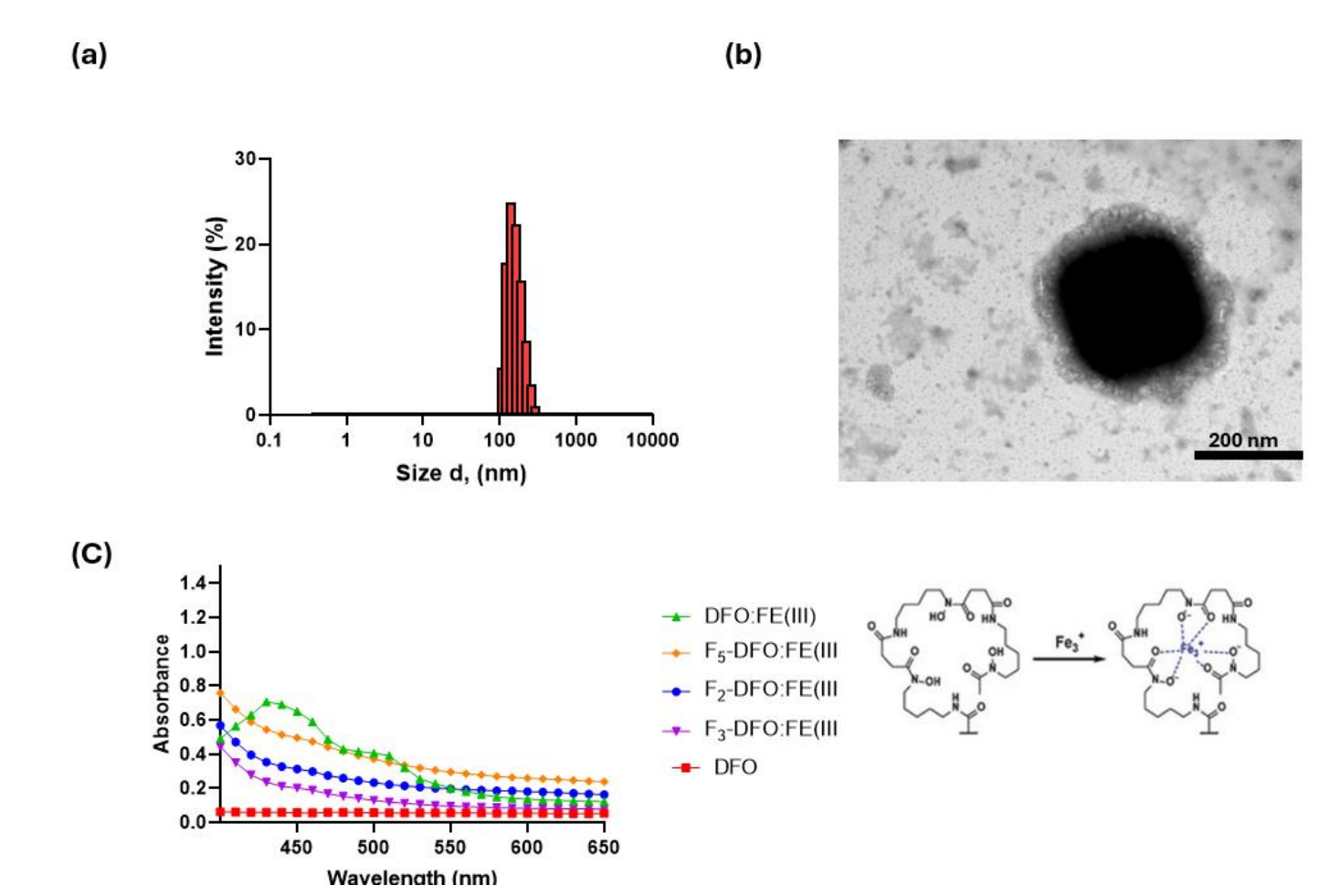


Figure 3.4. Physicochemical characterization of F2 DFO-NLC showing particle size analysis for (a) DLS, (b) TEM and (c) successful loading of F2, F3 and F5 DFO to NLC was confirmed by UV-Vis spectroscopy, where the presence of excess Fe (III) resulted in a strong absorbance peak at 430 nm, characteristic of DFO: Fe (III) complex formation.

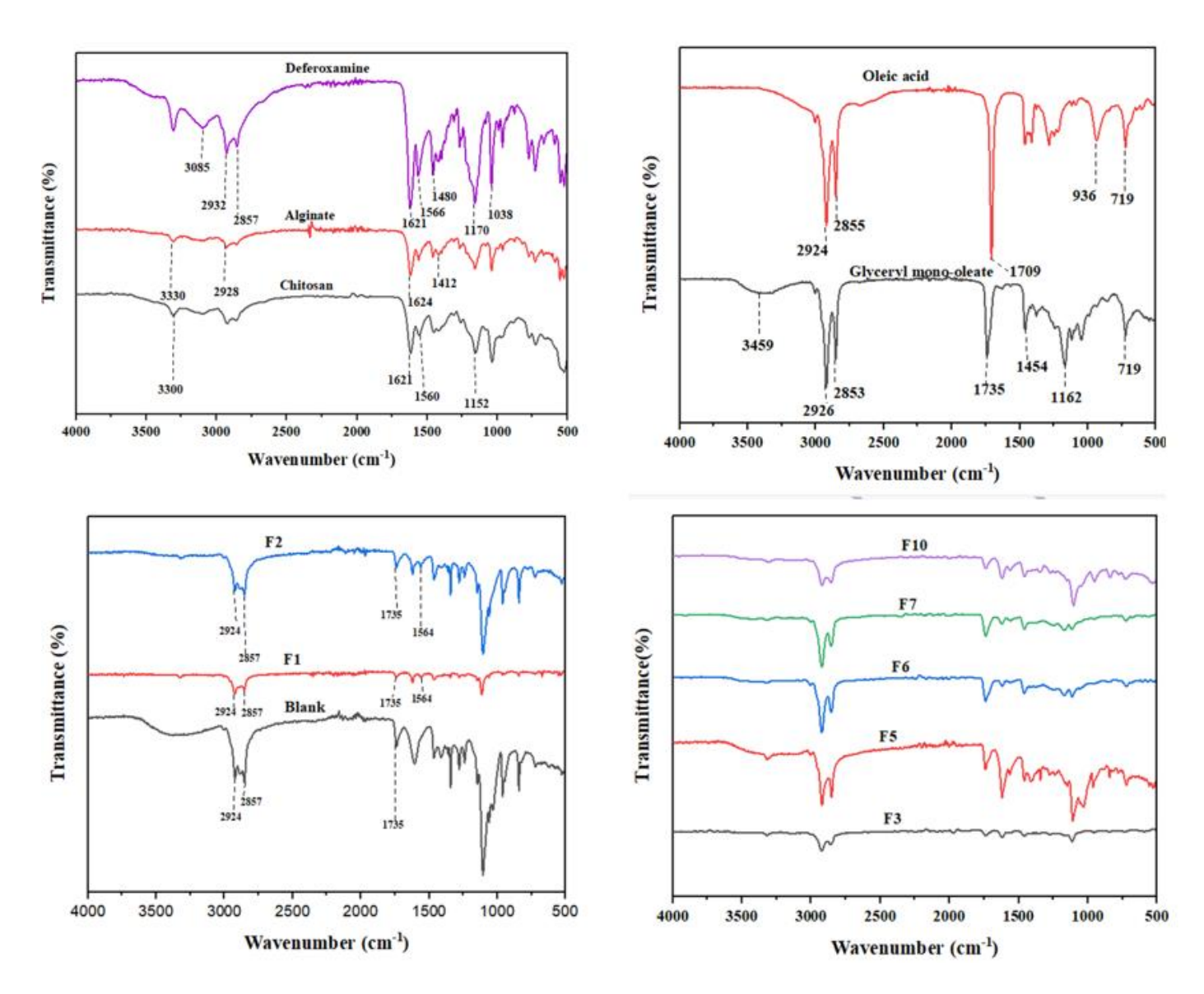


Figure 3.5. FTIR spectra of DFO, chitosan, alginate, GMO, oleic acid, NLC, and F1-F10 DFO nanostructured lipid carriers showing characteristic peaks indicative of DFO loading and cross-linking between chitosan and alginate

3.4.3. In Vitro DFO Release Study

It was important to study the drug release profile of the formulations to investigate how various lipid matrix compositions, and the presence of polymeric coating can impact the controlled release

properties. Based on the desirable physicochemical characteristics selected, F1, F2, F3, F5, F6, F7, and F10 DFO NLCs were studied for their cumulative DFO release over time as seen in **Figure 3.6**. It was observed that DFO release was lower in simulated gastric fluid in comparison to simulated intestinal fluid. For the simulated gastric fluid, less than 20 % of DFO was released at 2hrs for all the DFO-NLC formulations, while about 66.78 % of DFO was released for the free drug, which is representative of the drug's gastric residence time [122]. At 24 hours, less than 40% of DFO was released from all the DFO-NLC formulations, while about 88.64 % of DFO was released from the free drug. Also, at a pH of 7.4, it was observed that between 24.91 and 50.64 % of DFO was released from DFO-NLCs formulations, with F2 and F1 having the lowest DFO released, while F5 had the highest DFO released at 6 hours. In comparison, 93.76 % of DFO was released from the free drug at 6 hours. A similar trend was observed at 24 hours, where F2 DFO-NLC had the lowest DFO release of 34.53%, and F2 DFO-NLC had a DFO percentage release of 62.48 % while DFO had a percentage release of 94.82%.

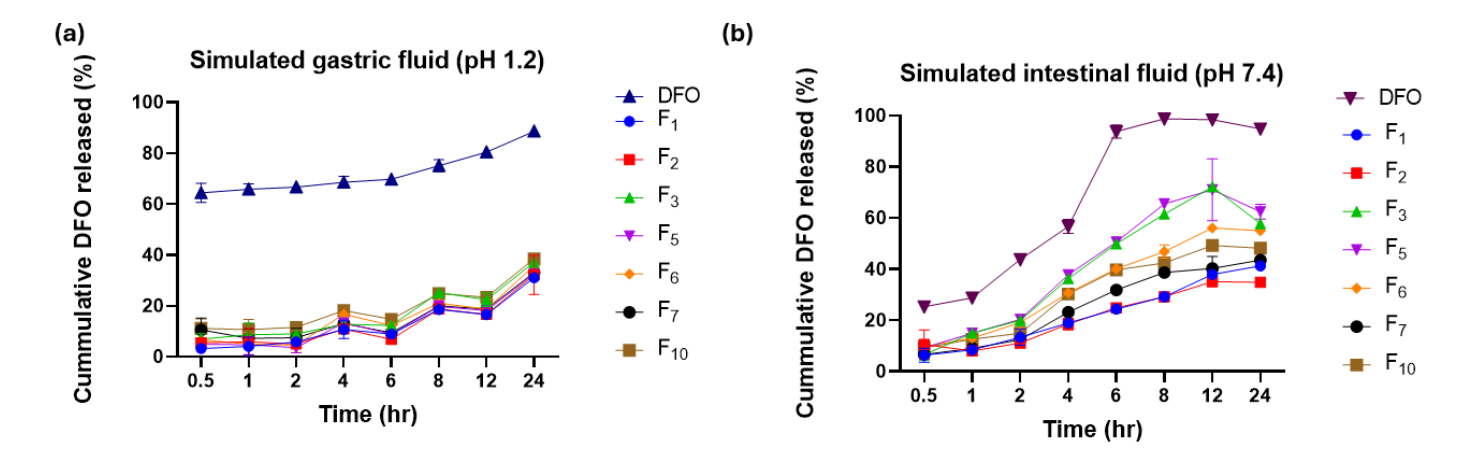


Figure 3. 6. Cumulative % drug release of DFO and F1, F2, F3, F5, F6, F7, and F10 DFO-NLCs (a) in simulated gastric fluid representative of pH 1.2, (b) in simulated fluid representative of pH 7.4. All DFO-NLC formulations had less DFO release in comparison to the free drug, indicative

of a more controlled release with the use of lipid matrix and polymeric coatings. Each data point is presented as the mean \pm standard deviation (SD) (n = 3)

3.4.4. Cytotoxicity Study in Mammalian Cells: J774A.1, HEPG2 and Caco-2

Based on the desirable DFO percentage drug release study, F2, F3, and F5 DFO NLCs were selected for the remaining in vitro cell studies. Free DFO significantly lowered cell viability in J774A.1 and HEPG2 cells; however, the presence of NLCs improved the cell viability of F2, F3, and F5 DFO-NLCs at equivalent DFO concentrations. For instance, in J774A.1 cells, the IC50 of free DFO was approximately 33.26 μ M, which increased to around 184.38 μ M, 96.207 μ M, and 169 μ M for F2, F3, and F5 DFO-NLC, respectively.

Similarly, in HepG2 cells, the IC₅₀ of free DFO was around 1000 μM, increasing to about 385.16μM, 196.71μM, and 244.32 μM for F2, F3, and F5 DFO-NLC, respectively. In contrast, Caco-2 cells indicated no cytotoxicity based on mitochondrial metabolism when up to 1000 μM of free DFO or equivalent concentrations of F2, F3, and F5 DFO-NLCs (**Figure 3.7**).

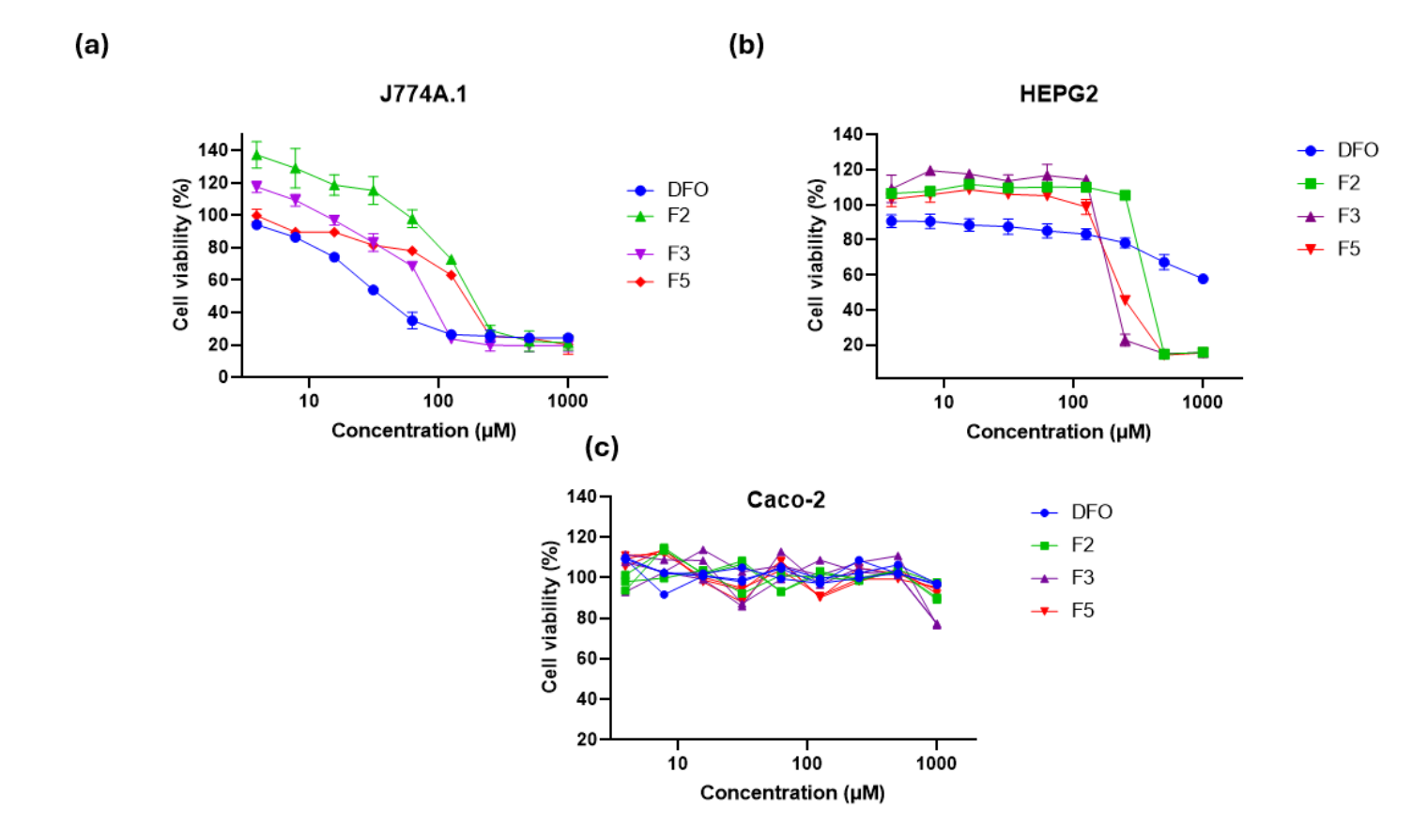


Figure 3.7. Cytotoxicity of free DFO (blue line), F2 DFO-NLC (green line), F3 DFO-NLC (purple line), and F5 DFO-NLC (red line) after 48 hrs. incubation on (a) J774A.1 cells, (b) HepG2 cells, and (C) Caco-2 cells. Each data point is presented as the mean ± standard deviation (SD) (n = 3).

3.4.5. In Vitro Iron Chelation Efficacy Studies

Figure 3.8a. shows that treating J774A.1 macrophage cells with 100 μM FAC elevated ferritin levels from a baseline of 4.86 ng/μg total protein (blue bar) to 6.45 ng/μg total protein (red bar). At equivalent DFO concentrations (50 μM), both free DFO (4.74 ng/μg total protein, green bar) and F5 DFO-NLC (3.70 ng/μg total protein, purple bar) produced similar reduction values to the baseline ferritin level, whereas F3 DFO-NLC and F5 DFO-NLC resulted in comparatively smaller

decreases. Similarly, as depicted in **Figure. 3.8b** FAC treatment (100 μM) increased ferritin concentrations in HepG2 liver cells from 4.53 ng/μg total protein (blue bar) to 9.11 ng/μg total protein (red bar). At equivalent DFO concentrations (50 μM), free DFO, F2 DFO-NLC, F5 DFO-NLC, and F3 DFO-NLC reduced ferritin levels to (5.45 ng/μg total protein, green bar), (3.28 ng/μg total protein, orange bar), (0.72 ng/μg total protein, purple bar), and (5.71 ng/μg total protein, brown bar), respectively.

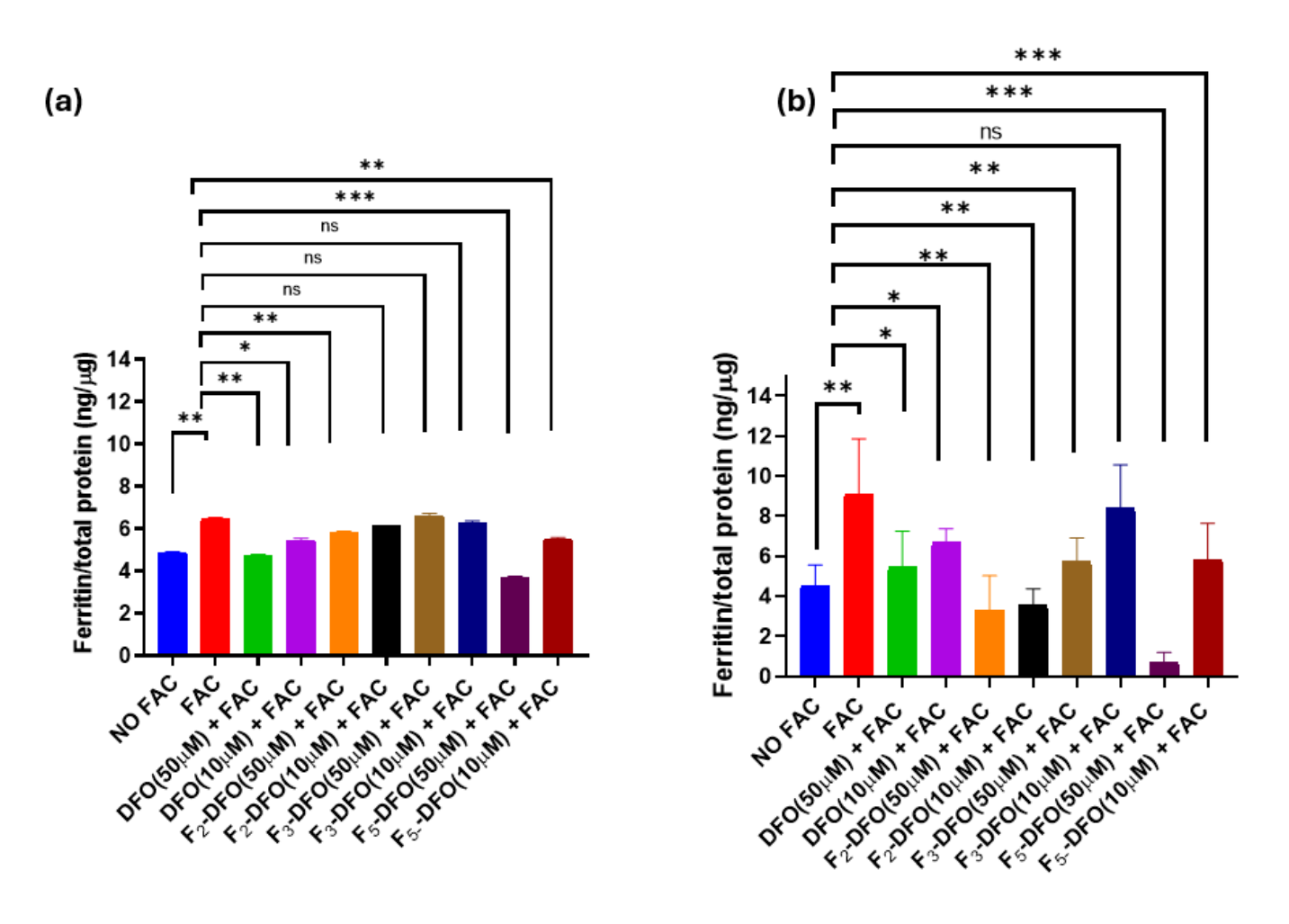


Figure 3.8. Ferritin reduction assay evaluating the iron chelation performance of DFO, F2 DFO-NLC, F3 DFO-NLC, and F5 DFO-NLC in (a) J774A.1 macrophages, (b) HepG2 iron-overloaded cells. Cells were exposed to DFO, F2 DFO-NLC, F3 DFO-NLC, or F5 DFO-NLC at

concentrations of either 10 μ M or 50 μ M for 48 hours. Following treatment, intracellular ferritin levels were quantified using a mouse / human ferritin ELISA kit. Data were normalized to total protein content (expressed as ng ferritin/ μ g protein) and are shown as mean \pm standard deviation (n=3). Statistical significance is indicated where applicable: "ns" denotes no significant difference; *p < 0.05, **p < 0.01, and *** p < 0.001.

3.4.5. In Vitro Permeation Studies

To quantitatively assess the ability of the DFO-NLCs to permeate through the small intestinal layer, a Caco-2 monolayer model of the gastrointestinal tract was used to investigate the extent to which DFO moved from the Caco-2 monolayer model of the gastrointestinal tract (Figure **3.9a**)[78]. From our findings, we saw that the absorbance readings of the DFO-Fe (III) complex demonstrated a time-dependent increase in DFO transport across the monolayer, as seen in Figure **3.9b.** F2 DFO-NLC, F3 DFO-NLC, and F5 DFO-NLC exhibited more DFO permeation in comparison to free DFO from 30 mins to 12 hours. Also, transepithelial electrical resistance (TEER) values were monitored to evaluate monolayer integrity following treatment with either free DFO or DFO nanoparticle formulations (Figure 3.9c). As reported by similar studies, the TEER values above 200 Ω·cm² indicate tight epithelial junctions for the Caco-2 monolayers [25]. After the 24-hour in-vitro permeation study, the cells were rinsed and incubated in fresh medium to investigate the recovery post-treatment for the monolayer cells. The TEER measurements revealed a transient decrease during treatment, followed by a reversible increase, with values returning near baseline within an additional 24 hours. This suggests that the nanostructure lipid carriers did not induce permanent tight junction disruption.

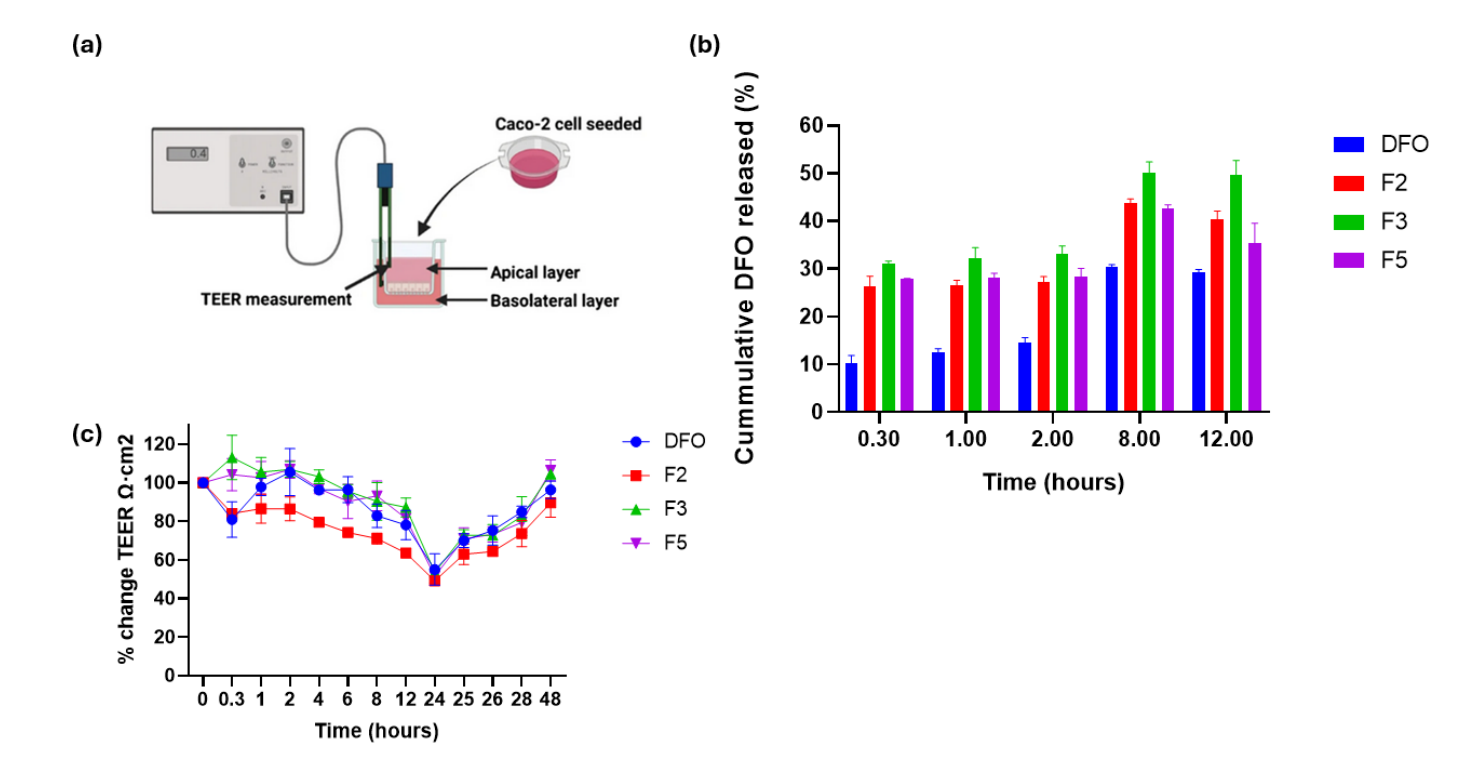


Figure 3.9. (a) Schematic representation of the Caco-2 monolayer permeability assay used to evaluate the cellular transport of DFO nanoparticles. The trans well system illustrates the key components of the experimental setup. (b) Caco-2 cells were treated with either 500 μM of equivalent DFO, F2 DFO-NLC, F3 DFO-NLC, or F5 DFO-NLC and incubated for 24 h. At each time point, 100 μl from the basolateral layers of each setup was added with Fe (III) and tested for absorbance at 430 nm. (c) TEER value measurements after incubation with DFO NLCs and removal of the DFO NLCs after 24 h

3.5. Discussion

As seen in **Figure 3.2**, DFO-NLCs were prepared by the solvent diffusion technique with the lipid core made of the solid lipid (GMO) and the liquid lipid (oleic acid) [39]. Prior studies have reported

that the presence of GMO in its liquid crystalline phase can ensure a more sustained release rate for both hydrophobic and hydrophilic drugs [123]. The NLCs were coated with a low molecular weight chitosan to ensure increased solubility in biological systems and absorption of the NLCs across the small intestine[124, 125]. Also, alginate was crosslinked with chitosan to protect the chitosan in the acidic environment of the stomach, which alters the positive charge of chitosan coated with the NLCs to a negative charge by the interaction of the protonated free amino groups on chitosan with the -OR groups on alginate [39]. While the NLCs ensure a high drug loading percentage for DFO, Chitosan ensures a more sustained release rate of the drug. After preliminary formulation with the use of the DOE, the data generated from the study of the effect of the variables on the response values showed that the various modifications of the variable greatly impacted the properties of the DFO-NLCs (Table 3.1). From the response surface diagrams, it was observed that increasing the lipid phase and aqueous phase also increases the particle size of the NLC at a concentration of 0.5-1.5 % of the surfactant. Regarding the EE, increasing the surfactant concentration increases DFO EE. Also, a higher ratio of the aqueous phase to the lipid phase increases DFO EE. Also, a higher ratio of the aqueous phase to the lipid phase increases DFO DL. Prior studies have reported that an increased aqueous phase can lead to an increase in the drug EE and DL with the use of both homogenization and sonication of particles due to enhanced solubilization [126, 127]. As you increase the drug to lipid matrix, it is also expected that this will lead to an increase in particle size because there will be more particle agglomeration. Similarly, increasing the surfactant concentration increases DFO DL. While the surfactant concentration impacts the sizes of the particles, it was observed that a broader size distribution observed with higher surfactant concentration may be due to an increased viscosity, which probably dissipates stirring energy more accurately, ultimately leading to reduced droplet breakup during emulsification[128]. While a smaller particle size is important in selecting the optimized formulation for this study, it was more important that the percentage EE and DL should be paramount because the goal was to load a hydrophilic drug (DFO) into the NLCs, which can be extremely difficult.

The zeta potential indicated a negative value, which is ideal since stable nanoparticles must have zeta potential values around -30 mV[99]. F2 DFO-NLC had spherical shape TEM images with an external coating indicative of the cross-linked chitosan-alginate coating (Figure 3.4). On further investigation of the DFO-NLC formulations, a new peak was observed at 1736 cm⁻¹, which indicates NH₂ bending vibration of the chitosan after being cross with alginate. The amino peak at 1152 cm⁻¹ also disappeared, which suggests electrostatic interaction between the (-COO⁻) of alginate and the (-NH₃⁺) of chitosan. The presence of DFO loading was confirmed by a characteristic peak at 1564, which indicates a bending vibration of N-H (amine II) while peaks at 2924 and 2857 suggest CH stretching vibrations due to oleic acid and GMO presence [39]. The FTIR study indicated that the polymers, NLC and DFO, did not interact with each other chemically but self-assembled with good stability (Figure 3.5). The drug release study for DFO showed that DFO release can be modified into a more controlled release rate with the presence of polymer coating and NLC, as seen in Figure 3.6. At pH 1.2, which indicates an acidic environment of the stomach, DFO had a higher release rate of 80% compared to DFO-NLCs, which had a significantly lower drug release rate. When compared to pH 7.4, which represents the basic environment of the small intestine, it was observed that there was an increased release rate of the DFO-NLCs, but still much lower than the free drug.

In-vitro cytotoxicity study showed that the presence of NLC further improved the cell viability profile of DFO on J774A.1 macrophage with an IC₅₀ of 33.26 μ M for free DFO and 184 μ M for

F2 DFO-NLC. Also, for HepG2 human liver cells, the presence of NLC improved the cell viability from an IC₅₀ of ABC µM for free DFO to 385 µM for free F2 DFO-NLCs. While in Caco-2 cells, both the free DFO drug and the DFO-NLCs did not induce any form of cellular toxicity up to a concentration of 1000 µM, as seen in Figure 3.7. This reduced cytotoxicity is particularly important for clinical applications, given that high doses of free DFO (>2.5 g per infusion) are associated with renal and hepatic complications, especially in elderly patients or those with preexisting organ impairments [90]. A type of intracellular protein called ferritin primarily stores iron, and the measurement of the ferritin concentration indirectly indicates the level of iron being stored in the body [90]. The ability of the DFO-NLCs to chelate excess iron was investigated with the use of a ferritin-specific ELISA assay. It was observed that F5 DFO-NLC chelated the most excess intracellular iron in comparison to free DFO, followed by F2 DFO-NLC, while F3 DFO-NLC chelated iron to a lesser degree (Figure 3.8). Also, the negative charge of the cross-linked polymers ensures enhanced uptake of NLC by Caco-2 cells, which can confer improved GIT permeation [129]. The human intestinal Caco-2 cell line, which is obtained from colorectal adenocarcinoma, can be used as an in vitro model for permeation studies due to its epithelial layer nature [130, 131]. We investigated the ability of the DFO-NLCs formulations to further increase the permeation ability of DFO with the Caco-2 cell line. It was observed that F2 DFO NLC, F3 DFO NLC, and F5 DFO NLC had an increased intestinal permeation compared to free DFO at 12 hrs. (Figure 3.9). Absorption of NLCs has been suggested to be due to their increase in permeability by surfactant, and adherence to the gut wall, which ultimately increases the ability to diffuse through the enterocytes of the small intestine [132-134]. While there was a transient change in the TEER values of the Caco-2 cell line, we observed that the values returned to normal after the removal of the DFO-NLCs, indicating no permanent damage.

3.6. Supplementary Information: DEVELOPMENT AND OPTIMIZATION OF NANOSTRUCTURED LIPID CARRIERS FOR ENHANCED ORAL ABSORPTION OF DEFEROXAMINE

S3.1. Materials and Instruments

Deferoxamine mesylate (DFO) was procured from Hospira, Inc. (Lake Forest, IL). Oleic acid, alginate, low molecular weight chitosan and poloxamer 188 were purchased from Sigma Aldrich (St. Louis, MO). Glyceryl mono oleate was donated by Gattefossé (Paramus, New Jersey). Ferric ammonium citrate (FAC) was purchased from VWR (Radnor, PA). The human epithelial colorectal adenocarcinoma (Caco-2), hepatoma (HepG2) and mouse macrophage (J774A.1) were purchased from the American Type Culture Collection (ATCC). Dulbecco's modified eagle medium (DMEM) with or without sodium pyruvate, penicillin/streptomycin solution (100×), nonessential amino acids (100×), heat-inactivated fetal bovine serum (FBS), Hank's Balanced Salt solution (HBSS), Dulbecco's Phosphate-Buffered Saline without CaCl₂ and MgCl₂, Resazurin, and Pierce BCA protein assay kit were purchased from Thermo Fisher Scientific Inc. The Human and Mouse ELISA kit was purchased from Immunology Consultants Laboratory, INC (Portland, OR). Ltd. The remaining reagents were procured from commercial sources and used without any additional purification.

Figure S3.2. A.

Experiment Constants

Constant Name	Constant Value	Units
DFO-API	1.0	*
ORGANIC PHASE	1.0	*

Experiment Design Matrix

Run No.	LIPID	AQUEOUS PHASE	SURFACTANT-POLOXAMER
1	5.00	15.00	1.00
2	5.00	10.00	1.50
3		15.00	1.50
	7.00		
4	3.00	5.00	1.50
5	3.00	10.00	1.00
6	7.00	5.00	0.50
7	5.00	10.00	0.50
8	5.00	5.00	1.00
9	3.00	15.00	1.50
10	5.00	10.00	1.00
11	5.00	10.00	1.00
12	5.00	10.00	1.00
13	7.00	5.00	1.50
14	3.00	15.00	0.50
15	7.00	10.00	1.00
16	7.00	15.00	0.50
17	3.00	5.00	0.50

Table S3.1. The experiment constants for the design of experiment included a drug: lipid ratio (1:3-1:7), organic: aqueous phase (1:5-1:15), and a surfactant concentration (0.5-1.5%). Table 1 shows the mixture variables output based on the experiment constants inputs that can be formulated. 15 runs were selected while run 11 and 12 were not selected because they were duplicates of run 10.

Table S3.2.

Variable Settings

Variable	Level Setting	
LIPID	7.00	
AQUEOUS PHASE	15.00	
SURFACTANT-POLOXAMER	1.50	

Predicted Results

Response Name	Goal	Predicted Result		
% DRUG LOADING	Maximize	28.08		
% ENCAPSULATION EFFICIENCY	Maximize	91.34		
PARTICLE SIZE(nm)	Minimize	281.34		

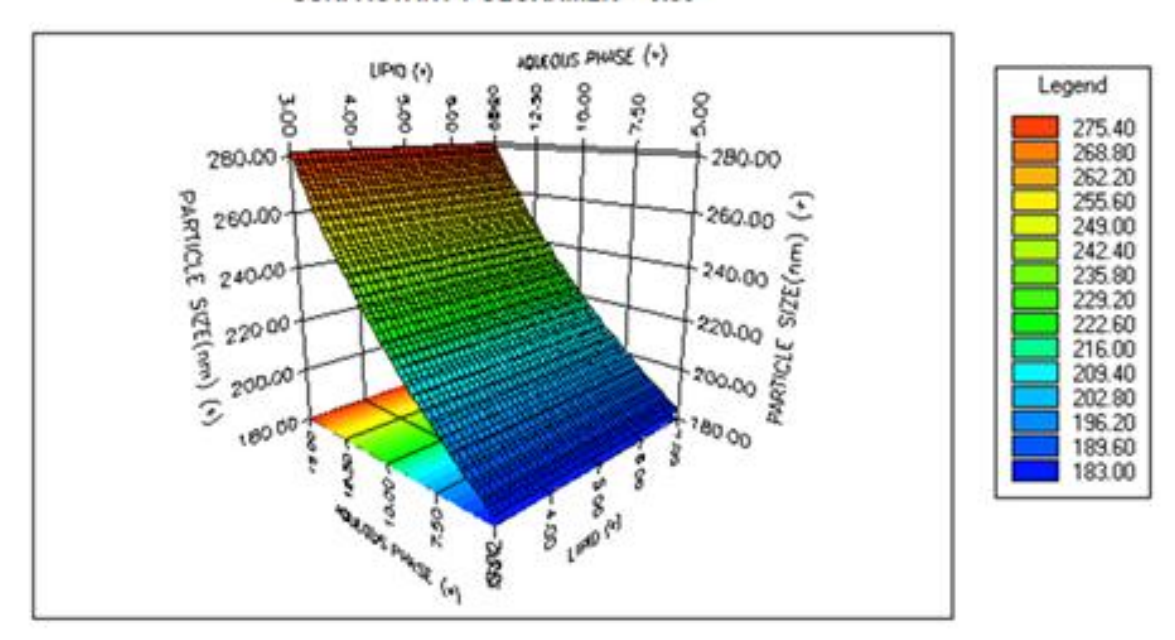
Cumulative Desirability Target = 1.0000 Cumulative Desirability Result = 0.8593

Table S3.2. Fusion pro predicted DFO-F2 as the overall best formulation with a drug: lipid ratio (1:7), organic: aqueous phase (1:15), and a surfactant concentration (1.5%). Table 1 shows the expected response values for Particle size, DL and EE.

Figure S3.1.A.

PARTICLE SIZE(nm) Response Surface SURFACTANT-POLOXAMER = 0.50

Fusion Pro Graph



PARTICLE SIZE(nm) Response Surface SURFACTANT-POLOXAMER = 1.00

Fusion Pro Graph

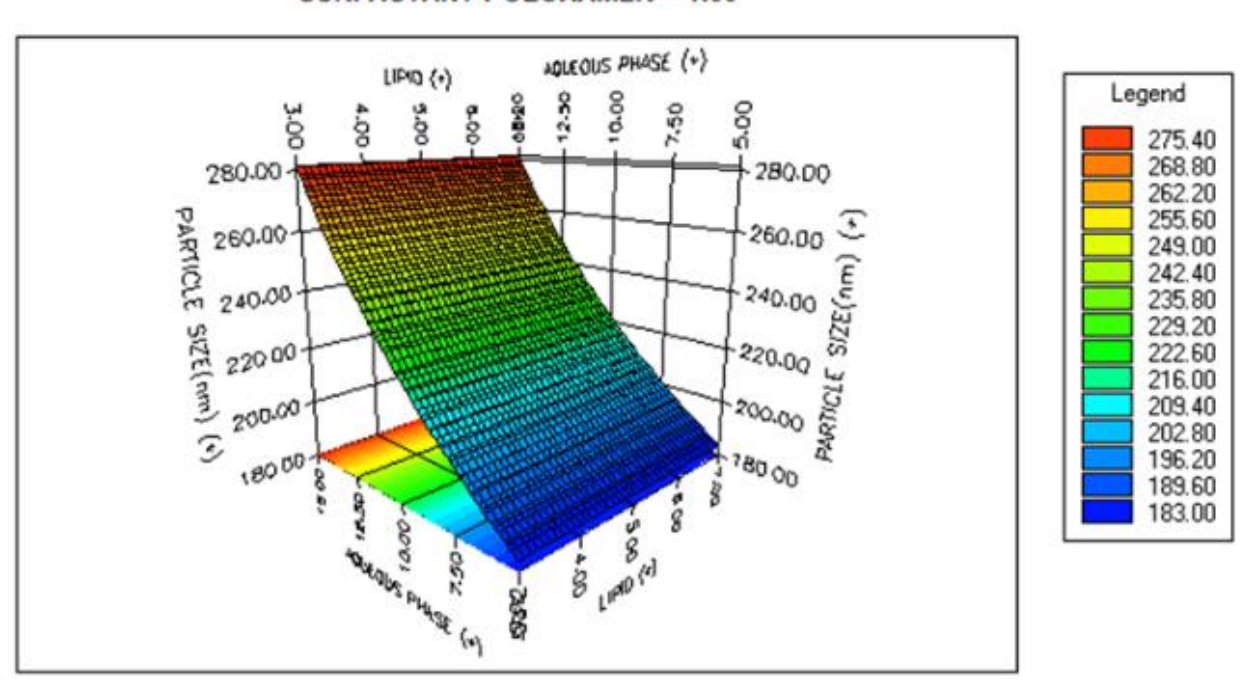


Figure S3.1B.

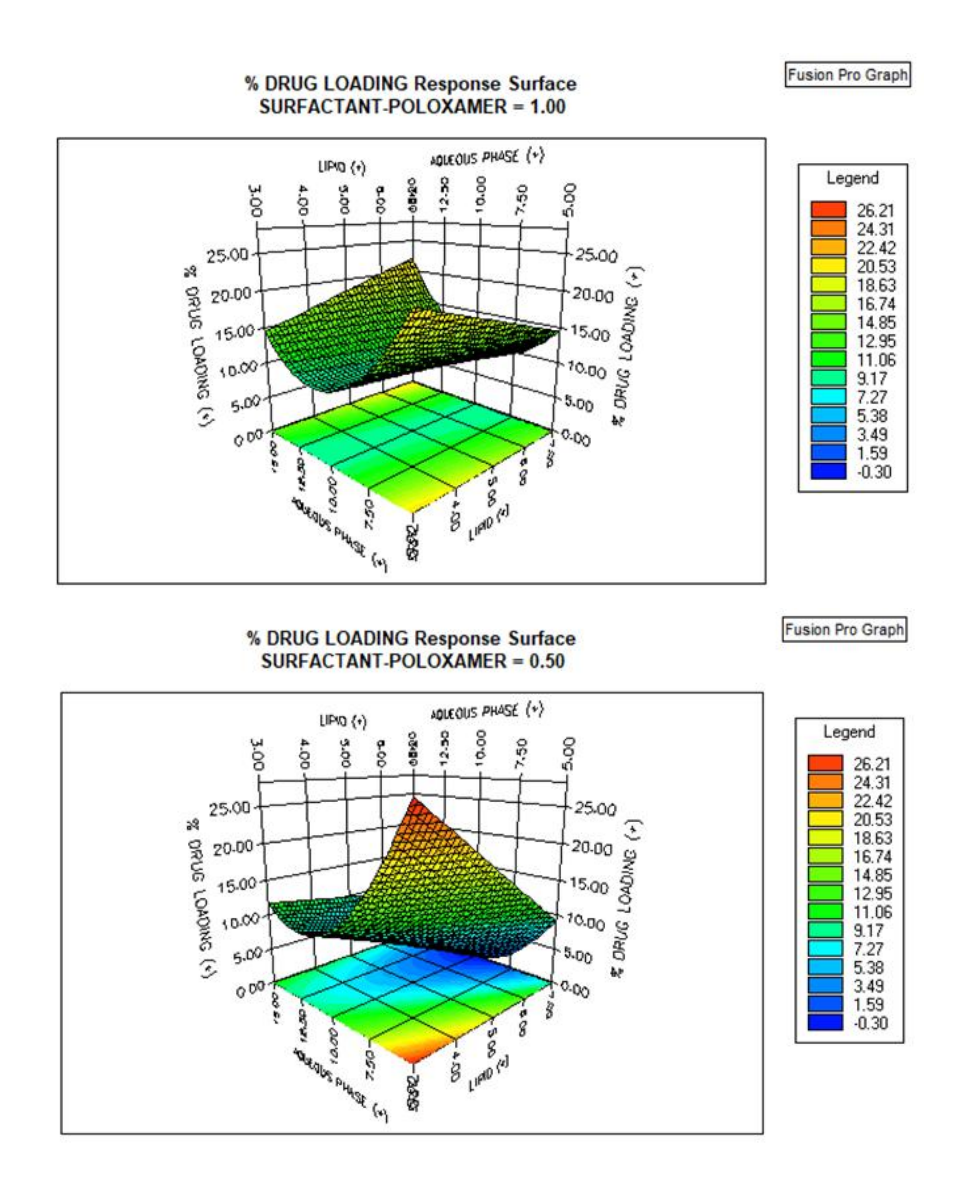


Figure S3.1. C.

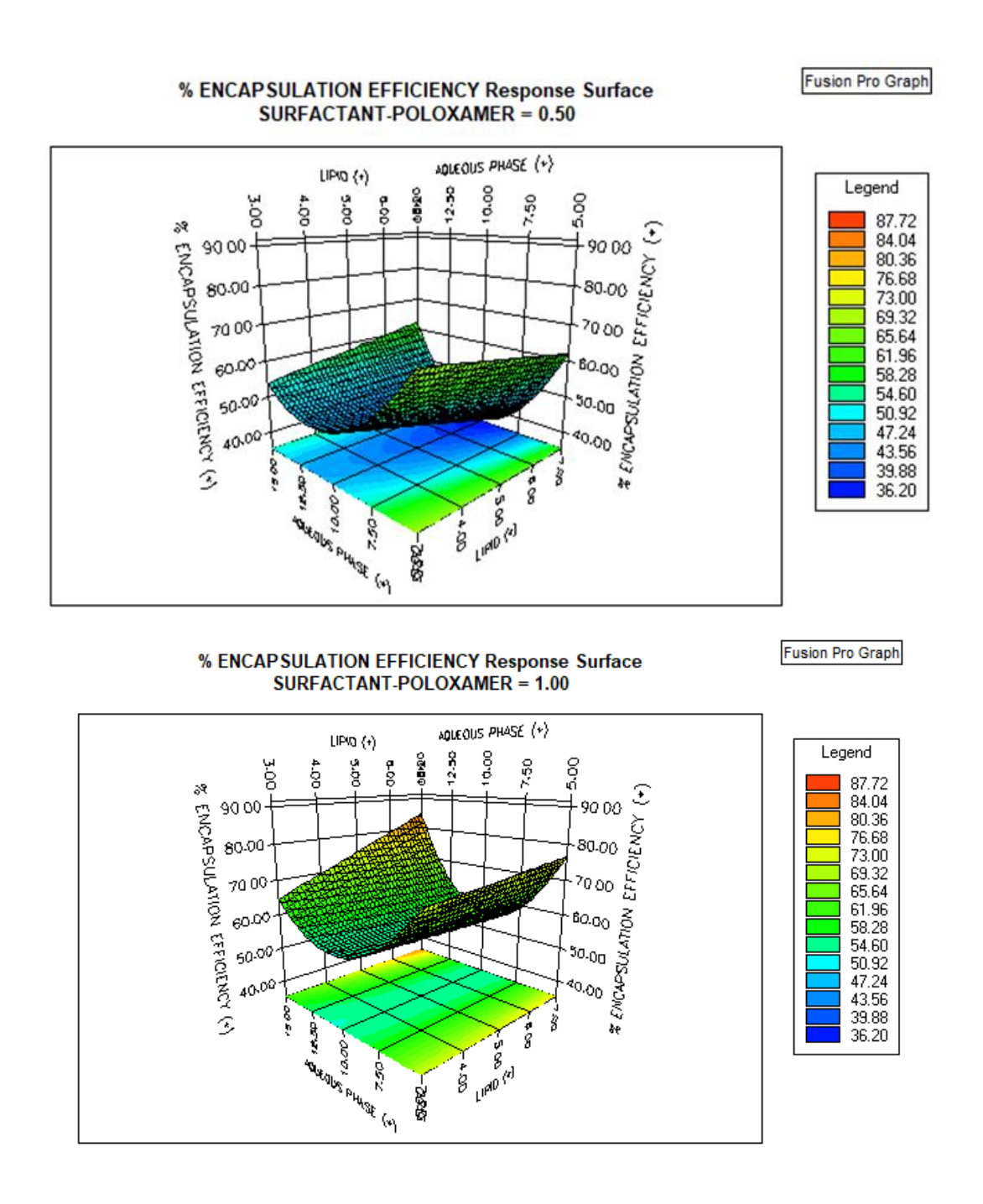


Figure S3.1. Three-dimensional (3D) response surface plots showing the effect of the variable on response (**A**) the effect of organic/aqueous phase ratio on particle size at a surfactant concentration

of 0.5-1.%. (**B**) The effect of organic/aqueous phase ratio on % DL at a surfactant concentration of 0.5-1.%. (**C**) the effect of organic/aqueous phase ratio on % EE at a surfactant concentration of 0.5-1.%.

CHAPTER 4

CONCLUSIONS

4.1. Bile Acid-Targeted Hyaluronic Acid Nanoparticles for Enhanced Oral Absorption of Deferoxamine

In this investigation, we have designed and evaluated HA nanoparticles through a self-assembly process to increase the absorption of deferoxamine. Previous research has indicated that HA itself exhibits strong adhesion to intestinal epithelial cells and thereby can enhance interactions between the carrier and the GIT wall [26]. To augment the oral absorption of DFO, we functionalized HA with BA (i.e., DOCA and TCA) and conjugated the HA-BA polymers with DFO to generate BA-HA-DFO nanoparticles. The first approach can be the use of a click chemistry-based reaction. Click chemistry has been described as an atom-economy reaction that produces high-yield results and selectivity. This will be done by coupling a hydroxyl group with the amino group of DFO. Studies have shown that click chemistry can increase the conjugation ratio for HA [28-30]. Another approach can be done by coupling the hydroxyl group on the HA backbone to the amino group on DFO with the use of borate buffer, chloride, and sodium triacetoxyhydroborate (STAB) with constant stirring for 4 days.

The creation of an oral DFO delivery system utilizing intestinal permeable nanocarriers holds promise for addressing the challenges associated with DFO's oral delivery. Up to 35% of aldehyde groups were created on HA backbones, and this was the rate-limiting step for the percentage of DFO conjugated to the HA backbone. To overcome this caveat, an alternative approach can be considered for conjugating DFO to the HA backbone.

4.2 Development and Optimization of Nanostructured Lipid Carriers for Enhanced Oral Absorption of Deferoxamine

In this study, we have been able to design and demonstrate that NLCs coated with chitosan crosslinked with alginate and formulated by a solvent diffusion technique can be used to increase the drug loading and encapsulation of a hydrophilic drug, specifically deferoxamine. The design of the experiment was also used to introduce quality by design into our investigation while accommodating all possible variables that could impact our response values. We further observed that the NLC ensured a controlled release rate of DFO from the formulation and an improved permeation across the Caco-2 cell line, which is representative of the small intestine, while improving the cell viability profile of DFO. This approach offers a promising strategy for overcoming the limitations of DFO's oral bioavailability in the management of either acquired or acquired hemochromatosis.

While comparing the effectiveness of the two strategies, it was observed that the polymeric conjugates had better gastrointestinal permeation when compared to nanostructured lipid carriers for the oral delivery of DFO. Apical sodium-dependent bile acid transporter-mediated endocytosis through binding of either taurocholic acid or deoxycholic acid is the proposed mechanism for the bile acid—targeted hyaluronic acid nanoparticles for enhanced oral absorption of deferoxamine project while the ability of chitosan to open up tight junctions and increase paracellular absorption of DFO is the proposed mechanism for the development and optimization of nanostructured lipid carriers for enhanced oral absorption of deferoxamine project as seen in **figure 4.1**. This holds a promising opportunity for translational studies for the oral delivery of DFO and larger molecules (peptides, antibodies, proteins, genes).

	Bile Acid-Targeted Hyaluronic Acid Nanoparticles for Enhanced Oral Absorption of Deferoxamine	Development and Optimization of Nanostructured Lipid Carriers for Enhanced Oral Absorption of Deferoxamine
Particle size	Smaller particle sizes	Larger particle sizes
Percentage DFO loading	Up to 42%	Up to 29%
Cytotoxicity	Taurocholic acid improved the cytocompatibility better when compared with deoxycholic acid	Lesser cytocompatibility when compared with bile acid—targeted hyaluronic acid nanoparticles
Absorption profile	Increased oral absorption of deferoxamine up to 33% at 24 hours	Increased oral absorption of deferoxamine up to 23% at 12 hours
Proposed Mechanism of action	Apical sodium-dependent bile acid transporter-mediated endocytosis through binding of either taurocholic acid or deoxycholic acid	Chitosan can open up tight junctions and increase paracellular absorption of DFO

Table 4.1: Comparison of the bile acid–targeted hyaluronic acid nanoparticles for enhanced oral absorption of deferoxamine efficiency and development and optimization of nanostructured lipid carriers for enhanced oral absorption of deferoxamine project

REFERENCES

- 1. Boldt, D.H., *New perspectives on iron: an introduction*. The American journal of the medical sciences, 1999. **318**(4): p. 207-212.
- 2. Briguglio, M., et al., *The central role of iron in human nutrition: from folk to contemporary medicine*. Nutrients, 2020. **12**(6): p. 1761.
- 3. Yun, S. and N.D. Vincelette, *Update on iron metabolism and molecular perspective of common genetic and acquired disorder, hemochromatosis*. Critical reviews in oncology/hematology, 2015. **95**(1): p. 12-25.
- 4. Pietrangelo, A., *Hereditary hemochromatosis: pathogenesis, diagnosis, and treatment.* Gastroenterology, 2010. **139**(2): p. 393-408. e2.
- 5. Adams, P.C. and J.C. Barton, *How I treat hemochromatosis*. Blood, The Journal of the American Society of Hematology, 2010. **116**(3): p. 317-325.
- 6. Chacon, A.H., B. Morrison, and S. Hu, *Acquired hemochromatosis with pronounced pigment deposition of the upper eyelids*. The Journal of clinical and aesthetic dermatology, 2013. **6**(10): p. 44.
- 7. Brissot, P., et al., *Current approach to hemochromatosis*. Blood reviews, 2008. **22**(4): p. 195-210.
- 8. Liu, Z., et al., *Enzymatically Biodegradable Polyrotaxane–Deferoxamine Conjugates for Iron Chelation*. ACS applied materials & interfaces, 2016. **8**(39): p. 25788-25797.
- 9. Salimi, A., B.S.M. Zadeh, and M. Kazemi, *Preparation and optimization of polymeric micelles as an oral drug delivery system for deferoxamine mesylate: In vitro: and: Ex vivo: Studies.* Research in pharmaceutical sciences, 2019. **14**(4): p. 293-307.
- 10. Neufeld, E.J., Oral chelators deferasirox and deferiprone for transfusional iron overload in thalassemia major: new data, new questions. Blood, 2006. **107**(9): p. 3436-3441.
- 11. Gupta, H., D. Bhandari, and A. Sharma, *Recent trends in oral drug delivery: a review.* Recent patents on drug delivery & formulation, 2009. **3**(2): p. 162-173.
- 12. Alqahtani, M.S., et al., *Advances in oral drug delivery*. Frontiers in pharmacology, 2021. **12**: p. 618411.
- 13. Lou, J., et al., Advances in oral drug delivery systems: Challenges and opportunities. Pharmaceutics, 2023. **15**(2): p. 484.
- 14. Sastry, S.V., J.R. Nyshadham, and J.A. Fix, *Recent technological advances in oral drug delivery—a review.* Pharmaceutical science & technology today, 2000. **3**(4): p. 138-145.
- 15. Homayun, B., X. Lin, and H.-J. Choi, *Challenges and recent progress in oral drug delivery systems for biopharmaceuticals.* Pharmaceutics, 2019. **11**(3): p. 129.
- 16. Zhang, L., et al., *Nanocarriers for oral drug delivery*. Journal of drug targeting, 2013. **21**(6): p. 515-527.
- 17. Aguilera-Garrido, A., et al., *Mucoadhesive properties of liquid lipid nanocapsules enhanced by hyaluronic acid.* Journal of Molecular Liquids, 2019. **296**: p. 111965.

- 18. Plapied, L., et al., *Fate of polymeric nanocarriers for oral drug delivery.* Current opinion in colloid & interface science, 2011. **16**(3): p. 228-237.
- 19. Reinholz, J., K. Landfester, and V. Mailänder, *The challenges of oral drug delivery via nanocarriers*. Drug delivery, 2018. **25**(1): p. 1694-1705.
- 20. Nagavarma, B., et al., *Different techniques for preparation of polymeric nanoparticles-a review.* Asian J. Pharm. Clin. Res, 2012. **5**(3): p. 16-23.
- 21. He, C., et al., Size-dependent absorption mechanism of polymeric nanoparticles for oral delivery of protein drugs. Biomaterials, 2012. **33**(33): p. 8569-8578.
- 22. Alai, M.S., W.J. Lin, and S.S. Pingale, *Application of polymeric nanoparticles and micelles in insulin oral delivery.* Journal of food and drug analysis, 2015. **23**(3): p. 351-358.
- 23. Wu, H., et al., *Hyaluronic-Acid-Coated Chitosan Nanoparticles for Insulin Oral Delivery: Fabrication, Characterization, and Hypoglycemic Ability.* Macromolecular Bioscience, 2022. **22**(7): p. 2100493.
- 24. Wang, S., et al., pH-responsive and mucoadhesive nanoparticles for enhanced oral insulin delivery: the effect of hyaluronic acid with different molecular weights. Pharmaceutics, 2023. **15**(3): p. 820.
- 25. Han, L., et al., *Insulin-loaded pH-sensitive hyaluronic acid nanoparticles enhance transcellular delivery.* Aaps Pharmscitech, 2012. **13**: p. 836-845.
- 26. Chen, Z., et al., Overcoming multiple absorption barrier for insulin oral delivery using multifunctional nanoparticles based on chitosan derivatives and hyaluronic acid. International journal of nanomedicine, 2020: p. 4877-4898.
- 27. Lu, Y., et al., *Double layer spherical nanoparticles with hyaluronic acid coating to enhance oral delivery of exenatide in T2DM rats*. European Journal of Pharmaceutics and Biopharmaceutics, 2023. **191**: p. 205-218.
- 28. Xiao, B., et al., *Orally targeted delivery of tripeptide KPV via hyaluronic acid*functionalized nanoparticles efficiently alleviates ulcerative colitis. Molecular Therapy, 2017. **25**(7): p. 1628-1640.
- 29. Hussein, H.A. and M.A. Abdullah, *Novel drug delivery systems based on silver nanoparticles, hyaluronic acid, lipid nanoparticles and liposomes for cancer treatment*. Applied nanoscience, 2022. **12**(11): p. 3071-3096.
- 30. Chen, M.-C., et al., A review of the prospects for polymeric nanoparticle platforms in oral insulin delivery. Biomaterials, 2011. **32**(36): p. 9826-9838.
- 31. Wang, Y., et al., *Polymeric nanoparticles (PNPs) for oral delivery of insulin*. Journal of Nanobiotechnology, 2024. **22**(1): p. 1.
- 32. Bhujbal, S. and A.K. Dash, *Metformin-loaded hyaluronic acid nanostructure for oral delivery.* AAPS PharmSciTech, 2018. **19**: p. 2543-2553.
- Dodero, A., et al., An up-to-date review on alginate nanoparticles and nanofibers for biomedical and pharmaceutical applications. Advanced Materials Interfaces, 2021.
 8(22): p. 2100809.
- 34. Sosnik, A., Alginate particles as platform for drug delivery by the oral route: state-of-the-art. International Scholarly Research Notices, 2014. **2014**(1): p. 926157.

- 35. Chia, J.J., et al., *Preparation and application of cross-linked alginate nanoparticles as drug carrier: A review.* Journal of Research in Nanoscience and Nanotechnology, 2022. **5**(1): p. 1-11.
- 36. Paques, J.P., et al., *Preparation methods of alginate nanoparticles*. Advances in colloid and interface science, 2014. **209**: p. 163-171.
- 37. Le Devedec, F., et al., *Aggregation behavior of pegylated bile acid derivatives*. Langmuir, 2012. **28**(37): p. 13431-13440.
- 38. Nemati, M., et al., *Bile acid-based advanced drug delivery systems, bilosomes and micelles as novel carriers for therapeutics*. Cell Biochemistry and Function, 2022. **40**(6): p. 623-635.
- 39. Velmurugan, R. and S. Selvamuthukumar, Development and optimization of ifosfamide nanostructured lipid carriers for oral delivery using response surface methodology. Applied nanoscience, 2016. **6**: p. 159-173.
- 40. Rassu, G., et al., *Nose-to-brain delivery of BACE1 siRNA loaded in solid lipid nanoparticles for Alzheimer's therapy.* Colloids and Surfaces B: Biointerfaces, 2017. **152**: p. 296-301.
- 41. Tian, H., et al., *Uniform core*—shell nanoparticles with thiolated hyaluronic acid coating to enhance oral delivery of insulin. Advanced healthcare materials, 2018. **7**(17): p. 1800285.
- 42. Zhang, M., et al., *The enhancing effect of N-acetylcysteine modified hyaluronic acid-octadecylamine micelles on the oral absorption of paclitaxel*. International journal of biological macromolecules, 2019. **138**: p. 636-647.
- 43. Wang, Y., et al., Nanogel-DFO conjugates as a model to investigate pharmacokinetics, biodistribution, and iron chelation in vivo. International journal of pharmaceutics, 2018. **538**(1-2): p. 79-86.
- 44. Liu, Z., et al., ROS-triggered degradable iron-chelating nanogels: Safely improving iron elimination in vivo. Journal of Controlled Release, 2018. **283**: p. 84-93.
- 45. Royal, C.D., et al., Sickle cell disease is a global prototype for integrative research and healthcare. Advanced Genetics, 2021. **2**(1): p. e10037.
- 46. Farshadpour, F., R. Taherkhani, and H. Farajzadeh, *Hepatitis B infection among β-thalassemia major patients in Bushehr province of southern Iran*. Journal of Immunoassay and Immunochemistry, 2023. **44**(2): p. 147-161.
- 47. USFD:, A. FDA approves first gene therapies to treat patients with sickle cell disease.

 . 2023 [cited 2023; Available from: https://www.fda.gov/news-events/press-announcements/fda-approves-first-gene-therapies-treat-patients-sickle-cell-disease.
- 48. Sheridan, C., *The world's first CRISPR therapy is approved: who will receive it.* Nat Biotechnol, 2024. **42**(1): p. 3-4.
- 49. Liu, Z., et al., Reactive oxygen species-triggered dissociation of a polyrotaxane-based nanochelator for enhanced clearance of systemic and hepatic iron. ACS nano, 2020. **15**(1): p. 419-433.

- 50. Hershko, C., et al., *Objectives and methods of iron chelation therapy*. Bioinorganic chemistry and applications, 2003. **1**(2): p. 151.
- 51. Pawlaczyk, M. and G. Schroeder, *Deferoxamine-modified hybrid materials for direct chelation of Fe (III) ions from aqueous solutions and indication of the competitiveness of in vitro complexing toward a biological system*. ACS omega, 2021. **6**(23): p. 15168-15181.
- 52. Poggiali, E., et al., *An update on iron chelation therapy.* Blood Transfusion, 2012. **10**(4): p. 411.
- 53. Farr, A.C. and M.P. Xiong, Challenges and opportunities of deferoxamine delivery for treatment of Alzheimer's disease, Parkinson's disease, and intracerebral hemorrhage. Molecular pharmaceutics, 2020. **18**(2): p. 593-609.
- 54. Liu, L., et al., Hyaluronic acid–zein core-shell nanoparticles improve the anticancer effect of curcumin alone or in combination with oxaliplatin against colorectal cancer via CD44-mediated cellular uptake. Molecules, 2022. **27**(5): p. 1498.
- 55. Zhao, L., et al., An efficient pH sensitive oral insulin delivery system enhanced by deoxycholic acid. Journal of Controlled Release, 2011. **152**: p. e184-e186.
- 56. Lei, C., et al., *Hyaluronic acid and albumin based nanoparticles for drug delivery.* Journal of Controlled Release, 2021. **331**: p. 416-433.
- 57. Yegappan, R., et al., *Nano polydopamine crosslinked thiol-functionalized hyaluronic acid hydrogel for angiogenic drug delivery.* Colloids and Surfaces B: Biointerfaces, 2019. **177**: p. 41-49.
- 58. Zhu, J., et al., *Applications and delivery mechanisms of hyaluronic acid used for topical/transdermal delivery—a review.* International journal of pharmaceutics, 2020. **578**: p. 119127.
- 59. Buckley, C., et al., *Hyaluronic acid: A review of the drug delivery capabilities of this naturally occurring polysaccharide.* Polymers, 2022. **14**(17): p. 3442.
- 60. Huang, P., et al., *Improving the oral delivery efficiency of anticancer drugs by chitosan coated polycaprolactone-grafted hyaluronic acid nanoparticles*. Journal of Materials Chemistry B, 2014. **2**(25): p. 4021-4033.
- 61. de Souza, A.B., M.V. Chaud, and M.H.A. Santana, *Hyaluronic acid behavior in oral administration and perspectives for nanotechnology-based formulations: A review.* Carbohydrate polymers, 2019. **222**: p. 115001.
- 62. Huang, G. and H. Huang, *Application of hyaluronic acid as carriers in drug delivery.*Drug delivery, 2018. **25**(1): p. 766-772.
- 63. Samstein, R.M., et al., *The use of deoxycholic acid to enhance the oral bioavailability of biodegradable nanoparticles.* Biomaterials, 2008. **29**(6): p. 703-708.
- 64. Li, Z., et al., Development of Liposome containing sodium deoxycholate to enhance oral bioavailability of itraconazole. asian journal of pharmaceutical sciences, 2017. **12**(2): p. 157-164.
- 65. Stojančević, M., et al., *Application of bile acids in drug formulation and delivery.* Frontiers in Life Science, 2013. **7**(3-4): p. 112-122.

- 66. Hanafi, N.I., et al., Overview of bile acids signaling and perspective on the signal of ursodeoxycholic acid, the most hydrophilic bile acid, in the heart. Biomolecules, 2018. **8**(4): p. 159.
- 67. Roda, A., et al., *Bile acid structure-activity relationship: evaluation of bile acid lipophilicity using 1-octanol/water partition coefficient and reverse phase HPLC.* Journal of lipid research, 1990. **31**(8): p. 1433-1443.
- 68. Nurunnabi, M., et al., *Design and strategies for bile acid mediated therapy and imaging*. RSC advances, 2016. **6**(78): p. 73986-74002.
- 69. Han, X., et al., Liver-targeting self-assembled hyaluronic acid-glycyrrhetinic acid micelles enhance hepato-protective effect of silybin after oral administration. Drug Delivery, 2016. **23**(5): p. 1818-1829.
- 70. Li, N.-N., C.-P. Fu, and L.-M. Zhang, *Using casein and oxidized hyaluronic acid to form biocompatible composite hydrogels for controlled drug release.* Materials Science and Engineering: C, 2014. **36**: p. 287-293.
- 71. Ossipov, D.A., et al., Functionalization of hyaluronic acid with chemoselective groups via a disulfide-based protection strategy for in situ formation of mechanically stable hydrogels. Biomacromolecules, 2010. **11**(9): p. 2247-2254.
- 72. Ujhelyi, Z., et al., Evaluation of cytotoxicity of surfactants used in self-micro emulsifying drug delivery systems and their effects on paracellular transport in Caco-2 cell monolayer. European Journal of Pharmaceutical Sciences, 2012. **47**(3): p. 564-573.
- 73. Li, J., et al., Redox-sensitive micelles self-assembled from amphiphilic hyaluronic acid-deoxycholic acid conjugates for targeted intracellular delivery of paclitaxel. Biomaterials, 2012. **33**(7): p. 2310-2320.
- 74. Dong, X. and C. Liu, *Preparation and Characterization of Self-Assembled Nanoparticles of Hyaluronic Acid-Deoxycholic Acid Conjugates*. Journal of Nanomaterials, 2010. **2010**(1): p. 906936.
- 75. Lee, E., et al., *Polyproline-type helical-structured low-molecular weight heparin (LMWH)-taurocholate conjugate as a new angiogenesis inhibitor.* International journal of cancer, 2009. **124**(12): p. 2755-2765.
- 76. Wei, W.-H., X.-M. Dong, and C.-G. Liu, *In vitro investigation of self-assembled nanoparticles based on hyaluronic acid-deoxycholic acid conjugates for controlled release doxorubicin: effect of degree of substitution of deoxycholic acid.* International journal of molecular sciences, 2015. **16**(4): p. 7195-7209.
- 77. Lai, J.-Y., Biofunctionalization of gelatin microcarrier with oxidized hyaluronic acid for corneal keratocyte cultivation. Colloids and Surfaces B: Biointerfaces, 2014. **122**: p. 277-286.
- 78. Cui, S., et al., *Oral Non-absorbable Polymer–Deferoxamine Conjugates for Reducing Dietary Iron Absorption*. Molecular Pharmaceutics, 2023. **20**(2): p. 1285-1295.
- 79. Li, L., et al., Biodegradable and injectable in situ cross-linking chitosan-hyaluronic acid based hydrogels for postoperative adhesion prevention. Biomaterials, 2014. **35**(12): p. 3903-3917.

- 80. Brittenham, G.M., *Iron-chelating therapy for transfusional iron overload*. New England Journal of Medicine, 2011. **364**(2): p. 146-156.
- 81. Bayanzay, K. and L. Alzoebie, *Reducing the iron burden and improving survival in transfusion-dependent thalassemia patients: current perspectives.* Journal of blood medicine, 2016: p. 159-169.
- 82. Annaba, F., et al., *Green tea catechin EGCG inhibits ileal apical sodium bile acid transporter ASBT.* American Journal of Physiology-Gastrointestinal and Liver Physiology, 2010. **298**(3): p. G467-G473.
- 83. Yao, W., et al., *Deoxycholic acid-functionalised nanoparticles for oral delivery of rhein*. European Journal of Pharmaceutical Sciences, 2021. **159**: p. 105713.
- 84. Park, J., et al., *Bile acid transporter mediated endocytosis of oral bile acid conjugated nanocomplex.* Biomaterials, 2017. **147**: p. 145-154.
- 85. Kim, S.K., et al., *Oral delivery of chemical conjugates of heparin and deoxycholic acid in aqueous formulation.* Thrombosis research, 2006. **117**(4): p. 419-427.
- 86. Kim, S.K., et al., *Physicochemical conjugation with deoxycholic acid and dimethylsulfoxide for heparin oral delivery.* Bioconjugate Chemistry, 2011. **22**(7): p. 1451-1458.
- 87. Khatun, Z., et al., *Oral absorption mechanism and anti-angiogenesis effect of taurocholic acid-linked heparin-docetaxel conjugates.* Journal of controlled release, 2014. **177**: p. 64-73.
- 88. Gupta, A., Secondary Hemochromatosis, in Decision Making Through Problem Based Learning in Hematology: A Step-by-Step Approach in patients with Anemia. 2024, Springer. p. 259-268.
- 89. Szczerbinska, A., et al., *Hemochromatosis—How Not to Overlook and Properly Manage "Iron People"—A Review.* Journal of Clinical Medicine, 2024. **13**(13): p. 3660.
- 90. Agboluaje, E.O., et al., *Bile Acid–Targeted Hyaluronic Acid Nanoparticles for Enhanced Oral Absorption of Deferoxamine*. The AAPS Journal, 2024. **26**(3): p. 46.
- 91. Liu, Z., et al., Oxidation-induced degradable nanogels for iron chelation. Scientific reports, 2016. **6**(1): p. 20923.
- 92. Marupudi, N. and M.P. Xiong, Genetic targets and applications of iron chelators for neurodegeneration with brain iron accumulation. ACS Bio & Med Chem Au, 2024. **4**(3): p. 119-130.
- 93. Salimi, A., B.S.M. Zadeh, and M. Kazemi, *Preparation and optimization of polymeric micelles as an oral drug delivery system for deferoxamine mesylate: In vitro and ex vivo studies*. Research in pharmaceutical sciences, 2019. **14**(4): p. 293.
- 94. Das, S. and A. Chaudhury, Recent advances in lipid nanoparticle formulations with solid matrix for oral drug delivery. Aaps Pharmscitech, 2011. **12**: p. 62-76.
- 95. Müller, R., M. Radtke, and S. Wissing, *Nanostructured lipid matrices for improved microencapsulation of drugs*. International journal of pharmaceutics, 2002. **242**(1-2): p. 121-128.

- 96. Hatem, S. and M. El-Kayal, *Novel anti-psoriatic nanostructured lipid carriers for the cutaneous delivery of luteolin: A comprehensive in-vitro and in-vivo evaluation*. European Journal of Pharmaceutical Sciences, 2023. **191**: p. 106612.
- 97. Ahalwat, S., et al., Mannose-Functionalized Isoniazid-Loaded Nanostructured Lipid Carriers for Pulmonary Delivery: In Vitro Prospects and In Vivo Therapeutic Efficacy Assessment. Pharmaceuticals, 2023. **16**(8): p. 1108.
- 98. Qizilbash, F.F., et al., *Thymoquinone-enriched naringenin-loaded nanostructured lipid carrier for brain delivery via nasal route: in vitro prospect and in vivo therapeutic efficacy for the treatment of depression.* Pharmaceutics, 2022. **14**(3): p. 656.
- 99. Rosli, N.A., R. Hasham, and A.A. Aziz, *Design and physicochemical evaluation of nanostructured lipid carrier encapsulated zingiber zerumbet oil by d-optimal mixture design.* Jurnal Teknologi (Sciences & Engineering), 2018. **80**(3).
- 100. Correia, A., et al., *Design of experiment (DoE) of mucoadhesive valproic acid-loaded nanostructured lipid carriers (NLC) for potential nose-to-brain application.*International Journal of Pharmaceutics, 2024. **664**: p. 124631.
- 101. Siahdasht, F.N., et al., *Enhanced delivery of melatonin loaded nanostructured lipid carriers during in vitro fertilization: NLC formulation, optimization and IVF efficacy.* RSC advances, 2020. **10**(16): p. 9462-9475.
- 102. Ahalwat, S. and D.C. Bhatt, *Development of novel lipid matrix for improved sustained release effect of a hydrophilic drug via response surface methodology.* Journal of Drug Delivery Science and Technology, 2022. **67**: p. 102993.
- 103. Kang, T., et al., *Physical, chemical, and biological characterization of ginsenoside F1 incorporated in nanostructured lipid carrier.* Journal of Food Biochemistry, 2021. **45**(8): p. e13860.
- 104. Khorrami, N.K., et al., Fabrication and characterization of alginate-based films functionalized with nanostructured lipid carriers. International Journal of Biological Macromolecules, 2021. **182**: p. 373-384.
- 105. Senna, J.P., et al., *Dual alginate-lipid nanocarriers as oral delivery systems for amphotericin B.* Colloids and Surfaces B: Biointerfaces, 2018. **166**: p. 187-194.
- 106. Werle, M., H. Takeuchi, and A. Bernkop-Schnürch, *Modified chitosans for oral drug delivery*. Journal of pharmaceutical sciences, 2009. **98**(5): p. 1643-1656.
- 107. Cunha, S., et al., Double optimization of rivastigmine-loaded nanostructured lipid carriers (NLC) for nose-to-brain delivery using the quality by design (QbD) approach: formulation variables and instrumental parameters. Pharmaceutics, 2020. **12**(7): p. 599.
- 108. Ahl, P.L., et al., Accelerating vaccine formulation development using design of experiment stability studies. Journal of Pharmaceutical Sciences, 2016. **105**(10): p. 3046-3056.
- 109. Kim, S., et al., Development and optimization of imiquimod-loaded nanostructured lipid carriers using a hybrid design of experiments approach. International Journal of Nanomedicine, 2023: p. 1007-1029.

- 110. Gadgil, P., J. Shah, and D.-L. Chow, *Enhanced brain delivery with lower hepatic exposure of lazaroid loaded nanostructured lipid carriers developed using a design of experiment approach*. International Journal of Pharmaceutics, 2018. **544**(1): p. 265-277.
- 111. Matarazzo, A.P., et al., Development of a Versatile Nanostructured Lipid Carrier (NLC) Using Design of Experiments (DoE)—Part II: Incorporation and Stability of Butamben with Different Surfactants. Pharmaceutics, 2024. **16**(7): p. 863.
- 112. Subramaniam, B., Z.H. Siddik, and N.H. Nagoor, *Optimization of nanostructured lipid carriers: Understanding the types, designs, and parameters in the process of formulations*. Journal of nanoparticle research, 2020. **22**: p. 1-29.
- 113. Hwang, R. and R.M. Noack, *Application of design of experiments to pharmaceutical formulation development*. International Journal of Experimental Design and Process Optimisation, 2011. **2**(1): p. 58-65.
- 114. Zhang, X., et al., Formulation optimization of dihydroartemisinin nanostructured lipid carrier using response surface methodology. Powder Technology, 2010. **197**(1-2): p. 120-128.
- 115. Cui, S., J. Qiao, and M.P. Xiong, *Antibacterial and biofilm-eradicating activities of pH-responsive vesicles against Pseudomonas aeruginosa*. Molecular Pharmaceutics, 2022. **19**(7): p. 2406-2417.
- 116. Hubatsch, I., E.G. Ragnarsson, and P. Artursson, *Determination of drug permeability* and prediction of drug absorption in Caco-2 monolayers. Nature protocols, 2007. **2**(9): p. 2111-2119.
- 117. Hashiba, A., et al., The use of design of experiments with multiple responses to determine optimal formulations for in vivo hepatic mRNA delivery. Journal of Controlled Release, 2020. **327**: p. 467-476.
- 118. Umemura, M., et al., *The iron chelating agent, deferoxamine detoxifies Fe (Salen)-induced cytotoxicity.* Journal of pharmacological sciences, 2017. **134**(4): p. 203-210.
- 119. Wanule, D., et al., Extraction and FTIR analysis of chitosan from American cockroach, Periplaneta americana. Extraction, 2014. **3**(3): p. 299-304.
- 120. Corazzari, I., et al., Advanced physico-chemical characterization of chitosan by means of TGA coupled on-line with FTIR and GCMS: Thermal degradation and water adsorption capacity. Polymer Degradation and Stability, 2015. **112**: p. 1-9.
- 121. Ng, W.S., et al., *Biocompatible polyurethane scaffolds prepared from glycerol monostearate-derived polyester polyol*. Journal of Polymers and the Environment, 2018. **26**: p. 2881-2900.
- 122. Kumar, R. and A. Philip, *Gastroretentive dosage forms for prolonging gastric residence time*. International Journal of Pharmaceutical Medicine, 2007. **21**: p. 157-171.
- 123. Boyd, B.J., et al., Lyotropic liquid crystalline phases formed from glycerate surfactants as sustained release drug delivery systems. International journal of pharmaceutics, 2006. **309**(1-2): p. 218-226.

- 124. Sannan, T., K. Kurita, and Y. Iwakura, *Studies on chitin, 2. Effect of deacetylation on solubility.* Die Makromolekulare Chemie: Macromolecular Chemistry and Physics, 1976. **177**(12): p. 3589-3600.
- 125. Thanou, M., J. Verhoef, and H. Junginger, *Chitosan and its derivatives as intestinal absorption enhancers*. Advanced drug delivery reviews, 2001. **50**: p. S91-S101.
- 126. Budhian, A., S.J. Siegel, and K.I. Winey, *Haloperidol-loaded PLGA nanoparticles:* systematic study of particle size and drug content. International journal of pharmaceutics, 2007. **336**(2): p. 367-375.
- 127. Li, Q., et al., A review of the structure, preparation, and application of NLCs, PNPs, and PLNs. Nanomaterials, 2017. **7**(6): p. 122.
- 128. Song, X., et al., *Dual agents loaded PLGA nanoparticles: systematic study of particle size and drug entrapment efficiency.* European journal of pharmaceutics and biopharmaceutics, 2008. **69**(2): p. 445-453.
- 129. Gaumet, M., R. Gurny, and F. Delie, *Localization and quantification of biodegradable particles in an intestinal cell model: the influence of particle size.* European Journal of Pharmaceutical Sciences, 2009. **36**(4-5): p. 465-473.
- 130. Vieira, R., et al., Sucupira oil-loaded nanostructured lipid carriers (NLC): Lipid screening, factorial design, release profile, and cytotoxicity. Molecules, 2020. **25**(3): p. 685.
- 131. Nasirizadeh, S. and B. Malaekeh-Nikouei, *Solid lipid nanoparticles and nanostructured lipid carriers in oral cancer drug delivery.* Journal of Drug Delivery Science and Technology, 2020. **55**: p. 101458.
- 132. Li, H., et al., Size-exclusive effect of nanostructured lipid carriers on oral drug delivery. International journal of pharmaceutics, 2016. **511**(1): p. 524-537.
- 133. Zhang, T., et al., Characterization and evaluation of nanostructured lipid carrier as a vehicle for oral delivery of etoposide. European journal of pharmaceutical sciences, 2011. **43**(3): p. 174-179.
- 134. Jaiswal, P., B. Gidwani, and A. Vyas, *Nanostructured lipid carriers and their current application in targeted drug delivery.* Artificial cells, nanomedicine, and biotechnology, 2016. **44**(1): p. 27-40.